

DOE/BETC/3251-12

**MEASUREMENT AND CORRELATION OF CONDITIONS  
FOR ENTRAPMENT AND MOBILIZATION OF RESIDUAL OIL**

**Final Report**

Work Performed for the Department of Energy  
Under Contract No. DE-AC03-79ET3251

Date Published—October 1981

New Mexico Petroleum Recovery Research Center  
New Mexico Institute of Mining and Technology  
Socorro, New Mexico



**National Petroleum Technology Office  
U. S. DEPARTMENT OF ENERGY  
Tulsa, Oklahoma**

**FOSSIL  
FUELS  
RESEARCH**

## DISCLAIMER

"This book was prepared as an account of work sponsored by an agency of the United States Government. Neither the United States Government nor any agency thereof, nor any of their employees, makes any warranty, express or implied, or assumes any legal liability or responsibility for the accuracy, completeness, or usefulness of any information, apparatus, product, or process disclosed, or represents that its use would not infringe privately owned rights. Reference herein to any specific commercial product, process, or service by trade name, trademark, manufacturer, or otherwise, does not necessarily constitute or imply its endorsement, recommendation, or favoring by the United States Government or any agency thereof. The views and opinions of authors expressed herein do not necessarily state or reflect those of the United States Government or any agency thereof."

Available from the National Technical Information Service, U.S. Department of Commerce, Springfield, Virginia 22161.

### NTIS price codes

Paper copy: \$11.00  
Microfiche copy: \$ 3.50

**MEASUREMENT AND CORRELATION OF CONDITIONS  
FOR ENTRAPMENT AND MOBILIZATION OF RESIDUAL OIL**

**Final Report**

Norman R. Morrow, *Principal Investigator*  
Ioannis Chatzis, *Research Engineer*  
New Mexico Petroleum Recovery Research Center  
New Mexico Institute of Mining and Technology  
Socorro, New Mexico 87801

Michael E. Crocker, *Technical Project Officer*  
Bartlesville Energy Technology Center  
P.O. Box 1398  
Bartlesville, Oklahoma 74005

Date Published—October 1981

Work Performed for the Department of Energy  
Under Contract No. DE-AC03-79ET3251

New Mexico Energy and Minerals Department  
Project No. 2-68-3302

UNITED STATES DEPARTMENT OF ENERGY

TABLE OF CONTENTS

Acknowledgement . . . . .	ii
Abstract . . . . .	1
Task 1. Capillary Number Relationships for Rock Samples . . . . .	3
(a) Tests of Capillary Number Correlation . . . . .	4
(b) and (c) Capillary Number Relationships for Displacement of Continuous and Discontinuous Oil for a Wide Range of Rock Samples . . . . .	7
(d) Relative Permeabilities at Reduced Residual Saturations . . . . .	12
Task 2. Residual Oil Saturations Near the Wellbore . . . . .	33
Task 3. Residual Oil Structure . . . . .	44
Task 4. Effect of Gravity on Residual Saturation . . . . .	53
Task 5. Magnitude of Residual Oil Saturation . . . . .	65
Task 6. Effects of Wettability on Capillary Number Relationships . . . . .	75
Appendix I (Task 6a) The Effects of Contact Angle Hysteresis and Pore Geometry on Blob Mobilization . . . . .	78
Appendix II (Task 6b) Effect of Interfacial Velocity on Dynamic Contact Angles at Rough Surfaces . . . . .	94

LIST OF ILLUSTRATIONS

Figure 1.1 . . . . .	19
Figure 1.2 . . . . .	20
Figure 1.3 . . . . .	21
Figure 1.4 . . . . .	22
Figure 1.5 . . . . .	23

Figure 1.6	24
Figure 1.7	25
Figure 1.8	25
Figure 1.9	26
Figure 1.10	27
Figure 1.11	28
Figure 1.12	29
Figure 1.13	30
Figure 1.14	31
Figure 1.15	32
Figure 2.1	39
Figure 2.2	40
Figure 2.3	41
Figure 2.4	42
Figure 2.5	43
Figure 3.1	49
Figure 3.2	50
Figure 3.3	51
Figure 3.4	52
Figure 4.1	60
Figure 4.2	61
Figure 4.3	62
Figure 4.4	63
Figure 4.5	64
Figure 5.1	72
Figure 5.2	73
Figure 5.3	74
Figure 6.1	77
Figure A1.1	90
Figure A1.2	91
Figure A1.3	92
Figure A1.4	93
Figure A2.1	105
Figure A2.2	106
Figure A2.3	107
Figure A2.4	108
Figure A2.5	109
Figure A2.6	110
Table 1.1	16
Table 1.2	17
Table 1.3	18
Table 4.1	58
Table 4.2	59
Table 5.1	71
Table A1.1	86
Table A1.2	87
Table A1.3	88
Table A1.4	89
Table A2.1	103
Table A2.2	103
Table A2.3	104

## ACKNOWLEDGEMENT

In addition to those named in the body of this report, the following people made contributions to this project: J. J. Taber (Senior Advisor); F. D. Martin and F. M. Orr (Consultants); R. W. Foster (Geologist); Cathy Fenn, Scott Mathews, Robert Mercogliano, and Lindley Paul (Technicians); Hal Delmuth, Scott Fedrowski, Suzanne Wood, Gian Bacigalupa, Pauline Kendeck, and Phil Mogen (Undergraduates).

## ABSTRACT

This report covers a two year research project concerned with factors which affect the entrapment and mobilization of residual oil. The project has six major tasks. A brief description of each task and highlights of results obtained to date are given below. Detailed results are given in the main body of the report.

Task 1 involves measurement of relationships between the ratio of viscous to capillary forces and the reduction in normal waterflood residual oil (capillary number relationships) for a variety of rock types. These measurements indicate the relative ease with which residual oil can be immiscibly displaced by a tertiary process. General correlations of results obtained for a variety of sandstones are presented.

Comparative results are presented for conditions required for a prevention of entrapment of a continuous phase as compared to those needed for mobilization of trapped oil. Results show that in reducing the amount of trapped oil to 50% of normal residual oil saturation, recovery of continuous oil is significantly easier than mobilization of trapped oil.

In application of these and previously reported results to surfactant flooding, the capillary number correlation is assumed to hold for changes of about four orders of magnitude in interfacial tensions. This assumption has been tested for more limited changes of 20-fold variation in interfacial tension. The system isooctane/isopropanol/2% CaCl<sub>2</sub> brine was used for tests of interfacial tension variation. Results given by varying the interfacial tension from 36 dyne/cm down to 4 dynes/cm gave excellent correlation. However, results for the 2 dyne/cm system in Berea sandstone showed consistent deviation from the general correlation. The use of reduced interfacial tensions permitted measurement of capillary number relationships down to very low residual saturations.

During the course of obtaining capillary number relationships, relative permeabilities of the water phase at reduced residual oil saturations were also being measured. The measured permeabilities were independent of the displacement mechanism of oil movement (i.e., via displacement of blobs or displacement of continuous oil) by which the reduced residual saturations were achieved and a good general correlation was obtained. Reduction in permeability with increase in pressure gradient at constant (residual) oil saturation was often observed, particularly in the higher permeability rocks.

Task 2 is the application of measured capillary number relationships to the problem of flushing as related to determining in situ residual oil saturations. The more widely accepted logging methods (pulsed neutron capture and nuclear magnetic logging) have depths of investigation which are limited to about 1" from the face of the wellbore. This region will

likely have been subjected to high flow rates during drilling which may be sufficient to cause stripping of residual oil. Reduction in residual oil saturation around the wellbore is estimated from the capillary number and relative permeability relationships obtained under Task 1. Corrections to residual oil saturations for flushing were obtained through integration of the residual oil distribution with assumed response functions for the logging tool.

Task 3 is to investigate the microscopic structure and distribution of residual oil. A technique involving solidification of the immobile oil phase and subsequent separation has been developed and electron micrographs have been made of the solid blobs. Preliminary results on the size distribution of residual blobs and change in size distribution with capillary number have been obtained for Berea sandstone samples.

Task 4 has been concerned with the effects of gravity on trapping. Relationships between residual saturation and the ratio of gravity to capillary forces have been measured, and the equivalence of gravity and viscous forces (i.e., the effect of the total potential) on trapping has been established. Topics considered within this work include detailed discussion of the microscopic mechanisms of trapping and mobilization, the effect of dip angle, relative permeabilities at the flood front, and the significance of buoyancy forces in low interfacial tension flooding. The results indicate that gravity forces can become important at the ultra-low interfacial tension values encountered; for example, in surfactant flooding.

Task 5 is to determine the main causes of variation in residual oil saturation from one rock to another. It has been shown, provided capillary forces are dominant, that residual saturation in unconsolidated media is independent of both particle size and size distribution. High residual saturations were achieved by inclusion of heterogeneities formed from clusters of large particles surrounded by smaller particles. The influence of pore structure on trapping mechanisms has been investigated using two-dimensional micromodel systems. In addition to providing visual demonstration of the effect of heterogeneities, it was also shown that when the aspect ratio (the ratio of pore body to pore throat size) was greater than about 3 to 4, extensive trapping of oil occurs as single pore blobs.

Task 6 concerns wettability and capillary number relationships and has two objectives. The first is to advance understanding of the effect of wettability on capillary number. Conjectures have been made as to the differences in effect that contact angle will have on the processes of trapping and mobilization. Experimental studies have been made of the effect of contact angle on mobilization in simple pore models. The second objective, which is in part supplementary to the aforementioned objective, is to investigate the effect of interface velocity at rough surfaces for advancing and receding conditions. For velocities ranging from below to well above typical field flow rates, contact angles at roughened low energy surfaces changed by no more than a few degrees for a wide range of wetting conditions.

## Task 1. Capillary Number Relationships for Rock Samples

- Objectives:
- (a) to test the capillary number concept by comparing capillary number relationships for various rock samples when parameters (in particular, the interfacial tension) of the capillary number are varied.
  - (b) to obtain capillary number relationships for various rock samples for the displacement of continuous oil at saturations much higher than normal waterflood residual oil saturations.
  - (c) to obtain accurate values of residual oil saturation and reduced residual as a function of capillary number for a wide range of rock specimens.
  - (d) to measure relative permeabilities at reduced residual oil saturations.

Capillary forces and the network nature of pore space interconnectedness are responsible for the entrapment of one phase by another during immiscible displacements in porous media. Laboratory studies have shown that residual oil can be recovered if the displacing phase causes viscous forces acting on the residual oil blobs to exceed the capillary retaining forces.<sup>1-10</sup> The magnitude of the capillary forces is set by the oil/water interfacial tension, wettability conditions, and the pore geometry in which trapped oil blobs exist. The apparent magnitude of the viscous forces acting on a trapped oil blob is set by the permeability of the rock sample to the displacing phase (e.g., water), the imposed pressure gradient, and the viscosity of the displacing phase.

The ratio of viscous to capillary forces is often referred to as the "capillary number" by workers dealing with surface phenomena and oil recovery. Its magnitude determines the relative importance of viscous and capillary forces on the mobilization of residual oil. More than a dozen expressions have been used in the literature to express the ratio of viscous to capillary forces in immiscible displacement experiments in porous media,<sup>11</sup> many of which are equivalent.<sup>12</sup> They include the following expressions that are also used in this paper:

$$N_{c_1} = \frac{v\mu}{\sigma} \quad (1.1)$$

$$N_{c_2} = \frac{K_w \Delta P}{L\sigma} \quad (1.2)$$

$$N_{c_3} = \frac{K_a \Delta P}{L\sigma} \quad (1.3)$$

where  $v$  is the Darcy velocity of the displacing phase,  $\mu$  is the viscosity of the displacing phase,  $\sigma$  is the interfacial tension,  $\Delta P/L$  is the imposed pressure gradient across the sample of length  $L$ , and  $K_a$ ,  $K_w$  are the specific permeabilities of the sample to air and aqueous phase, respectively. Whatever the specific definition used for the "capillary number," use of this term in this paper implies generic reference to the ratio of viscous to capillary forces.

#### (a) Tests of Capillary Number Correlation

Estimates of the reduction in interfacial tension required for tertiary oil recovery based on the capillary number relationships measured at normal oil-water interfacial tensions involve the assumption that the effect of change in interfacial tension will hold for reductions of about 4 orders of magnitude. This assumption has been tested by making interfacial tension the principal variable in capillary number measurements on a few sandstone samples. Interfacial tension was varied more than an order of magnitude by using equilibrated fluid pairs formed from mixtures of isooctane, isopropanol (IPA) and 2%  $\text{CaCl}_2$  brine, hereafter referred to as the OAW system. Phase composition, interfacial tension, density and viscosity data at room temperature have been measured and results are presented in Figures 1.1, 1.2 and 1.3. The upper phase, rich in isooctane, serves the purpose of the oil phase, and the lower phase, rich in brine, serves the purpose of the wetting phase. The gradual variation of interfacial tensions with composition (see Figure 1.1) is such that the OAW system is well suited for varying the tension in the range of 0.5 to 10 dynes/cm.

### Experimental Procedures, Results and Discussion

Cores used in mobilization experiments using the OAW system were sandstone samples about 3 inches long by 1.5 inches in diameter. For the mobilization of residual oil saturation, the experimental procedure was as follows:

- (1) The cores properties  $K_a$ ,  $\phi$ ,  $K_w$  were first determined.
- (2) The core was saturated with brine, and an initial oil saturation,  $S_{oi}$ , (upper phase saturation) was established by oil flooding the sample at pressure gradients of about 250 psi/ft.
- (3) Normal waterflood residual oil saturation ( $S^*$ ) was established by waterflooding the sample using the lower phase<sup>or</sup> of the OAW system at pressure gradients of about 2 to 5 psi/ft. Water breakthrough curves were typical of low viscosity oil in a water-wet rock, there being little or no oil production after injection of about 2 PV of the lower phase.

- (4) The pressure drop across the core was then increased in a stepwise manner, and above some critical value, residual oil production is observed. For each step change of pressure drop across the sample, about 3.5 PV of lower phase are passed through the sample. At the end of every step change in  $\Delta P$ , the sample is weighed in order to keep track of the residual oil saturation remaining in the sample. In addition, the volume of residual oil produced is monitored. Effective permeabilities to water are also measured at the end of every step change in  $\Delta P$  as a matter of course.

The major problem areas in the capillary number measurements using the OAW system have been: 1) the difficulty of monitoring saturation changes volumetrically, particularly for interfacial tensions smaller than 10 dynes/cm because of emulsification and long-time periods required for phase separation; and 2) difficulties in weight measurements at the end of an incremental step change in pressure drop. Loss of core sample weight was experienced when core samples were flooded in the Hassler type core holder primarily due to 1) loss of rock grains; and 2) air entering the rock sample during application of overburden pressure to the rubber sleeve. Recently, these problem areas have been eliminated by using core samples cast in an epoxy resin which had unusually good mechanical strength (e.g., the epoxied core sample assembly could stand pressure gradients of about 650 psi/ft) and satisfactory resistance to chemical attack by IPA and brine.

Capillary number relationships using the OAW system have been obtained for a number of Berea sandstone samples having air permeabilities in the range of 200 md to 800 md, and for a Fountainbleau sandstone sample with  $K_a \approx 1360$  md. A summary of core properties and flooding data is given in Table 1.1<sup>a</sup> using equilibrated mixtures of the OAW system having interfacial tensions ranging from 2 dynes/cm to 6.6 dynes/cm. Designations by which cores will be referred to are included in this Table. Examining the results of Table 1.1, one finds the normal waterflood residual oil saturation for Berea sandstone samples to vary between 28% to 33.5%, with one exception; run No. 2 for the Berea CQ-A8 sample, the relative permeability to the aqueous phase varied from 0.13 to 0.25. The initial oil saturations in the Berea samples tested varied from 50% to 65%. Although the initial oil saturations attained with the OAW system are consistently lower than those obtained using the Soltrol oil-brine system (details of which will be discussed under tasks 1(b) to 1(c)), the residual oil saturation and relative permeabilities at waterflood residual oil are typical of high interfacial tension systems under water-wet conditions. The results obtained with the same Fountainbleau sandstone sample using 2 dynes/cm mixtures, with one exception, gave reproducible residual oil saturation and relative permeability values at normal waterflood residual oil conditions. It must be noted, however, that saturation determinations made by carrying out gravimetric material balance in our experiments are subject to an experimental error of  $\pm 1\%$  for samples having a pore volume of about 15 cm<sup>3</sup>.

Residual oil saturation data and values normalized with respect to  $S^*$ , were determined for the core samples listed in Table 1.1. These are  
or

plotted against capillary number. Typical capillary number plots with  $\frac{K_w \Delta P}{L\sigma}$  are presented in Figure 1.4 for a Berea sandstone. Plots of three forms of capillary number versus reduced residual oil saturation for three core samples are presented in Figure 1.5.

Comparison of capillary number curves for various sandstone samples and various interfacial tension conditions is made in Figure 1.6. The data, shown in Figure 1.6 for the cases of the Berea R9-11 sample and the Fountainbleau sample with interfacial tensions of 4.8 and 34.8 dynes/cm respectively, correlate very satisfactorily. The capillary number curves obtained with the 2 dynes/cm fluid pair for the Fountainbleau sandstone sample and other samples are different from the correlation defined by the 4.8 and 34.0 dynes/cm data. Figure 1.7 shows capillary number curves obtained with tensions of 2 and 6.6 dynes/cm using the same Berea BE-1 sample; the capillary number curve of Berea BE-1 corresponding to 2 dynes/cm is compared with that of Berea CQ-10 sample. It appears from the capillary number data of Berea BE-1 that the capillary number curve does not exactly scale with surface tension, when  $\sigma$  is smaller than about 4 dynes/cm. This is similar to the behavior shown by the results presented in Figure 1.6 for various samples and interfacial tensions. However, for the two different sandstones at a given interfacial tension, capillary number curves in the form of  $S_{or}/S_{or}^*$  versus  $\frac{K_w \Delta P}{L\sigma}$  (or  $\frac{K_a \Delta P}{L\sigma}$ ) correlate well. The effect of

interfacial tension and fluid pair on capillary number curve can also be examined through the data shown in Figure 1.8; capillary number data obtained with the OAW system in various samples with interfacial tension of about 5 dyne/cm are compared with capillary number data obtained with the Soltrol oil-brine system which had an interfacial tension of about 35 dynes/cm. As can be seen from Figure 1.8, the two sets of data compare satisfactorily. In recently completed experiments on displacement of oil from bead packs, capillary number appears to correlate satisfactorily with interfacial tension for systems ranging from 2 dynes/cm up to 11 dynes/cm for the complete capillary number curve.

The critical  $\frac{K_w \Delta P}{L\sigma}$  values for the samples used with the OAW system fall in the range of  $1 \times 10^{-5}$  to  $2.5 \times 10^{-5}$ . These values compare favorably with the results of other studies<sup>1,5</sup> as well as with results obtained in the present work for systems having interfacial tension of 35 dynes/cm (see Table 1.2).

The capillary number relationships indicate that almost complete mobilization corresponds to capillary numbers of about  $1.5 \times 10^{-3}$ . This value of capillary number is smaller than that indicated by literature data<sup>1,4,1.8</sup> which suggest the value of  $1 \times 10^{-2}$  for complete recovery. It may be noted that there is only a limited amount of data on the capillary numbers required to achieve very high oil recovery.

## Conclusions

(1) Normalized reduced residual oil saturation versus capillary number defined by  $\frac{K_w \Delta P}{L\sigma}$  (or  $\frac{K_a \Delta P}{L\sigma}$ ) correlate satisfactorily for various sandstone samples for interfacial tensions of 4 dynes/cm and higher.

(2) From the limited amount of data obtained to date using the OAW system, it appears that capillary number curves for a given rock sample do not always scale as expected when the interfacial tension was reduced to about 2 dynes/cm. This conclusion is tentative and needs to be tested through further experiments.

(3) Complete mobilization of residual oil in water-wet rocks, as indicated by displacement results for OAW systems corresponds to displacement at a capillary number of  $1.5 \times 10^{-3}$ .

### (b) and (c) Capillary Number Relationships for Displacement of Continuous and Discontinuous Oil for a Wide Range of Rock Samples

Two types of measurements have been made for a wide variety of sandstone samples:

- (1) Capillary number relationships for the displacement of discontinuous oil. They are obtained by starting at normal waterflood residual oil saturation and increasing the pressure gradient in increments.
- (2) Capillary number relationships for the displacement of continuous oil. They are obtained by beginning with high oil saturation in the rock sample and displacing it at some set pressure to give a residual saturation. High oil saturation is then restored and the set displacement pressure is increased.

Experiments have been conducted on a wide variety of Berea sandstone samples, Boise sandstone, Cottage Grove sandstone, Fountainbleau sandstone, and Torpedo sandstone samples. The immiscible fluid pair used in these experiments was mineral oil (Soltrol 130, Soltrol 170) and 2%  $\text{CaCl}_2$  brine, hereafter referred to as the OW system, having interfacial tension of about 35 dynes/cm. Displacement experiments were carried out in Hassler type core holders using core samples of about 3 inches long by 1.5 inches in diameter.

## Experimental Procedure

After measuring air permeabilities, the core samples were saturated with 2%  $\text{CaCl}_2$  brine and the porosity of the sample determined. Subsequently,

the permeability to brine was measured for a range of pressure drops and the core was then flooded with oil at about 300 to 500 psi/ft to establish an analogue of connate water saturation. Capillary number curves for displacement of continuous oil were obtained by displacing oil at some pressure drop,  $\Delta P$ , across the sample, and measuring the corresponding residual oil saturation. The connate water saturation was reestablished in the same core sample by one of the following two ways: 1) flowing oil through the core, or 2) cleaning the core sample with IPA, then saturating the sample with brine, followed with oil flooding at a high pressure gradient as in the first oil flooding. The sample with reestablished high oil saturation was waterflooded again at an increased pressure. This cycle was repeated about twelve times to give a relationship between residual oil and capillary number for displacement of continuous oil. Residual oil saturation and initial oil saturation determinations were made based on gravimetric material balance. As such, the test sample was weighed at the end of every displacement. (Saturation determination by volumetric material balance alone was found to be unreliable.)

Capillary number curves for displacement of discontinuous oil were obtained by starting at normal waterflood residual oil saturation,  $S^*$ , obtained by displacing continuous oil at pressure gradients of about 10-20 psi/ft, and increasing the applied pressure drop incrementally. The volume throughput of brine for each data point was kept to about 5 PV. Residual oil saturation corresponding to each capillary number condition was monitored by 1) weighing the sample after a particular increase in  $\Delta P$  had been applied, and 2) monitoring volumetrically the amount of oil mobilized.

## Experimental Results and Discussion

Established residual oil saturations and reductions in residual oil saturation achieved by changing capillary number are summarized in Table 1.2 for a wide range of rock specimens. Multiple runs performed for a number of sandstone samples gave reproducible values of normal waterflood residual oil saturations to within experimental error of about  $\pm 1.0\%$  of pore volume for most of the samples tested as can be seen from Table 1.2. Most of the core samples listed in Table 1.2 were fired to about  $800^\circ\text{C}$  for one hour and cleaned with IPA between runs. This was found to enhance the reproducibility of results for permeability to brine, values of  $S^*$  achieved at given flow conditions, and relative permeabilities at given values of  $S^*$ . The initial oil saturations attained in Berea sandstone samples with air permeabilities in the range of 100 md to 1000 md were in the range of 60% to 70%. Residual oil saturations varied between 30% to 43%. However, there does not appear to be a strong correlation between residual oil saturation and sample permeability for the various Berea sandstone samples, although the low permeability samples (e.g., Berea C-0) gave higher residual oil saturation values than the high permeability Berea samples (e.g., Berea BL-2).

Typical capillary number curves and reproducibility of results for the case of displacement of discontinuous and continuous oil are illustrated by

the data obtained for Fountainbleau sandstone, shown in Figure 1.9, and the data presented in Figure 1.10 for four Berea sandstones.

The capillary number curves of  $S_{or}/S_{or}^*$  versus  $\frac{K_w \Delta P}{L\sigma}$  and  $S_{or}/S_{or}^*$  versus  $\frac{K_a \Delta P}{L\sigma}$  run parallel to each other, since  $K_w$  and  $K_a$ , are constants for a given system ( $K_w$  usually  $< K_a$ ) in the above definition of capillary number (see Figure 1.5). The forms of capillary number used  $\left( \frac{K_w \Delta P}{L\sigma} \text{ and } \frac{K_a \Delta P}{L\sigma} \right)$  as compared with the more widely used  $\frac{v\mu}{\sigma}$  for the case of discontinuous oil offers the advantages of 1) providing a better estimation of the critical capillary number defined at the pressure gradient conditions above which mobilization occurs, and 2) showing reduced residual oil values corresponding to  $S_{or}/S_{or}^*$  values lower than 0.95 as a straight line when  $S_{or}/S_{or}^*$  is plotted against the logarithm of  $\frac{K_w \Delta P}{L\sigma}$  or  $\frac{K_a \Delta P}{L\sigma}$ . By plotting the data of  $S_{or}/S_{or}^*$  versus  $\frac{K_w \Delta P}{L\sigma}$  for a number of samples, the values of capillary number corresponding to  $S_{or}/S_{or}^*$  equal to 1.0, 0.95 and 0.5 respectively were read from the graphs. Because limitations on pressure gradients of about 940 psi/ft were necessary to avoid obvious core damage, 50% reductions of residual oil saturation were not attainable with the high interfacial tension in OW systems. This problem is aggravated by use of low permeability samples. If a 50% reduction in saturation was not achieved by experiment, whenever judged appropriate, the capillary number corresponding to 50% reduction was approximated by extrapolation (e.g., see Figure 1.13). A summary of the capillary number corresponding to the aforementioned  $S_{or}/S_{or}^*$  conditions is given in Table 1.2.

As can be seen from Table 1.2, the critical capillary number for onset of oil displacement, calculated as  $\frac{K_w \Delta P}{L\sigma}$ , varied between  $8 \times 10^{-6}$  to  $3 \times 10^{-5}$  with the value of  $2 \times 10^{-5}$  being typical for most of the samples. The variations of the capillary number for various rocks when evaluated at  $S_{or}/S_{or}^*$  values of 0.95 and 0.5 respectively were somewhat smaller on the average, ranging between  $2 \times 10^{-5}$  to  $6.5 \times 10^{-5}$  at  $S_{or}/S_{or}^* = 0.95$  and  $2 \times 10^{-4}$  to  $4.4 \times 10^{-4}$  at  $S_{or}/S_{or}^* = 0.5$ . This magnitude of variation of the capillary number for a given reduction in residual oil from one sample to another can be accounted for by microscopic pore structure parameters involving normalized size (length) distributions of trapped oil blobs and differences between drainage and imbibition curvatures, respectively, that do not vary more than a factor or two. Bearing this in mind, the experimental results suggest that capillary number curves of various sandstones correlate satisfactorily.

A correlation was sought between the critical displacement ratio  $\left( \frac{\Delta P}{L\sigma} \right)_{cr}$ , and sample permeability. Based on mobilization conditions of an oil blob trapped in a periodically constricted tube of diameters  $D_1$  and  $D_2$ , and neglecting effects of change in pore shape, the critical displacement condition is given by:

$$\left( \frac{\Delta P}{L\sigma} \right)_{cr} = \frac{1}{C_1 D_1^2} \left( \cos\theta_R - \frac{\cos\theta_A}{C_2} \right) \quad (1.4)$$

where  $C_1$  is a dimensionless quantity that relates the length of the oil blob with respect to the equivalent pore throat diameter,  $D_e$ , at the leading edge of the blob,  $C_2$  is the aspect ratio of diameters  $D$  to  $D_e$ ;  $\theta_R$  and  $\theta_A$  are the receding and advancing contact angles, respectively.

By analogy with a porous medium,  $C_1$  will be related to the blob length size distribution and pore throat size, and  $C_2$  will be related to the mean aspect ratio of pore body size to pore throat size. The permeability of the medium is strongly determined by the pore throats and as such is proportional to  $D_e^2$ . Therefore, if the porous media are geometrically similar, the parameters  $C_1$  and  $C_2$  in equation (1.4) are scaled from one porous medium to another, and  $K_a$  and  $K_w$  are proportional to  $D_e^2$  so that  $\left(\frac{\Delta P}{L\sigma}\right)_{cr} \propto \frac{1}{K}$ . Log-log plots of  $\left(\frac{\Delta P}{L\sigma}\right)_{cr}$  versus  $K_a$  and  $K_w$  shown in Figure 1.11 provide a comparison of the data obtained in this work with those reported by Taber.<sup>1,5</sup> Although there is a considerable variation in the critical displacement ratio values for a given value of air permeability, there is a general trend showing  $\left(\frac{\Delta P}{L\sigma}\right)_{cr}$  decreasing as the air permeability of the sample increases. A least square fit performed on the data obtained in this work with the OW system gave a slope of -0.94 (e.g.,  $1/K^{0.94}$ ), and a correlation coefficient of -0.90. The scatter in results is not unexpected. The critical displacement ratio cannot be expected to be fully determined by the rock permeability alone, since the pore structure of residual oil blobs are strongly affected by microscopic pore structure parameters such as the pore body to pore throat aspect ratio, and microscopic heterogeneities consisting of clusters of relatively large pores surrounded by relatively small pores that influence important factors such as the length size distribution of residual oil blobs.

Comparisons of the capillary number curves obtained when displacing continuous oil with the capillary number curves obtained when trying to mobilize residual oil are illustrated in Figure 1.10 for a number of samples. It is clearly demonstrated that for a given reduction of residual oil saturation, the corresponding capillary number for the displacement of continuous oil is significantly lower than that required for mobilization of discontinuous oil, for reduced residual oil saturations in the range  $S_{Or}/S_{Or}^* = 0.5$  to 1.0. After the residual oil saturation,  $S_{Or}$ , has been reduced to about 50% of its initial value ( $S_{Or}^*$ ), the capillary number relationships for the continuous oil and discontinuous oil<sup>or</sup> become almost indistinguishable. These experimental results are consistent with the comparison of capillary number results drawn by various authors<sup>1,9,1.10</sup> from published literature, and with the analysis of how oil can be prevented from trapping.<sup>1.11,1.12</sup> The data presented in this work are the most extensive yet available for a given rock sample.

Preliminary studies of displacement of discontinuous and continuous oil in 2-D network models gave similar results to those obtained in rock samples. Basic reasons for the relative ease of displacing continuous oil were suggested

in a discussion of displacement mechanisms at the microscopic level, given in the first annual report.<sup>1.11</sup> From the micromodel studies, it was observed, in addition to the previously described mechanisms, that under dynamic conditions a trapped oil blob behind the flood front can become mobilized at higher capillary numbers. A mobilized blob can coalesce with a stationary blob to create a larger oil blob which is sometimes able to catch up with the continuous oil at the flood front and add to the total oil recovery. It has also been observed that at capillary numbers needed to achieve an  $S_{or}/S_{or}^*$  value less than 0.5, the blob size distributions of residual oil are very narrow (e.g., much of the oil is held in single pores), with blob sizes greater than one pore body having very small probability of existence. A similar type of blob size distribution is anticipated for sandstones at low residual saturation and is suggested by the results presented under Task 3. This is likely related to the similarity of results for displacement of continuous and discontinuous oil at capillary numbers higher than those corresponding to  $S_{or}/S_{or}^* = 0.5$ .

### Conclusions

(1) Waterflood residual oil saturations obtained at capillary numbers lower than  $10^{-6}$  for a number of sandstone samples that vary in permeability by well over an order of magnitude were reproducible for many samples to within  $\pm 1\%$  of PV but varied from one sandstone sample to another.

(2) Capillary number relationships obtained with the oil initially continuous demonstrated the increased ease with which oil can be recovered by prevention of entrapment as compared with mobilization of discontinuous blobs of oil.

(3) At reduced residual oil saturations smaller than 50% of  $S_{or}^*$ , the capillary number curves for the displacement of initially continuous and discontinuous oil respectively fall close together.

(4) The critical displacement ratio is a strong function of sample permeability. Data of this work, and literature data for a total of 32 different sandstone samples having air permeabilities in the range 40 md to 2190 md, led to the following correlation:

$$\left(\frac{\Delta P}{L\sigma}\right)_{cr} = \frac{1422}{K_a}$$

the units of  $\frac{\Delta P}{L\sigma}$  being (psi/ft)/(dyne/cm).

(5) Capillary number curves for the mobilization of discontinuous oil at normal waterflood residual saturation,  $S_{or}^*$ , for various sandstones correlate satisfactorily when capillary number is expressed as

$$\frac{K_w \Delta P}{L\sigma} \quad \text{or} \quad \frac{K_a \Delta P}{L\sigma}$$

#### (d) Relative Permeabilities at Reduced Residual Saturations

The effect of reduction of residual oil saturation on relative permeability is obviously important to simulation of processes such as chemical flooding. Relative permeabilities to the displacing phase at reduced residual saturations were measured as a matter of course during tests related to parts (a), (b) and (c) of Task 1. In runs where the capillary number relationships were most reproducible for a given core, there was also good reproducibility of specific permeabilities. Firing of the Berea sandstone samples was found to enhance the reproducibility of specific permeabilities and permitted use of the same core sample in a number of capillary number experiments.

#### Experimental Results and Discussion

The reproduction of specific permeabilities for a given rock sample after each core cleaning step of the capillary number experiments was essential to quantifying the effect of reduction of residual oil saturation on relative permeability. Table 1.3 shows typical reproduction of specific permeabilities after each regeneration for a Berea sandstone sample used in capillary number tests involving the OW system.

Good reproducibility has been obtained for relative permeability at reduced residual saturations for both OW and OAW systems. Figure 1.12 shows sample results of relative permeability at reduced residual oil conditions obtained for the Berea CQ-11 sample when displacing continuous and discontinuous oil, respectively. Relative permeabilities did not differ greatly from each other, although a given saturation was attained at distinctly different capillary numbers for the two conditions.

Figure 1.13 shows the relative permeability plotted against the applied pressure drop across the sample. Note that for the case of displacement of continuous oil (i.e., initial high oil saturation), the relative permeability to brine increases as the applied displacement pressure is increased. For discontinuous oil, behavior is somewhat anomalous. When one tries to mobilize trapped residual oil by increasing the applied pressure gradient, there is no change in sample saturation until a critical  $\Delta P/L$  is reached. However, the relative permeability plots in Figure 1.12 for the case of discontinuous oil, show that there is a decrease in relative permeability to brine as  $\Delta P/L$  is increased, even though there is no change in residual oil saturation. The relative permeability plots of Figure 1.13 were plotted in this unconventional form for the purpose of illustrating this phenomenon. The basic reasons for this, we believe, are: 1) the blobs of residual oil must change shape as the pressure gradient increases even though the critical pressure gradient for blob mobilization has not been reached and no oil is observed to be produced; as a result, their action as check valves within the pore spaces becomes increasingly effective; and 2) at pressure gradients smaller than the critical pressure gradient, large oil blobs trapped at  $S_{or}^*$  conditions may be locally mobilized and broken up to smaller size oil blobs as soon as the large oil blob encounters pathways that permit the capillary retention forces to stabilize the blob. Blob breakup into a larger number of stable blobs may also occur in a manner which increases the hindrance to flow of water. These speculations are

also consistent with observations of the mobilization process made in transparent 2-D micromodels.

Figure 1.14 shows relative permeability characteristics obtained with the OW system in a relatively low permeability Berea sandstone sample. The results obtained for this sample are of similar form to those described above. The relative permeability curves at reduced residuals are independent of the saturation history of the sample, but the corresponding  $\Delta P/L$  values needed to obtain a specified reduced residual saturation differ. This is consistent with the behavior of capillary number relationships discussed earlier.

Figure 1.15 shows relative permeability characteristics at reduced residual oil saturations for various Berea sandstone samples obtained with the OAW system at different interfacial tensions. The relative permeability characteristics obtained with the OW system for Berea CQ-11 sample are also shown in Figure 1.15 for the purpose of comparison. It is evident that the various relative permeability data for a given water saturation are in good agreement. These results show no significant difference in relative permeability values for a given reduced residual saturation among the various samples, and no significant effect due to variation in interfacial tension for a given core sample, as indicated in Figure 1.15.

Note that the relative permeability curve to the displacing phase at reduced residuals cannot be assumed to be simply an extrapolation of the relative permeability to the water phase measured by conventional techniques. Such extrapolation does not take into account the S shape nature of the curve, and in general, predicts relative permeabilities that are too low. At reduced residual oil saturation, for relative permeabilities corresponding to  $S_w$  in the range of 74% to 82%, there is a dramatic increase in the relative permeability to the wetting phase. When the relative permeability data reported by Abrams<sup>1,7</sup> are plotted on linear graph paper, the relative permeabilities to water at reduced residual oil appear to fall close to a straight line relationship.<sup>1,9</sup> This type of relative permeability behavior at reduced residual oil saturation was not observed in the present work.

## Conclusions

(1) In water-wet sandstone samples, the relative permeability curves at reduced residual oil conditions were found to be strongly dependent on the sample saturation and independent of the history by which a given reduced residual oil saturation was attained.

(2) Relative permeability curves at reduced residual oil saturations obtained with the OAW system were consistent with those obtained with the OW system.

(3) For a given rock sample, using the OAW system, the present data suggest that relative permeability curves at reduced residuals are not dependent on interfacial tension for interfacial tensions down to about 2 dynes/cm.

(4) In displacement experiments for the mobilization of residual oil, reduction in the relative permeability to water at constant saturation (namely, the waterflood residual oil saturation) has been observed, particularly for the less permeable samples, as the capillary number is increased towards its critical value.

(5) Relative permeability curves at reduced residual oil saturation should not be approximated by extrapolation of relative permeability curves to the wetting phase measured by conventional means.

#### Acknowledgement

Laboratory measurements involving the OW system have been made by Earl Barber and Hau Lim. Measurements involving the OAW system have been made by Mary Paneral.

#### References

- 1.1 Moore, T. F. and Slobod, R. L., "The Effect of Viscosity and Capillarity on the Displacement of Oil by Water," Producers Monthly 20, 20 (1956).
- 1.2 Taber, J. J., "Static and Dynamic Forces Required to Remove a Discontinuous Oil Phase from Porous Media Containing both Oil and Water," Soc. Pet. Eng. J. (March 1969).
- 1.3 Melrose, J. C. and Brandner, C. F., "Role of Capillary Forces in Determining Microscopic Displacement Efficiency for Oil Recovery by Water Flooding," J. Can. Pet. Tech. 13, 42 (1974).
- 1.4 Foster, W. R., "A Low Tension Waterflooding Process Employing a Petroleum Sulfonate, Inorganic Salts, and a Biopolymer," J. Pet. Tech. 25, 195 (1973).
- 1.5 Taber, J. J., "Research on Enhanced Oil Recovery, Past, Present and Future," presented at 3rd Int. Conf. on Surface and Colloid Science, Stockholm, Sweden (Aug. 20-25, 1979). (Manuscript available on request.)
- 1.6 Stosur, J. J. and Taber, J. J., "Critical Displacement Ratio and Its Effect on Wellbore Measurement of Residual Oil Saturation," J. Pet. Tech. 28, 865-868 (Aug. 1976).
- 1.7 Abrams, A., "The Influence of Fluid Viscosity, Interfacial Tension, and Flow Velocity on Residual Oil Saturation Left by Waterflooding," Soc. Pet. Eng. J., 435-447 (Oct. 1975).

- 1.8 Gupta, S. P. and Trushenski, S. P., "Micellar Flooding - Compositional Effects on Oil Displacement," Soc. Pet. Eng. J. (April 1974).
- 1.9 Larson, R. G., Davis, H. T. and Scriven, L. E., "Displacement of Residual Nonwetting Phase from Porous Media," Chem. Eng. Sci. (In Press).
- 1.10 Stegemeier, G. L., "Mechanisms of Entrapment and Mobilization of Oil in Porous Media," in Improved Oil Recovery by Surfactant and Polymer Flooding, 55-91, Academic Press (1977).
- 1.11 Morrow, N. R., "Measurement and Correlation of Conditions for Entrapment and Mobilization of Residual Oil," First Annual Report, submitted to the U. S. Department of Energy, November 1979.
- 1.12 Morrow, N. R. and Songkran, B., "Effect of Viscous and Buoyancy Forces on Nonwetting Phase Trapping in Porous Media," in Surface Phenomena in Enhanced Oil Recovery," Plenum Press. In Press.

Table 1.1 Core Properties and Core Flooding Data Obtained with the OAW System

Core Sample	Core Properties			Fluid Properties			Core Flooding Data				
	$\phi$ %	$K_a$ md	$K_w$ md	$\mu_w$ cp	$\mu_o$ cp	$\sigma$ dyne/cm	Run No.	$S_{oi}$ %	$S_{or}^*$ %	$K_{rw}$ at $S_{or}^*$	Flooding $\frac{\Delta P}{L}$ (psi/ft)
Berea BE-1	21.5	370	296	3.08	0.72	2.0	1	65.4	28.7	0.23	2.3
		382	285	2.42	0.71	6.6	2	60.3	32.3	0.18	2.3
Berea BD1-9	19.1	488	314	2.72	0.68	4.6	1	50.0	28.0	0.25	4.1
Berea CA	19.6	234	169	2.42	0.71	6.6	1	61.0	32.7	0.13	2.4
		234	148	"	"	"	2	60.0	31.0	0.15	2.4
Berea CQ-A8	22.7	427	342	3.08	0.72	2.0	1	58.2	28.3	0.26	2.4
		---	256	"	"	"	2	57.7	43.8	0.13	2.4
Berea CQ-1	22.4	764	612	3.08	0.72	2.0	1	55.2	29.6	0.17	2.4
	22.2	766	602	"	"	"	2	53.6	32.3	0.14	2.4
Berea CQ-10	21.0	196	172	3.08	0.72	2.0	1	60.6	32.7	0.15	2.8
Berea R9-11	20.0	543	417	2.62	0.69	4.8	1	52.3	29.9	0.128	4.8
Berea V-10	20.7	562	497	2.72	0.68	4.6	1	62.0	33.5	0.17	5.0
Fountainbleau	16.3	1344	1060	3.08	0.72	2.0	1	64.7	31.7	0.25	2.0
		---	1080	"	"	"	2	76.0	32.4	0.27	2.0
	16.4	---	1202	"	"	"	3	69.6	27.0	0.29	3.0
		1405	1202	"	"	"	4	79.5	44.0	0.25	2.0
		---	1082	"	"	"	5	77.2	28.8	0.25	3.9

Table 1.2 Summary of Core Properties and Capillary Number Measurements

Sandstone Sample	Transport Properties			Waterflooding Data						K <sub>w</sub> AP at various S <sub>or</sub> conditions				Critical AP L <sub>c</sub> kPa mN	
	φ (%)	K <sub>a</sub> (md)	K <sub>w</sub> (md)	Run No.	μ <sub>w</sub> mPa·s	μ <sub>o</sub> mPa·s	σ mN/m	Sol %	S <sub>or</sub> %	K <sub>w</sub> at S <sub>or</sub> *	S <sub>or</sub> = 1 S <sub>or</sub> *	S <sub>or</sub> = 0.95 S <sub>or</sub> *	S <sub>or</sub> = 0.5 S <sub>or</sub> Discontinuous Oil		S <sub>or</sub> = 0.5 S <sub>or</sub> Continuous Oil
Berea B-L2	22.5	982	584	1	0.94	2.05	34.8	64.7	34.0	0.202	2 × 10 <sup>-5</sup>	4.5 × 10 <sup>-5</sup>	2.8 × 10 <sup>-4</sup>	3 × 10 <sup>-4</sup>	37.3
			534	2	"	"	"	66.2	33.2	0.240					
			542	3	"	"	"	68.9	34.2	0.245					
Berea CQ-11	21.4	859	641	1	0.94	2.05	34.8	56.9	32.3	0.311	2 × 10 <sup>-5</sup>	6 × 10 <sup>-5</sup>	2.7 × 10 <sup>-4</sup>	2.7 × 10 <sup>-4</sup>	40.3
			506	2	"	"	"	63.9	30.1	0.218					
			508	3	"	"	"	63.8	31.8	0.273					
			428	4	"	"	"	63.1	32.1	0.25					
Berea CQ-5	20.4	772	425	1	0.94	1.42	35.9	63.2	29.4	0.255	2 × 10 <sup>-5</sup>	6 × 10 <sup>-5</sup>	2.7 × 10 <sup>-4</sup>	2.5 × 10 <sup>-4</sup>	49.3
			407	2	"	"	"	64.0	28.4	0.175					
Berea CQ-A7	21.1	825	485	1	0.94	1.42	35.9	62.5	30.2	0.246	2.8 × 10 <sup>-5</sup>	5.5 × 10 <sup>-5</sup>	2.2 × 10 <sup>-4</sup>	2.2 × 10 <sup>-4</sup>	59.3
			347	2	"	"	"	64.6	30.6	0.219					
Berea CQ-9	20.3	625	378	1	0.94	1.42	35.9	63.5	32.5	0.111	2.2 × 10 <sup>-5</sup>	5.5 × 10 <sup>-5</sup>	2.5 × 10 <sup>-4</sup>	---	61.5
			366	2	"	"	"	64.7	34.7	0.147					
			690	3	"	"	"	66.1	36.0	0.080					
Berea CQ-A4	21.2	774	418	1	0.94	1.42	35.9	67.2	29.8	0.326	1.5 × 10 <sup>-5</sup>	3.7 × 10 <sup>-5</sup>	3.6 × 10 <sup>-4</sup>	---	36.9
Berea CQ-A	21.5	674	300	1	0.94	2.05	34.8	58.7	34.7	0.113	3 × 10 <sup>-5</sup>	4.6 × 10 <sup>-5</sup>	2.0 × 10 <sup>-4</sup>	---	102.5
			300	2	"	"	"	64.3	34.9	0.111					
Berea DOE-1	18.5	719	476	1	0.94	2.05	35.9	68.2	32.4	0.174	2.5 × 10 <sup>-5</sup>	6 × 10 <sup>-5</sup>	3.3 × 10 <sup>-4</sup>	---	53.8
Berea B-J	22.1	604	342	1	0.94	2.05	34.8	66.8	38.7	0.186	2.2 × 10 <sup>-5</sup>	6.5 × 10 <sup>-5</sup>	4.0 × 10 <sup>-4</sup>	---	66.1
Berea B-5	18.7	303	117	1	0.94	2.05	34.8	60.5	37.2	0.0318	1.3 × 10 <sup>-5</sup>	2.1 × 10 <sup>-5</sup>	3.0 × 10 <sup>-4</sup>	---	123.3
			102	2	"	"	"	64.5	37.2	0.0548					
			303	3	"	"	"	68.5	43	0.0485					
Berea HB-2	17.7	188	76	1	0.94	2.05	34.8	61.0	34.4	0.101	8.0 × 10 <sup>-5</sup>	2 × 10 <sup>-5</sup>	1.7 × 10 <sup>-4</sup>	---	113.8
			68	2	"	"	"	60.9	35.5	0.093					
Berea C-0	18.3	148	67	1	0.94	2.05	34.8	65.0	41.3	0.0625	1.3 × 10 <sup>-5</sup>	2.0 × 10 <sup>-5</sup>	---	---	190.2
			72	2	"	"	"	64.4	41.0	0.0623					
			84	3	"	"	"	60.0	42.7	0.060					
Boise	25.3	1600	745	1	0.94	2.05	34.8	79.1	27.0	0.410	1.5 × 10 <sup>-5</sup>	5 × 10 <sup>-5</sup>	3.5 × 10 <sup>-4</sup>	---	19.9
			785	2	"	"	"	72.3	27.6	0.380					
Cottage Grove 1H	25.1	296	155	1	0.94	2.05	34.8	62.6	35.3	0.0746	2.0 × 10 <sup>-5</sup>	5 × 10 <sup>-5</sup>	2.0 × 10 <sup>-4</sup>	---	146.4
			133	2	"	"	"	63.9	38.3	0.0738					
			133	3	"	"	"	63.4	37.2	0.0738					
Fountainbleau	15.6	1455	665	1	0.94	2.05	34.8	63.3	36.7	0.268	1 × 10 <sup>-5</sup>	4.5 × 10 <sup>-5</sup>	2.2 × 10 <sup>-4</sup>	2.2 × 10 <sup>-4</sup>	15.4
			665	2	"	"	"	73.9	28.9	0.387					
			623	3	"	"	"	70.0	33.7	0.341					
			706	4	"	"	"	61.5	35.2	0.270					
			1320	5	"	"	"	73.0	31.3	0.310					
Torpedo 1N-1	27.3	564	239	1	0.94	2.05	34.8	66.5	34.1	0.209	2.2 × 10 <sup>-5</sup>	6.5 × 10 <sup>-5</sup>	---	---	94.3

Table 1.3 Reproduction of Specific Permeabilities after each  
Regeneration Step for a Fired Berea Sample

<u>Run No.</u>	<u><math>K_w (S_w=1)</math> (md)</u>	<u><math>K_o (S_w=S_{wc})</math> (md)</u>	<u><math>K_a</math> (md)</u>	<u>Core Previously Dried</u>
1	500	550	875	yes
2	506	600	860	yes
3	500	540	860	yes
B1	425	430	-	no
B2	440	480	-	no
B3	440	500	-	no
B4	425	525	-	no
B5	430	430	-	no
B6	430	440	-	no
B7	451	480	-	no
B8	410	450	-	no
B9	435	430	-	no

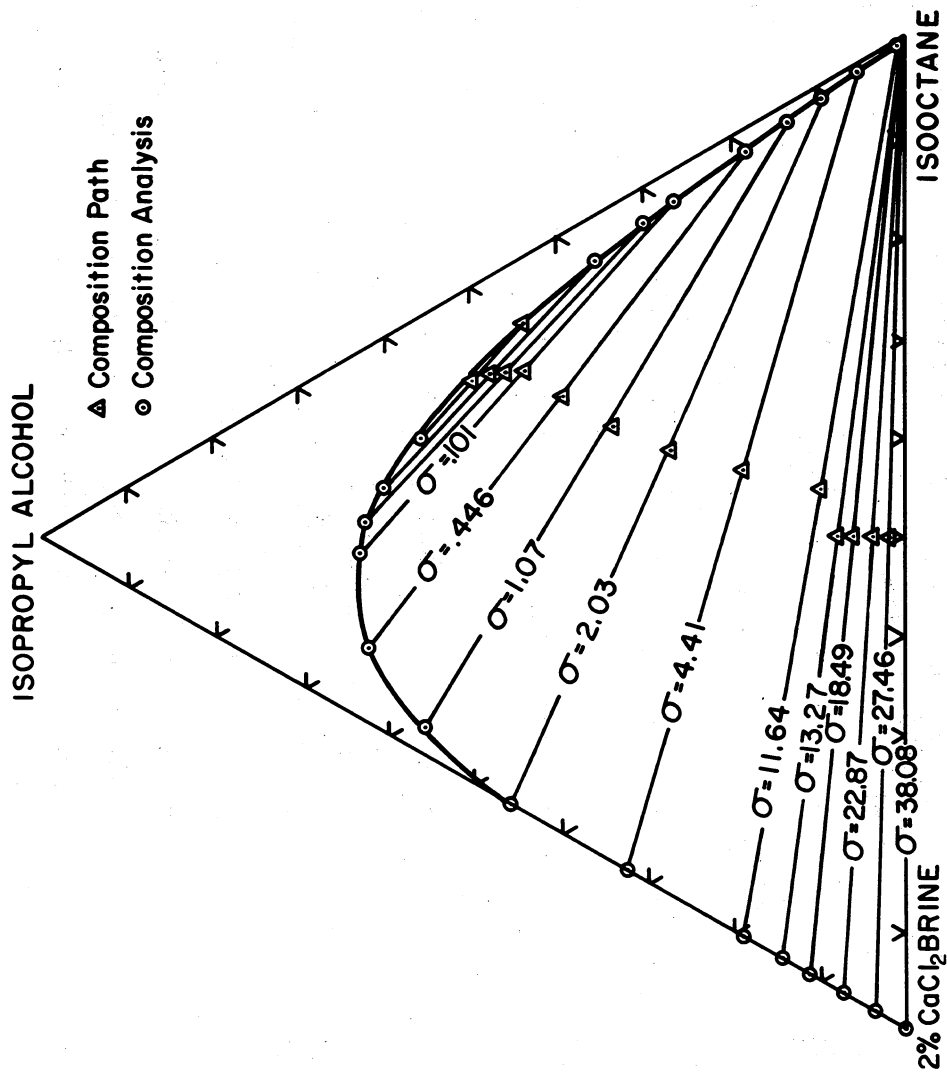


FIG. 1.1 Phase envelope and interfacial tensions for 2% CaCl<sub>2</sub> brine, iso-octane and isopropyl alcohol.



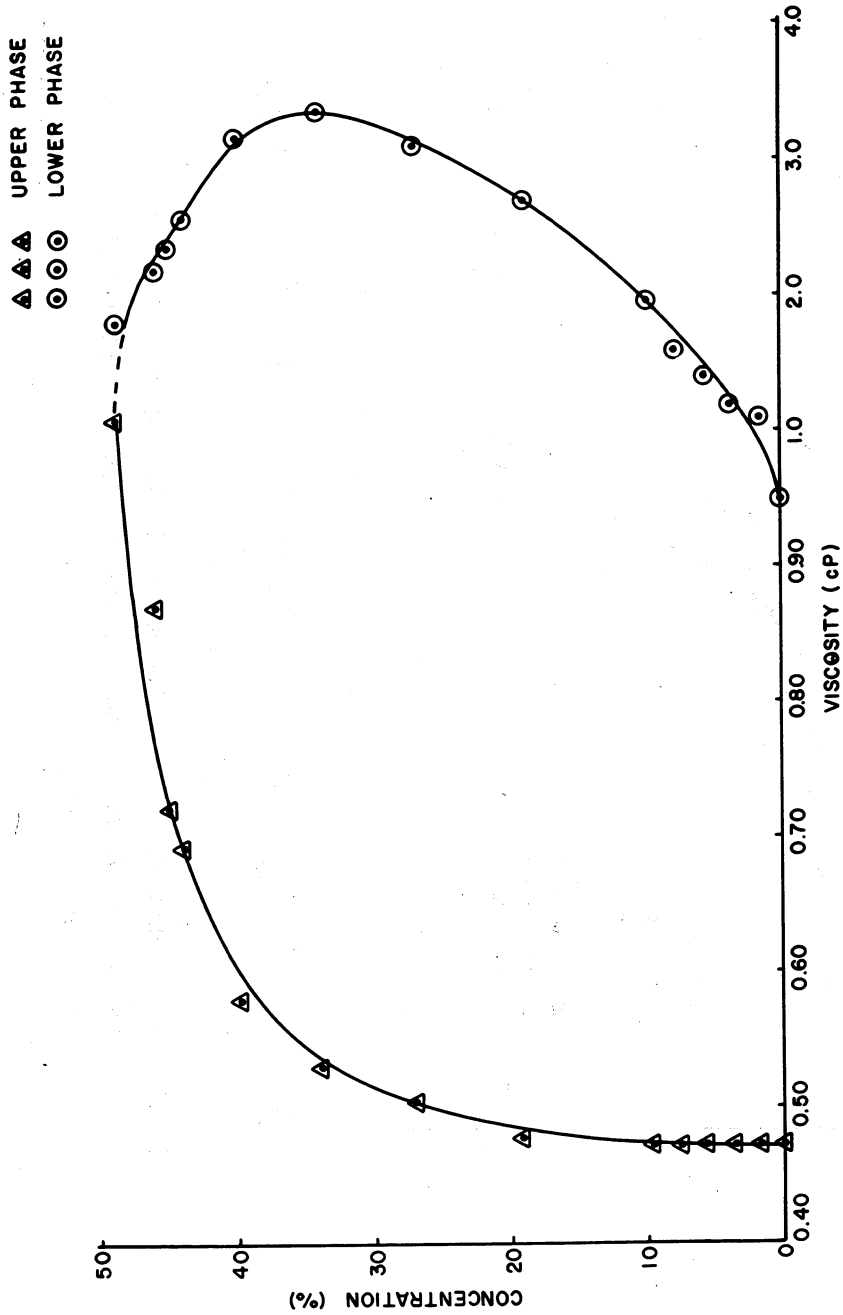


FIG. 1.3 Viscosities of liquid phases formed by 2% CaCl brine, isooctane and isopropyl alcohol for tie lines indicated by alcohol concentrations of composition path shown in figure 1.1

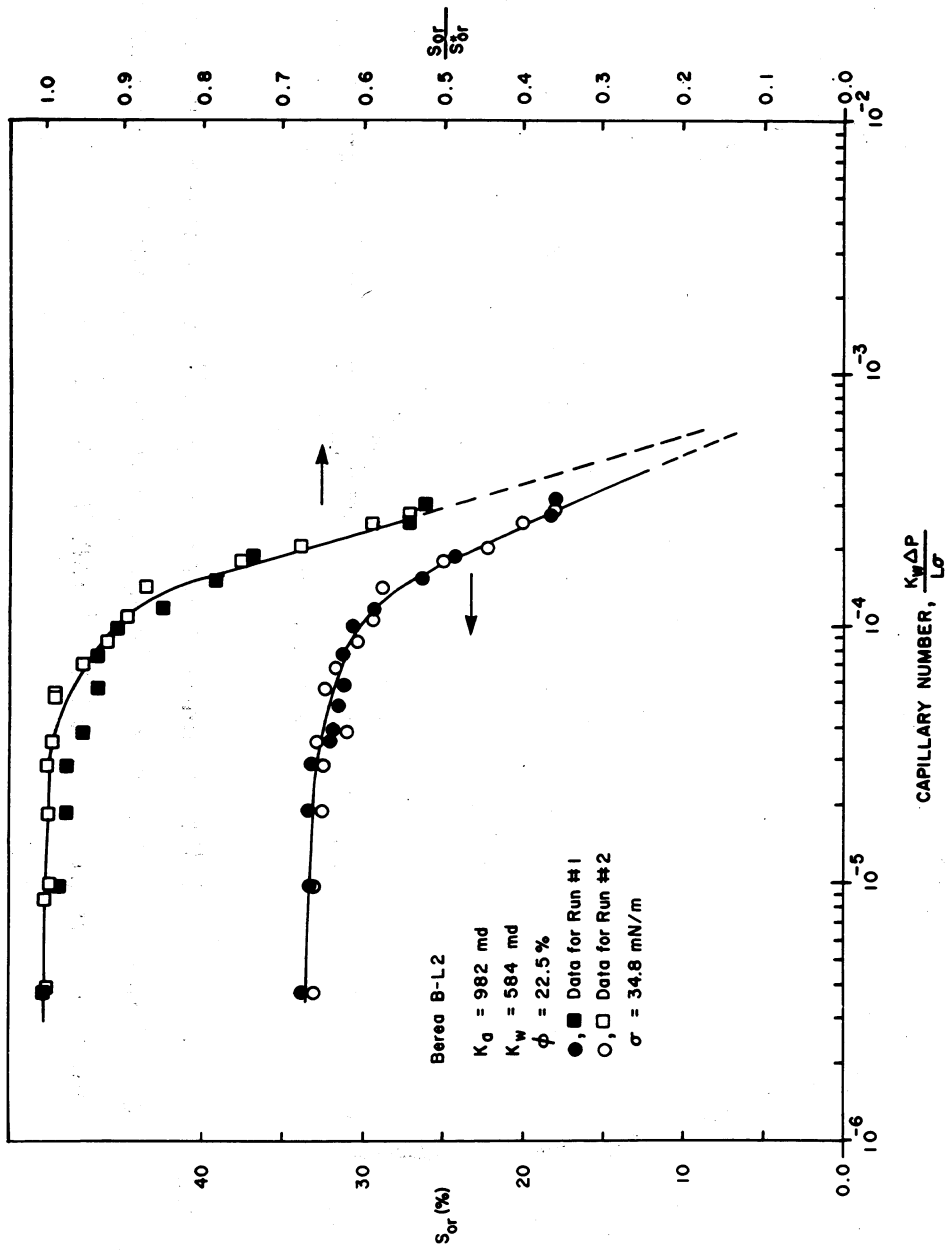


FIG. 1.4 Reproducibility of results when displacing discontinuous oil and capillary number curves for the Berea B-L2 sandstone sample.

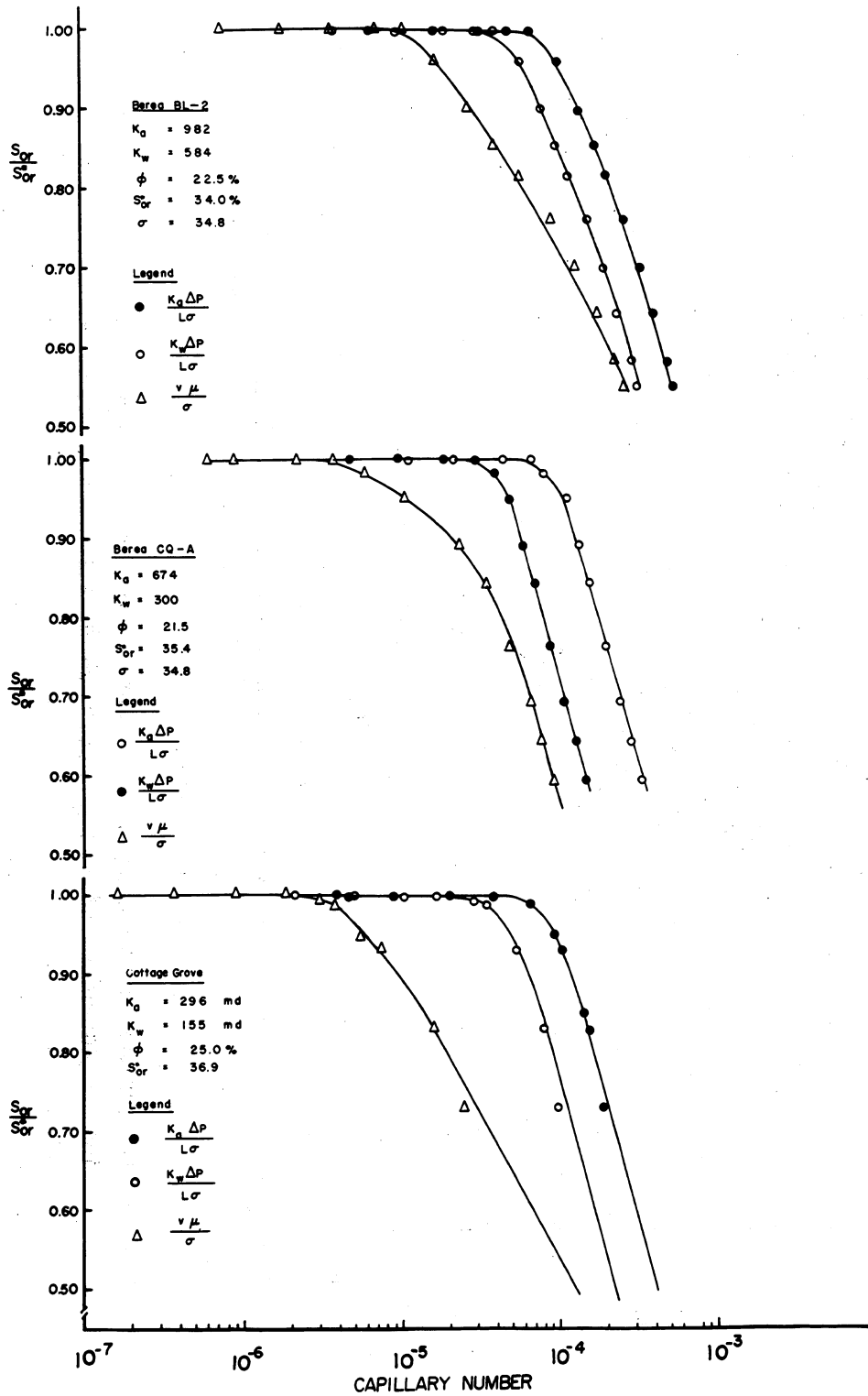


FIG 1.5 Plots of residual oil ratio versus various definitions of capillary number when displacing discontinuous oil from various samples.

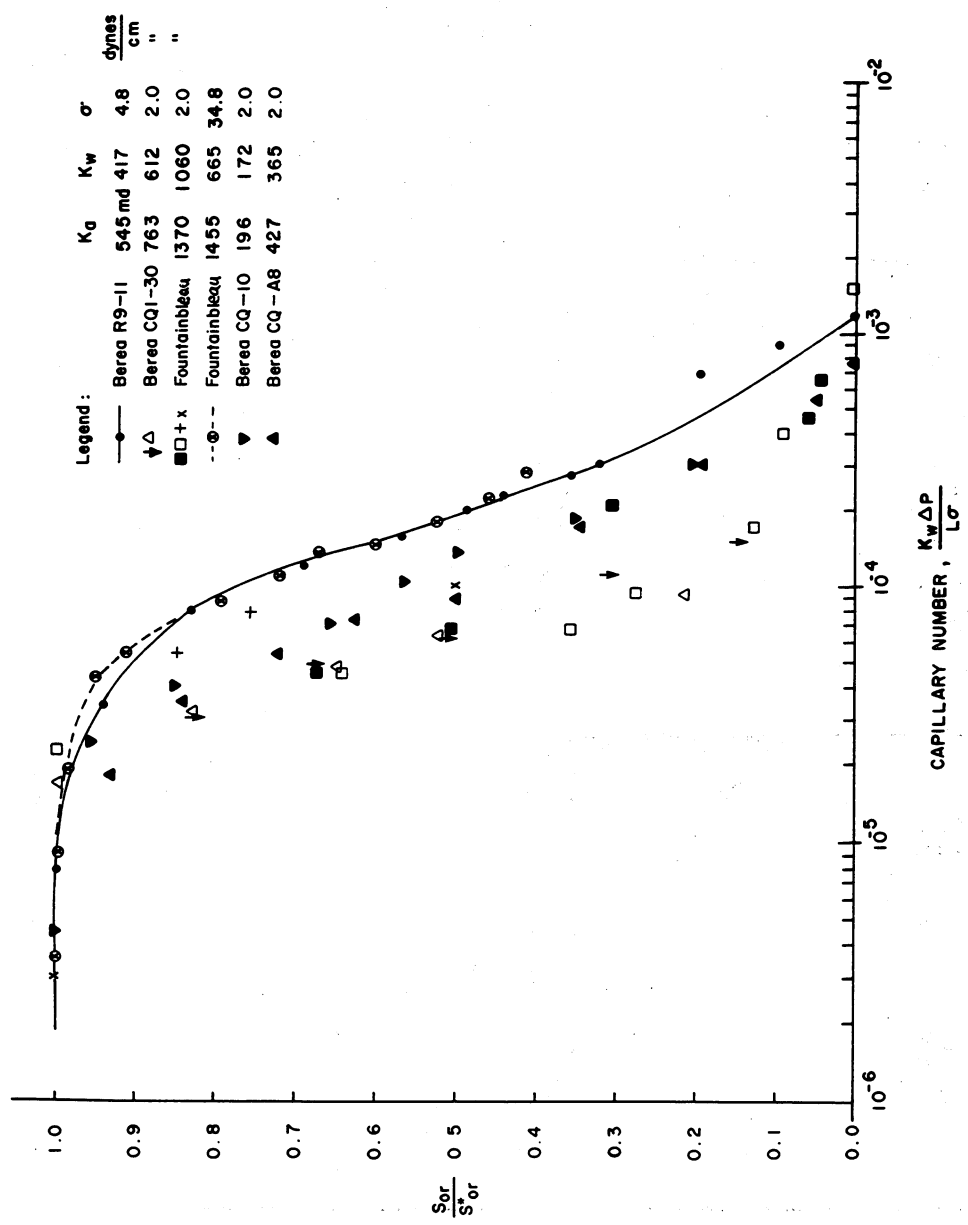


FIG. I.6 Comparison of capillary number curves of various sandstones for the displacement of discontinuous oil at various interfacial tension conditions.

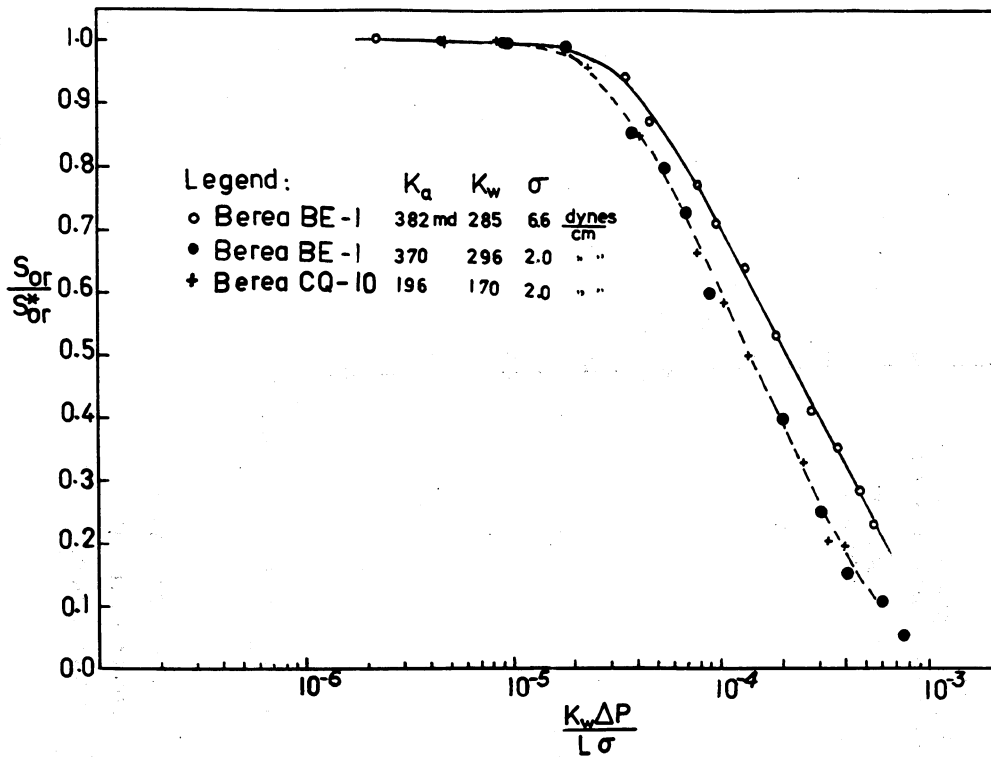


Fig.1.7 Effect of interfacial tension on the capillary number curve for the Berea BE-1 sample and comparison of results for two sandstone samples at interfacial tension of 2 dynes/cm.

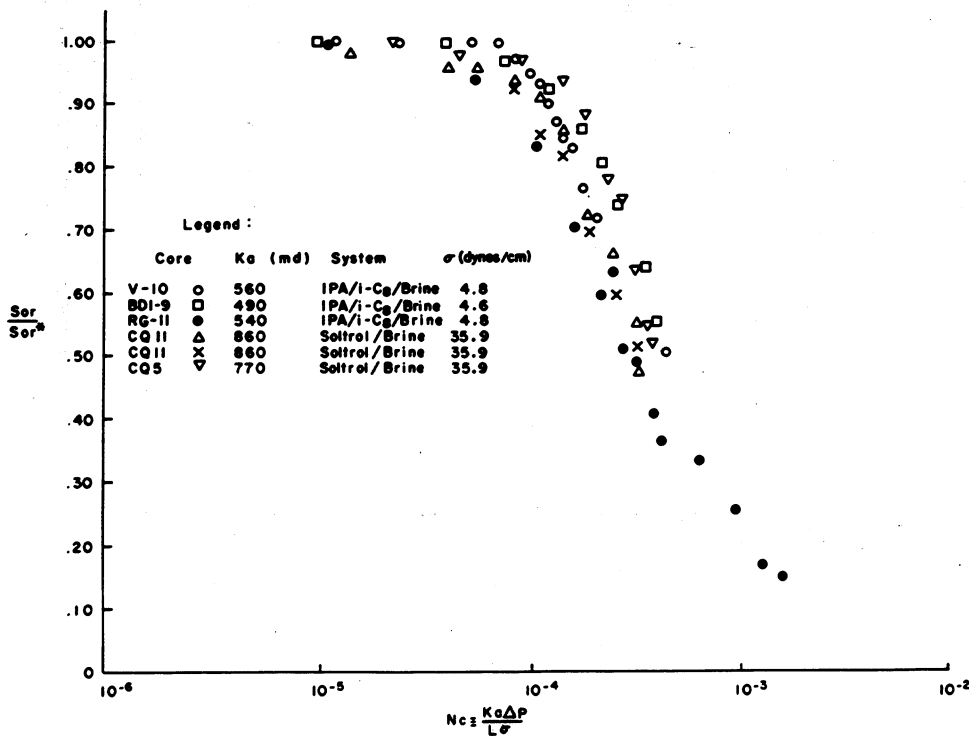


FIG. 1.8 Effect of interfacial tension on capillary number curve.

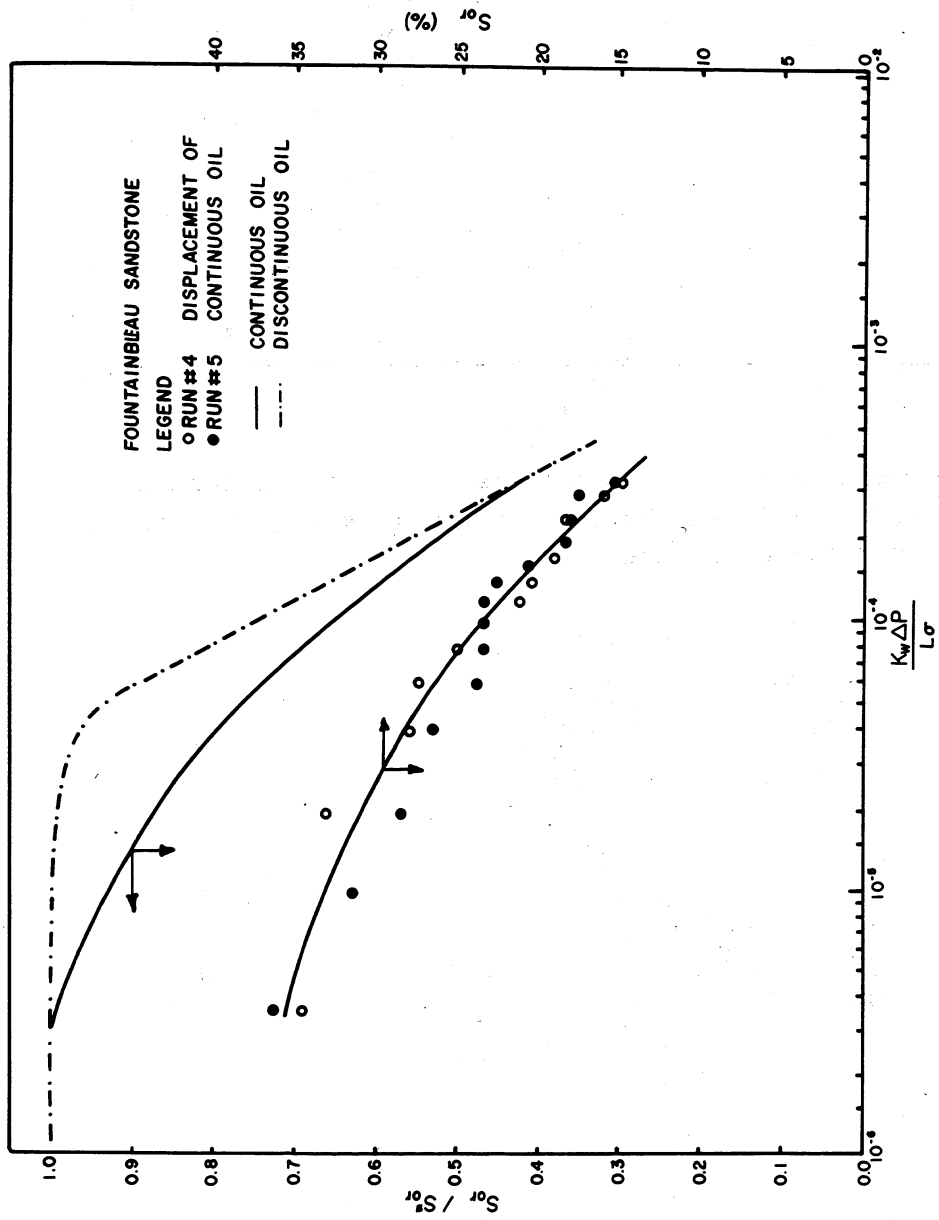


FIG. I.9 Reproducibility of results when displacing continuous oil and comparison of capillary number curves for displacement of discontinuous and continuous oil in Fountainbleau sandstone.

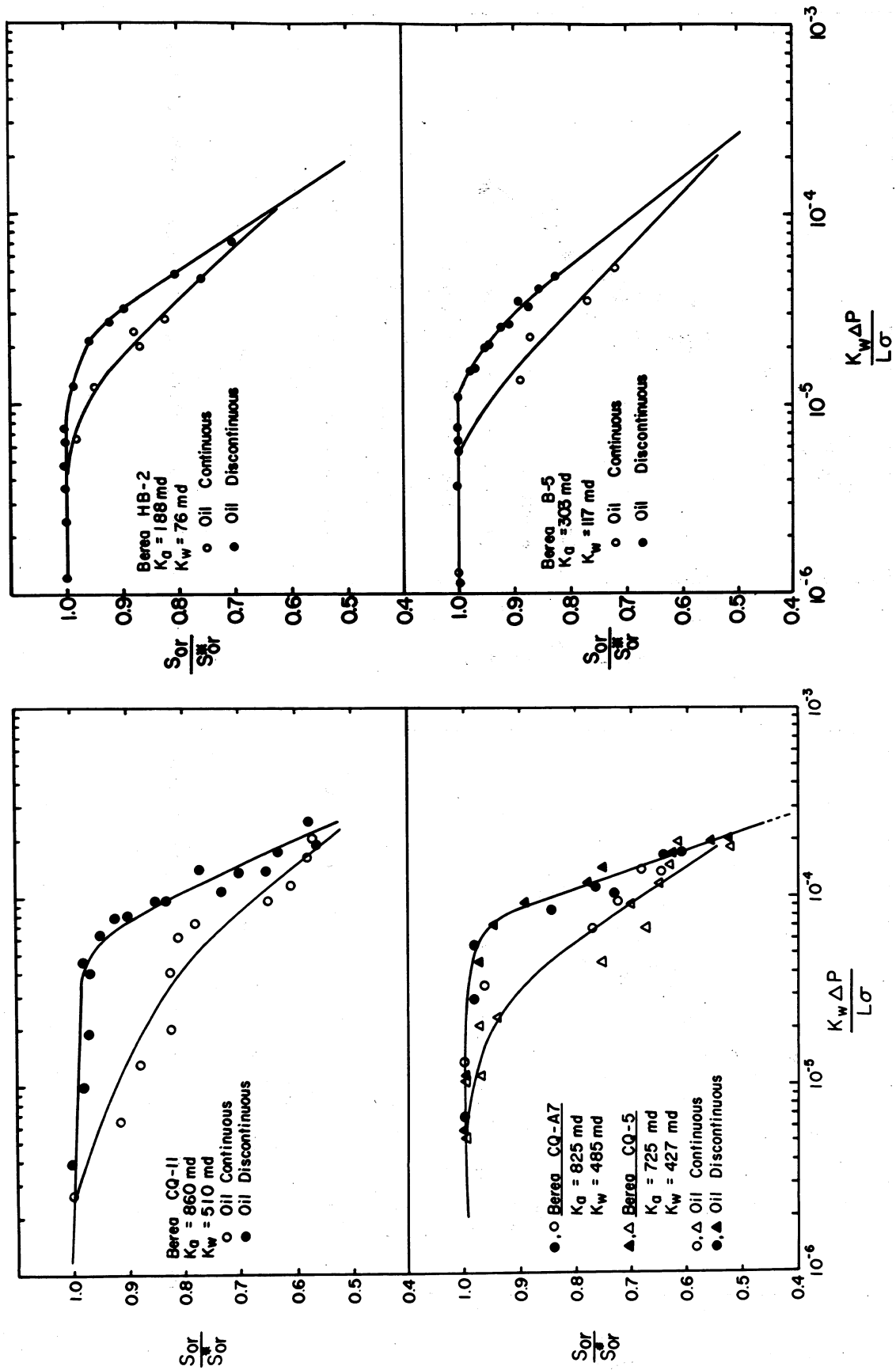


FIG. 110 Comparison of capillary number curves of various sandstones.

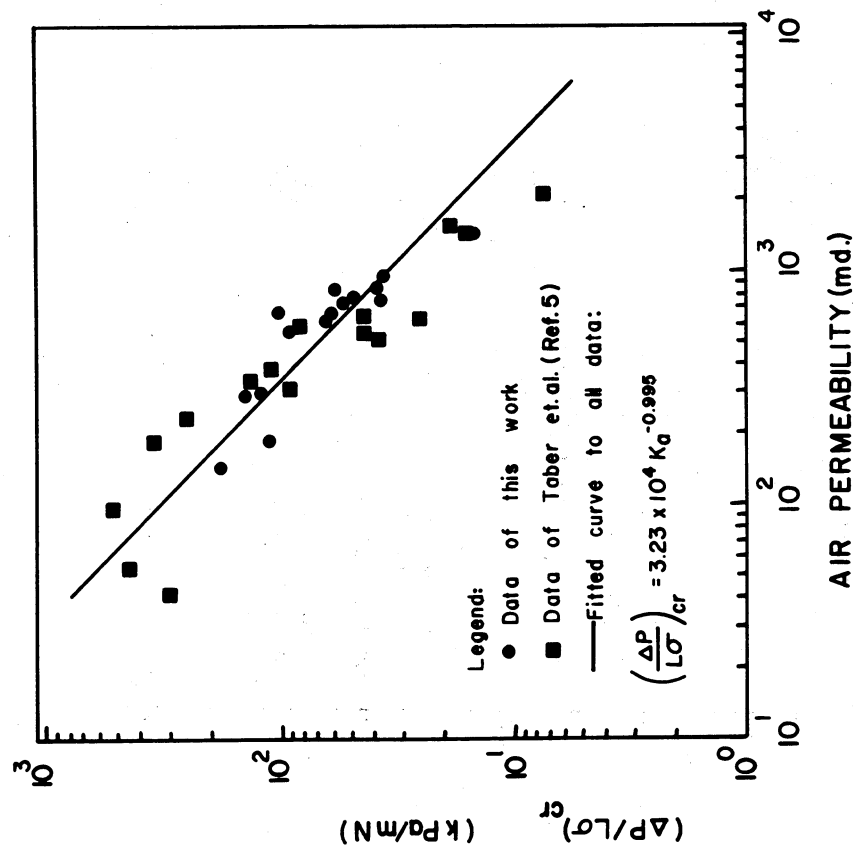
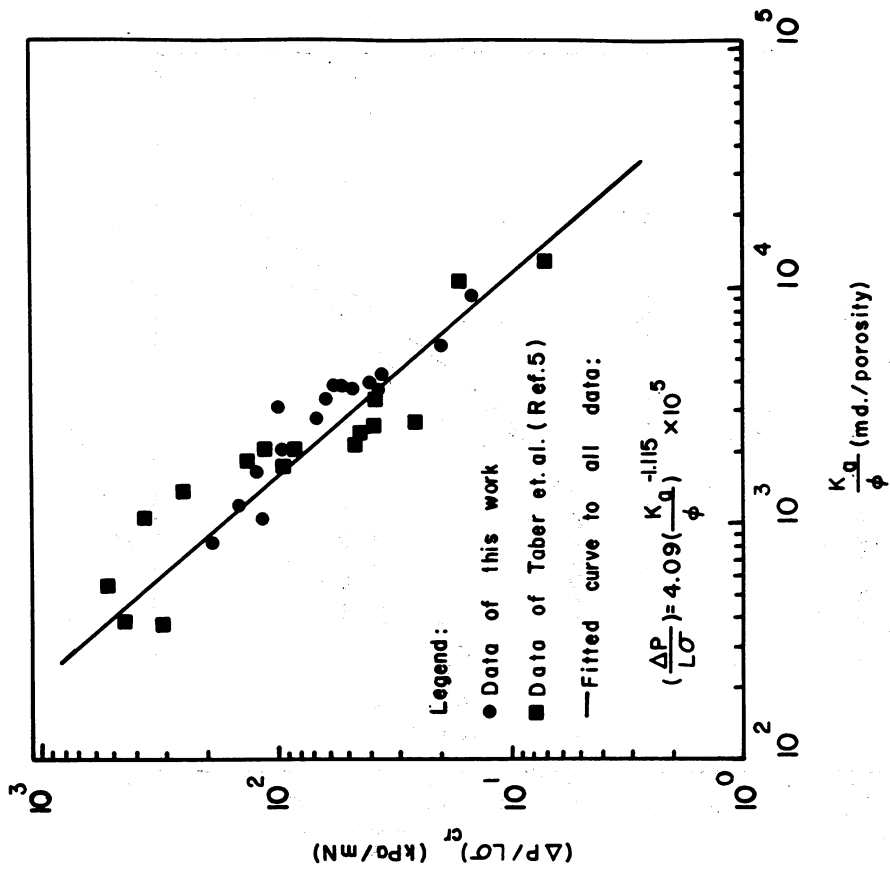


FIG. III Relationship between the critical displacement ratio and the parameters  $K_a$  and  $K_a/\phi$ , respectively.

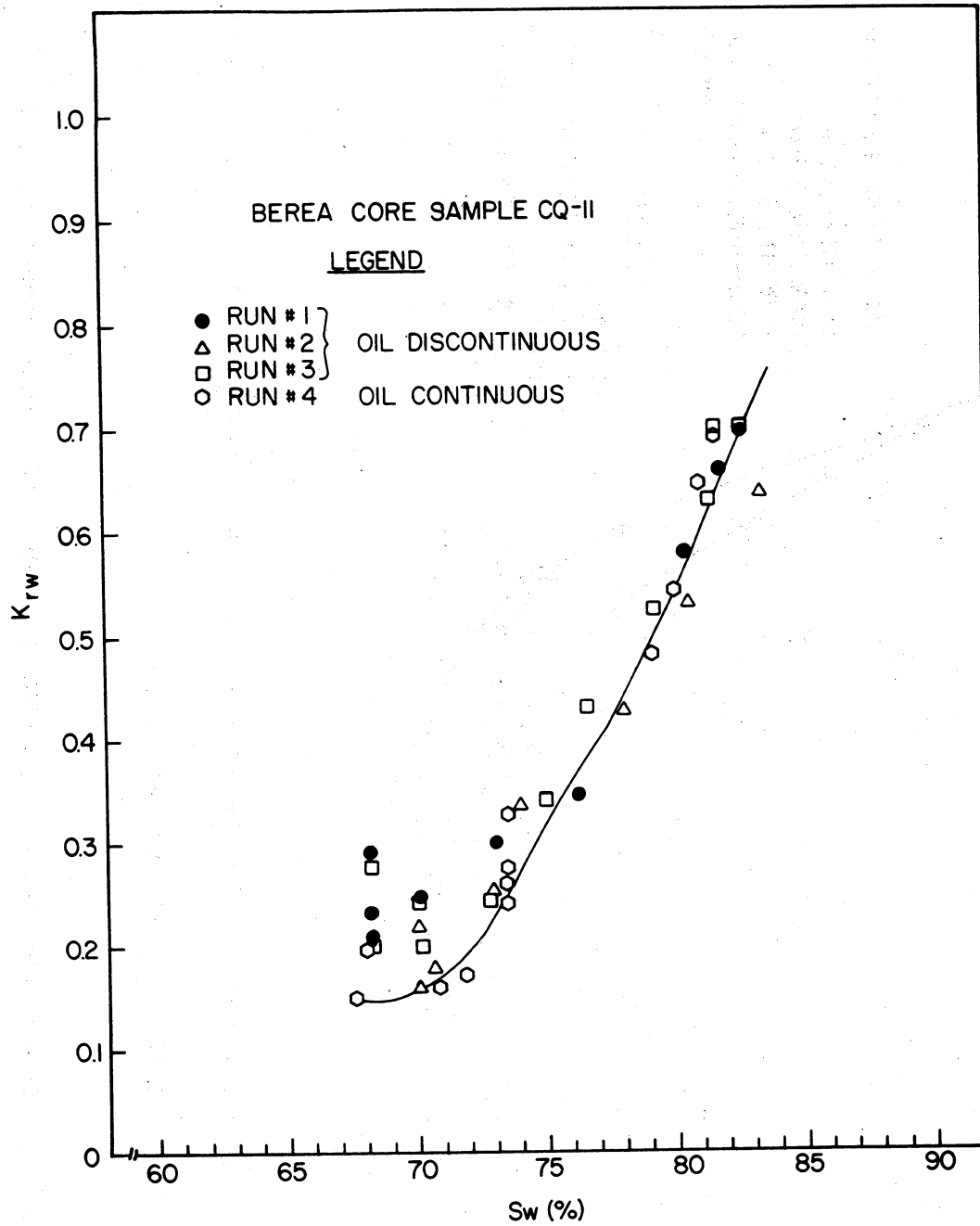


FIG. II.2 Relative permeabilities at reduced residual oil.

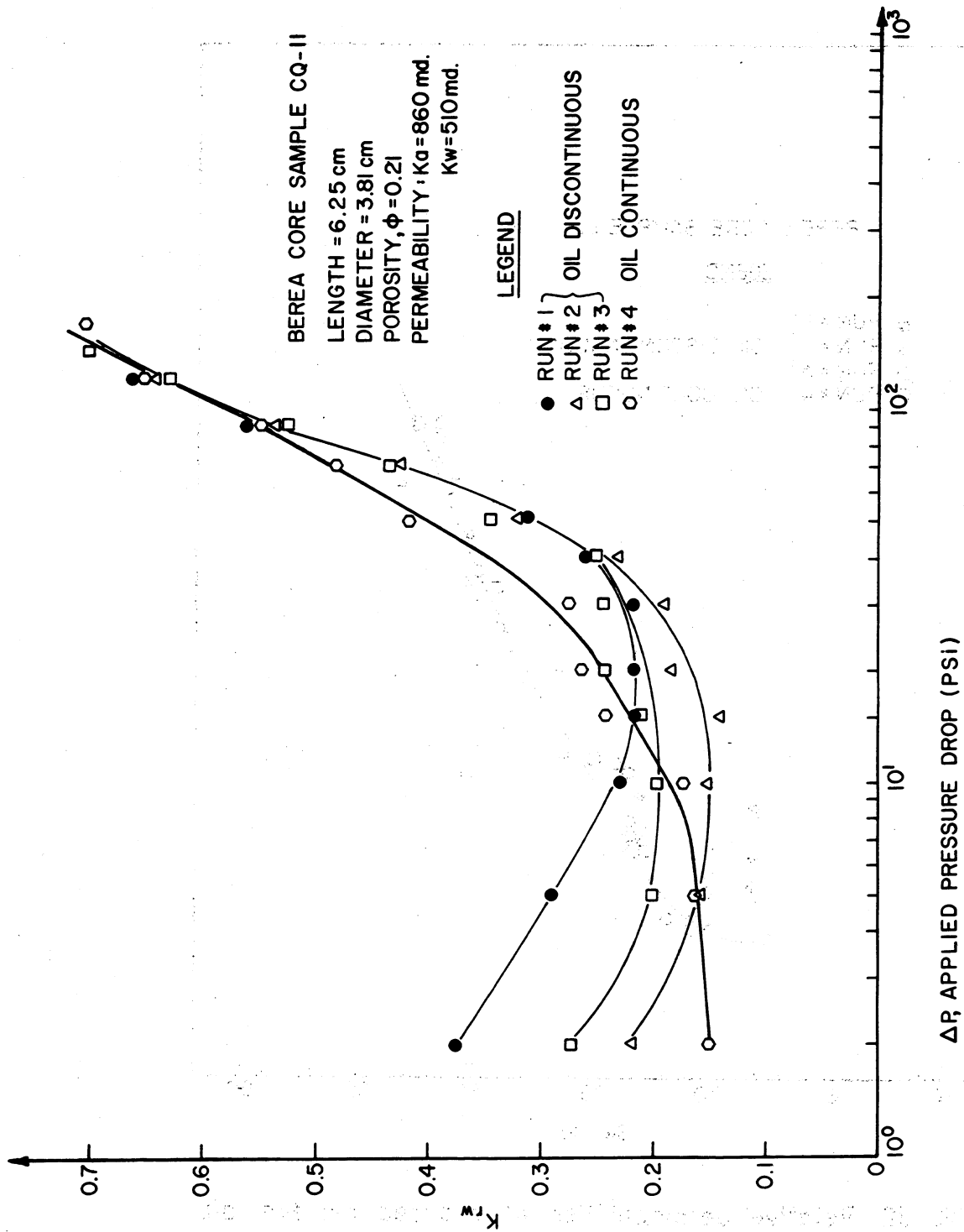


FIG. I.13 Relative permeability at reduced residual oil versus applied pressure drop.

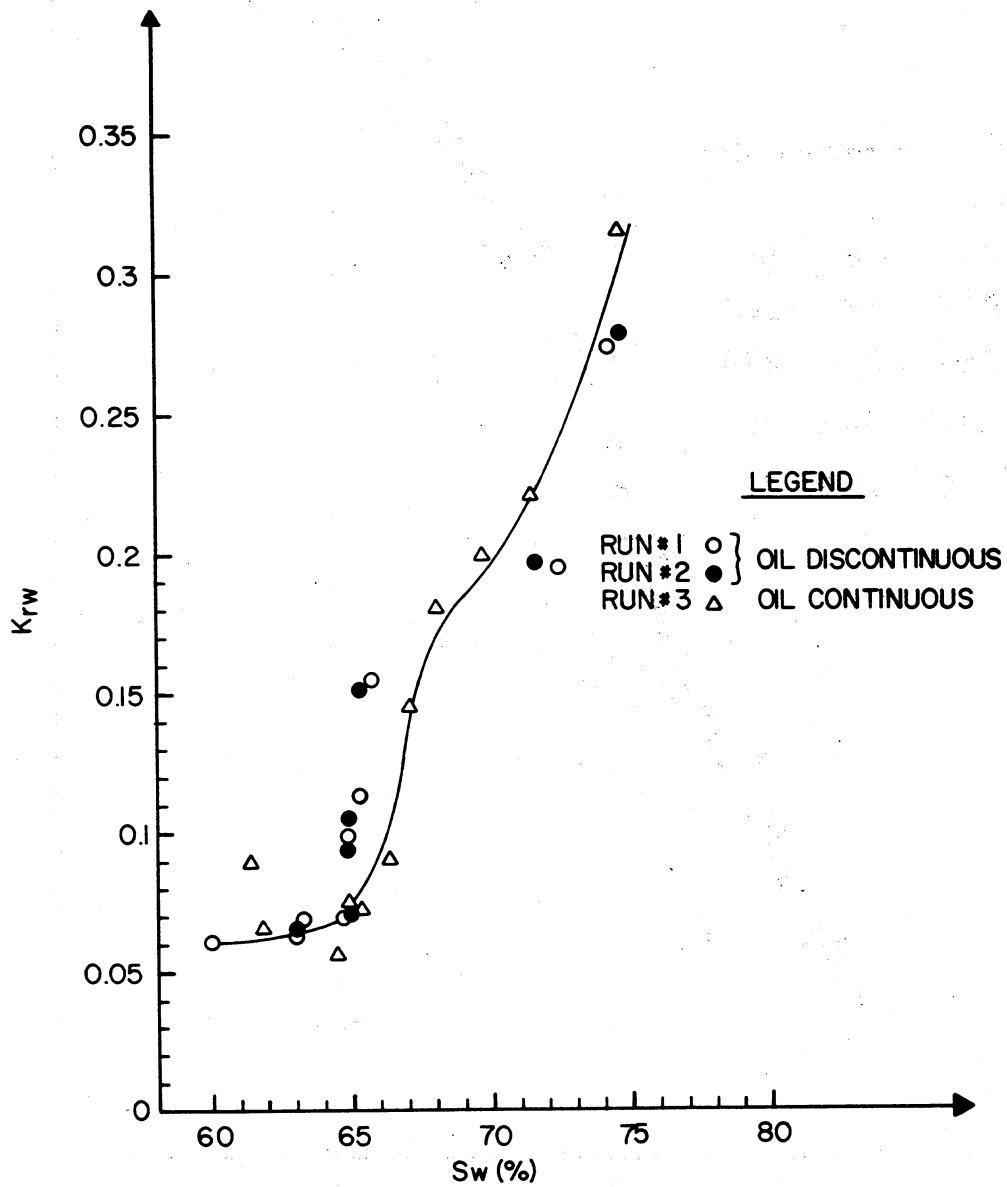


FIG. 1.14 Relative permeability characteristics at reduced residual oil saturation in a low permeability Berea core ( $K_w \approx 70-90$  md).

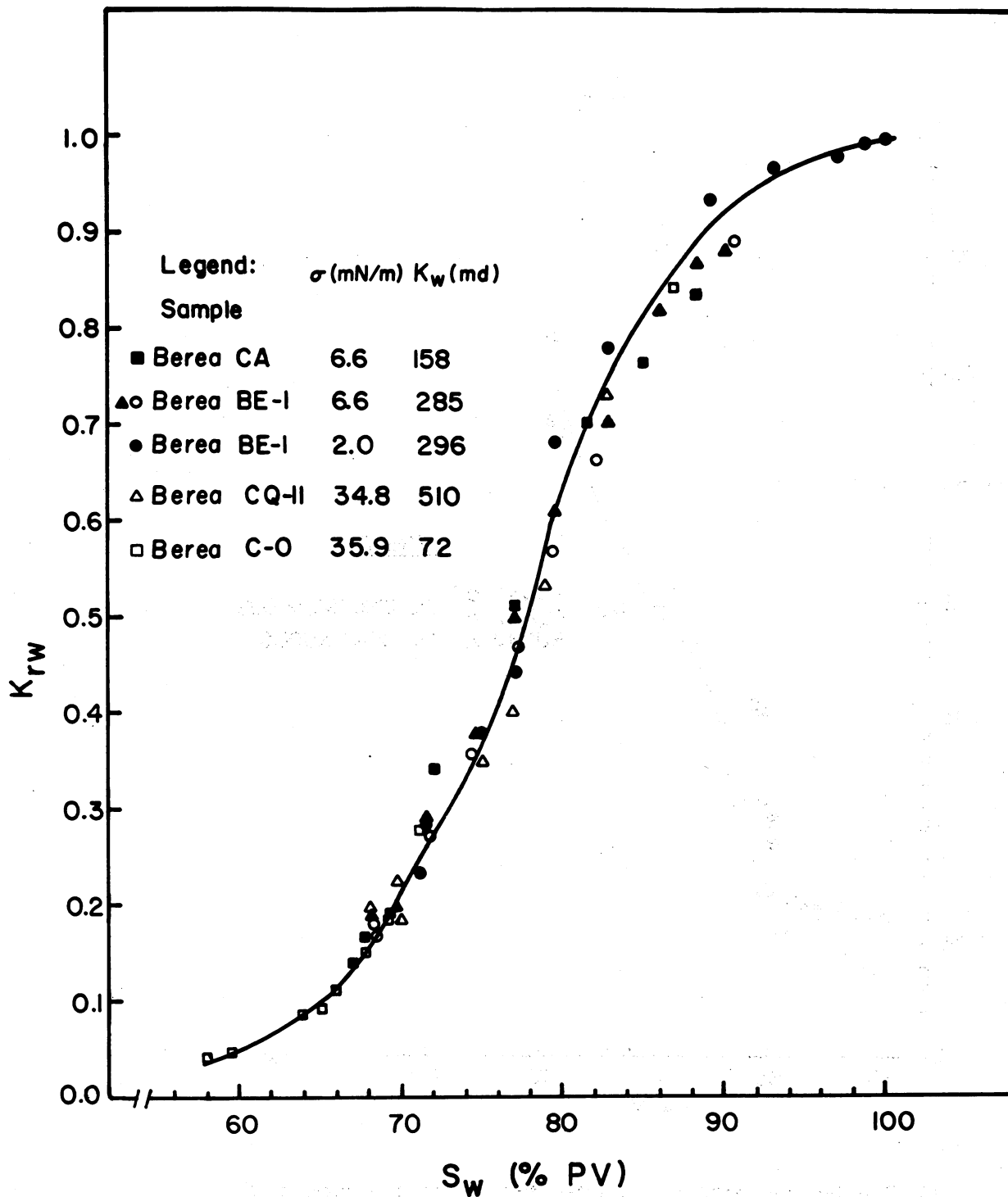


FIG. 1.15 Relative permeability at reduced residual oil saturation in Berea sandstone samples at various interfacial tensions.

## Task 2. Residual Oil Saturations Near the Wellbore

Objective: to provide a correction or residual oil saturation measured close to the wellbore for loss of oil caused by stripping.

### Background

Accurate values of residual oil saturation are essential for economic evaluation of any tertiary oil process. Methods of determining in situ residual oil saturations have been reviewed.<sup>2,1-2,3</sup> Currently, the industry is devoting much effort to in situ measurements of residual oil by specialized logging techniques such as pulsed neutron capture and nuclear magnetic logs. Most of these measurements involve a relatively small portion of the formation near the wellbore. This region will generally have been subjected to high pressure gradients which may be sufficient to cause significant reduction in the amount of residual oil retained close to the wellbore compared to that trapped in the swept zone as a whole. Similarly, when coring for residual oil, as when using a pressure retaining barrel, flushing caused by high local pressure gradients can result in retrieved cores having anomalously low residuals.

The conditions at which residual oil becomes displaced, and the extent to which residual saturations are reduced will depend in part on the individual formations. This point is illustrated by the variation observed in capillary number curves from one rock to another for similar (water-wet) wettability conditions.

It follows that logging or coring techniques, which involve the region close to the wellbore and do not allow for flushing, may provide a conservative estimate of the residual oil with respect to application of tertiary recovery methods or an optimistic value with respect to judging the success of a secondary waterflood operation. Increased accuracy in reserves determination may require that residual oil saturations be corrected for the effect of high pressure gradients around the wellbore which can arise during both drilling and production.

In wells drilled for the purpose of determining residual oil by coring and logging, the overbalance pressure (the pressure between the mud outside the drill bit and the pressure of the formation fluid) is a key variable.<sup>2,4</sup> Stosur and Taber investigated the conditions under which residual oil will be mobilized close to the wellbore.<sup>2,5</sup> This treatment is now extended to the problem of determining the distribution of oil around the wellbore when critical displacement conditions are exceeded and to estimating the effect of the given distribution on logging tool response.

### Theory of Mobilization

Consider a water-wet system which has been flooded to residual oil saturation. A modified form of Darcy's Equation for flow through a packing containing immobile residual oil is:

$$v = \frac{k_r K_w}{\mu} \frac{\Delta P}{\Delta L} \quad (2.1)$$

where  $v$  is the apparent fluid velocity

$K_w$  is the absolute permeability to brine

$k_{rw}$  is the relative permeability to water

$\mu$  is the fluid viscosity

$\frac{\Delta P}{\Delta L}$  is the pressure gradient

An expression for capillary number  $\frac{v\mu}{\sigma}$  is obtained from Equation (2.1) as follows:

$$\frac{v\mu}{\sigma} = \frac{k_{rw} K_w}{\sigma} \frac{\Delta P}{\Delta L} \quad (2.2)$$

where  $\sigma$  is the interfacial tension.

For geometrically similar porous media, conditions for blob mobilization are independent of any chosen characteristic microscopic length of the media.<sup>2,6</sup>

Larson, et al<sup>2,7</sup> have compared all available literature on capillary number relationships and shown that most results fall within a fairly well defined range. Results of the present study for various core samples (see Task 1) provide extensive confirmation of this observation. In the present study, capillary number curves for three cores, considered to be representative of a wide range of media have been selected. The cores, designated Berea B-L2, Berea CQ-A and Cottage Grove in Table 1.2 had air permeabilities of 982, 674 and 296 md respectively. Other properties are listed in Table 1.2.

### Calculation Procedure

In order to determine how stripping depends on the overbalance pressure, an indirect method of calculation was used. The reduction in residual oil saturation was expressed as a ratio,  $S_{rr}$ , of the saturation at the face of the wellbore  $S_{owb}$  to the residual oil obtained in the absence of flushing,  $S_{or}^*$ . Preliminary calculations indicated values in the range 0.8 to 1.0 as suitable choices of  $S_{rr}$  with respect to overbalance pressures likely to be encountered in practice. Having selected a value of  $S_{rr}$ , arbitrarily from within the range of importance, the capillary number curve for a given rock gives a corresponding velocity at the wellbore. It is clear from Equation (2.2) that comparison of  $\frac{v\mu}{\sigma}$  with  $\frac{k_w}{\sigma} \frac{\Delta P}{\Delta L}$  for a given reduction in residual provides a value of pressure gradient for a given core at the specified reduction in saturation. Note that this procedure automatically accounts for variation in relative permeability with residual oil saturation.

For constant flow rate, the velocity in the reservoir is inversely proportional to distance from the center of the wellbore. The capillary number curves can, therefore, be used to give the pressure gradient and relative oil saturation,  $S_{rr}$ , as functions of distance, as presented in Figures 2.1 and 2.2. In Figure 2.1, the graphs terminate at the critical

pressure gradient,<sup>2.5</sup> below which there should be no oil flushing. Beyond this point, the relative permeability to the water phase is constant and the curves can be extended as functions inversely proportional to distance. With this extension, the area under the pressure gradient curve between the wellbore,  $r_w = 4$  in, and a commonly selected radial distance,  $r_e = 2000 r_w$ , gives the overbalance pressure at the wellbore. Figure 2.3 shows relative wellbore-face saturation versus overbalance pressure for three permeabilities.

### Logging Tool Response

The manner in which the distribution of residual oil around the wellbore affects logging tool response will depend on the depth of investigation characteristics of the logging tool. Calculation of flushing factors for any given response function is fairly straightforward. For the purposes of a general treatment, some response function of the form  $1/r^n$  for an element in the formation at distance  $r$  from the center of the wellbore is an obvious choice. The response of an annular ring is then proportional to  $\frac{2\pi}{n-1} \cdot \frac{S_r}{r}$ . A correction factor, given by the ratio of the logging tool response in the absence of flushing to that which is obtained with flushing, can be written as:

$$F_f = \frac{2000 \int \frac{1}{r^{n-1}} dr}{\int \frac{S_r}{r^n} dr}$$

The methods of particular interest for measuring residual oil saturation are the pulsed neutron capture log which can operate in both open and cased holes, and the nuclear magnetic log which is strongly recommended for open hole measurements.<sup>2.2</sup> For the nuclear magnetic log,<sup>2.8</sup> a reasonable estimate of tool response is given by  $n=4$ . A plot of correction factor versus overbalance pressure for the core designated CQ-A is presented in Figure 2.4. The pulsed neutron capture log is favored for measurement of residual oil in cased holes. Factors which determine the tool response are more complicated,<sup>2.9, 2.10</sup> but setting  $n=2$  gives a reasonable approximation. The effect of tool response on correction factors for the PNC log as compared with the NML log is apparent from the estimates presented in Figure 2.4. Effect of change of permeability is shown in Figure 2.5 for tool response given by  $n=4$ .

## Dynamic Effects and Resistance of the Mud Cake

One approach to reduction of flushing is the use of low invasion muds.<sup>2.11</sup> In general, drilling mud filter cake will greatly reduce flow into the formation. However, as the drill bit cuts fresh rock face, there will be a local region, not yet protected by the mud cake, which will be subjected to maximum local pressure gradient. Furthermore, experimental studies<sup>2.4</sup> have shown that dynamic effects, such as described by Van Lingen,<sup>2.12</sup> around the drill bit, including the pressure gradient across the bit face at a given pressure gradient, can, in some cases, double the amount of residual oil stripping measured under linear flow conditions. Thus, even though the local pressure gradient in the formation is decreased as the mud filter cake builds up, the reductions in residual oil by flushing predicted from the foregoing calculations are probably underestimates. Comparison of reductions in residual oil in laboratory simulation of coring with flushing measured by linear displacement in similar core material indicates that the amount of flushing is unlikely to exceed that estimated by assuming an overbalance pressure which is double the actual value.

The presented calculations could be modified to allow for the restriction of flow away from the bit with build up of the mud cake. This would tend to reduce the pressure gradient in the region of the bit, but the effect would not be severe, and the modeling would be considerably more complicated and would involve a number of fairly arbitrary estimates as to conditions close to the working drill bit.

## New Applications

One possible approach to developing improved knowledge of local flushing effects is to carry out in situ measurements of changes caused by deliberate flushing. This might be especially useful in wells where records of injection pressures experienced by the well were incomplete or not available. It is assumed that the effect of mud cake can be avoided or allowed for. The results would be, in essence, in situ capillary number measurements which would indicate the relative ease of mobilization of residual oil. Such a procedure could be used as a minitest of a recovery process. Changes in the vertical distribution of residual oil would also indicate the amenability of the formation to enhanced recovery with respect to vertical sweep efficiency.

## Conclusions

- 1) Capillary number relationships can be used to relate pressure gradient around the wellbore and associated overbalance pressure to reduction in residual oil saturation.

2) Interfacial tension is a key scaling parameter in estimating flushing effects. Above a critical overbalance pressure, oil flushing will occur with its extent depending on formation characteristics and distance from the wellbore. Usually, stripping decreases with decrease in formation permeability.

3) Corrections to logging measurements for flushing of residual oil are strongly dependent on response characteristics of the logging tool; in particular, the nuclear magnetic log is considerably more sensitive to the effects of flushing around the wellbore than the pulsed neutron capture log.

4) Development of generalized correlations of flushing factor corrections will follow from development of improved correlations of capillary number characteristics and relative permeabilities at reduced residual saturations.

#### Acknowledgement

Computations were made by David Siegel and Hau Lim. Information on logging tool response was provided by Chuck Newmann of Chevron and R. N. Chandler and other members of Schlumberger.

#### References

- 2.1 Wyman, R. E., "How Should We Measure Residual Oil Saturation?" Bull. of Can. Pet. Geol., 25, 2 (May 1977) 233.
- 2.2 Residual Oil, Interstate Oil Compact Commission, Oklahoma City, 1978.
- 2.3 Martin, F. D., Morrow, N. R. and Moran, J., "A Survey of Methods for Estimating Waterflood Residual Oil Saturations," PRRC Report, New Mexico Institute of Mining and Technology (May 1979).
- 2.4 Jenks, L. H., Huppler, J. D., Morrow, N. R. and Salathiel, R. A., "Fluid Flow Within a Porous Medium Near a Diamond Core Bit," J. Can. Pet. Tech. 7, No. 4 (1968) 172.
- 2.5 Stosur, J. J. and Taber, J. J., "Critical Displacement Ratio and Its Effect on Wellbore Measurement of Residual Oil Saturation," J. Pet. Tech. 28, (Aug. 1976) 865.
- 2.6 Melrose, J. C. and Brandner, C. F., "Role of Capillary Forces in Determining Microscopic Displacement Efficiency for Oil Recovery by Water Flooding," J. Can. Pet. Tech. 13, (1974) 42.
- 2.7 Larson, R. G., Scriven, L. E. and Davis, H. T., "Displacement of Residual Nonwetting Phase from Porous Media," Chem. Eng. Sci. 36 (1981) 57-73.

- 2.8 Herrick, R. C., Couturie, S. H. and Best, D. L., "An Improved Nuclear Magnetism Logging System and Its Application to Formation Evaluation," SPE 8361, presented at the 54th Annual Fall Meeting of SPE of AIME, Las Vegas, Nevada, September 23-26, 1979.
- 2.9 Hopkinson, E. C., Youmans, A. H. and Johnson, R. B., Jr., "Depth of Investigation of the Neutron Lifetime Log," SPWLA 15th Annual Logging Symposium, June 2-5, 1974.
- 2.10 Antkiw, S., "Depth of Investigation of the Dual-Spacing Thermal Neutron Decay Time Logging Tool," SPWLA 17th Annual Logging Symposium, June 9-12, 1976.
- 2.11 Willmon, G. J., "A Study of Displacement Efficiency in the Redwater Field," J. Pet. Tech., April 1967, 449.
- 2.12 Van Lingen, N. H., "Bottom Scavenging-A Major Factor Governing Penetration Rates at Depth," J. Pet. Tech., Feb. 1962, 187.

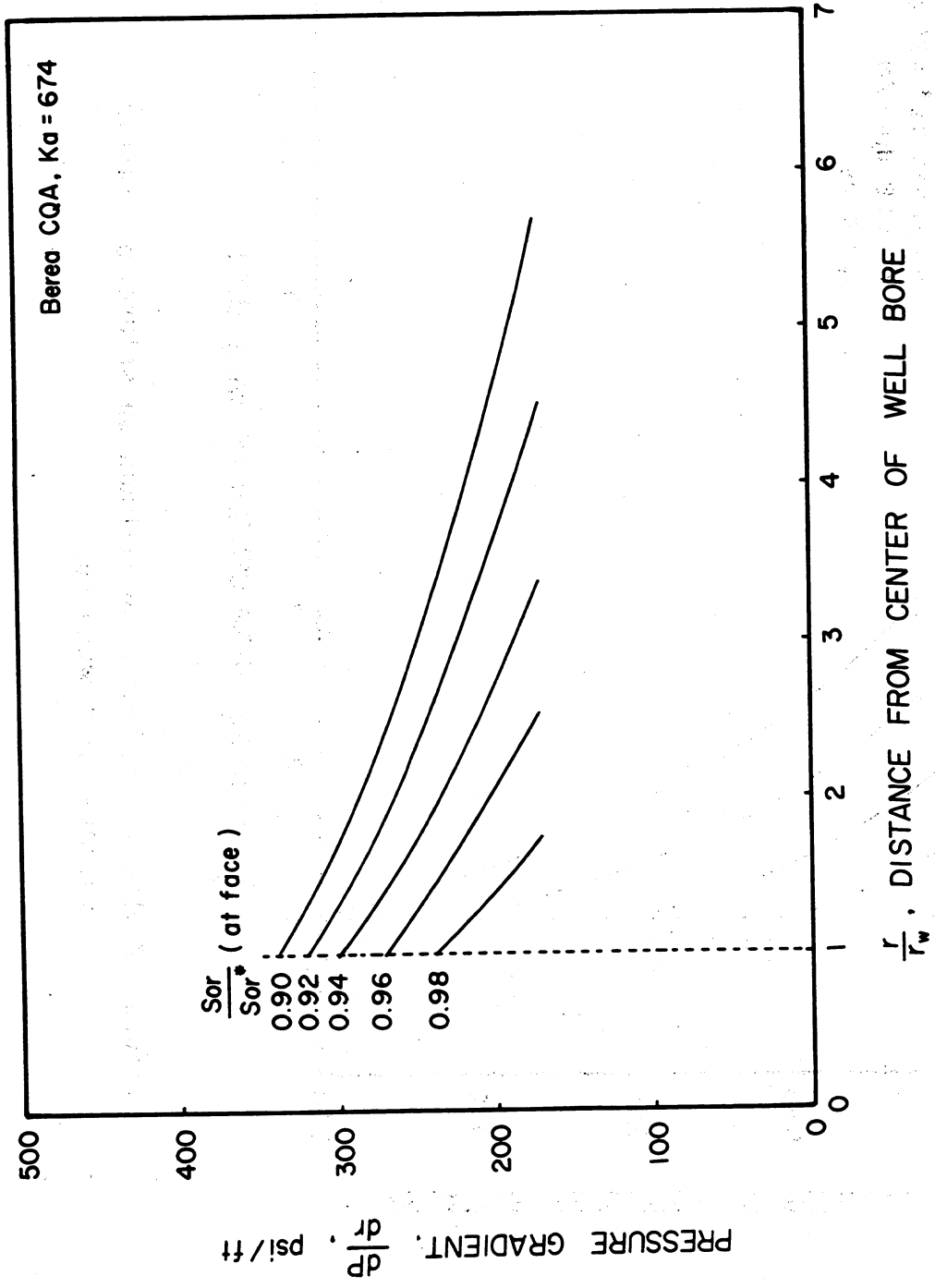


Figure 2.1 Pressure gradient versus distance with relative reduction in residual oil saturation at face of wellbore as parameter.

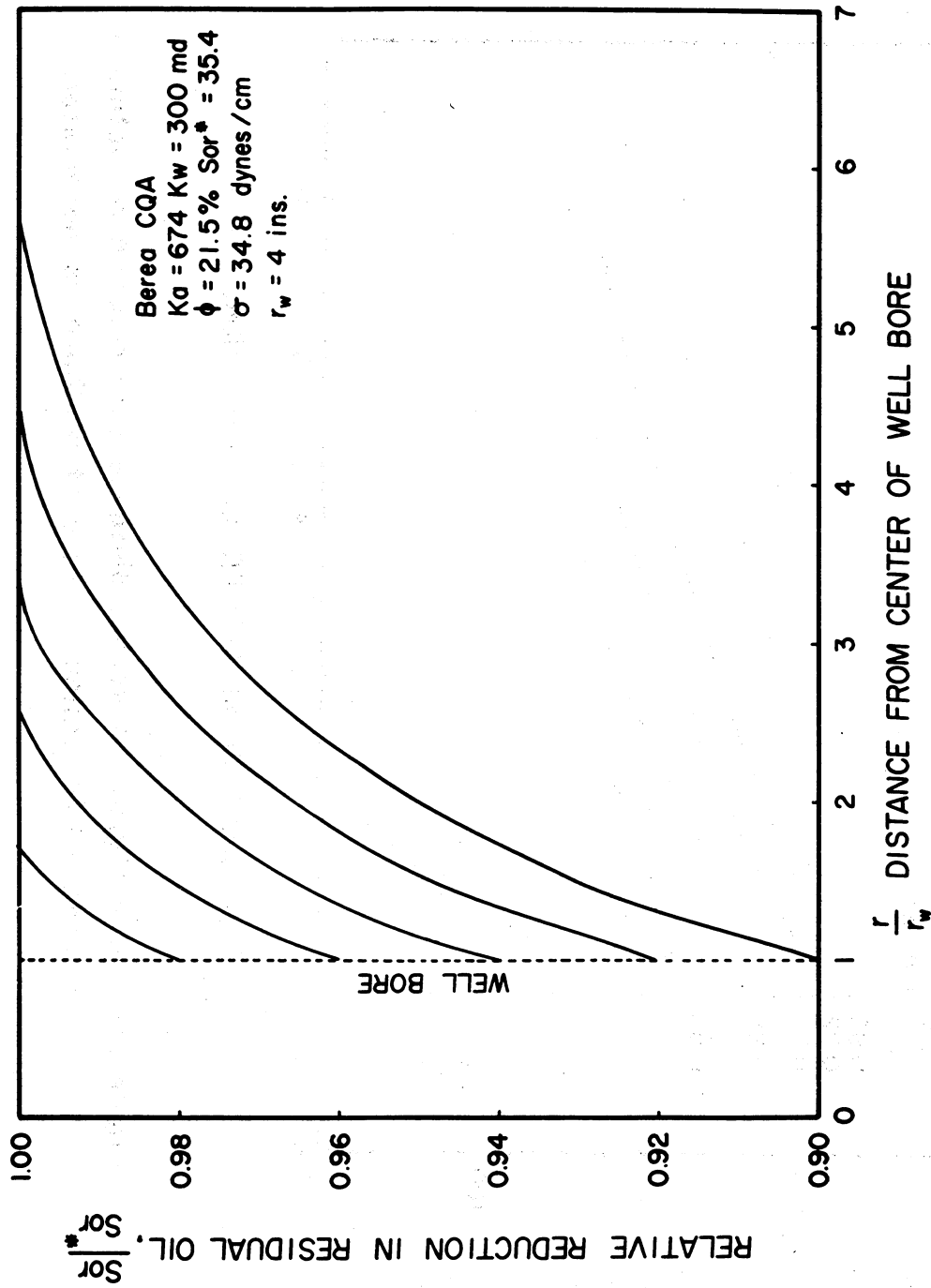


Figure 2.2 Relative reduction in residual oil saturation versus distance from wellbore.

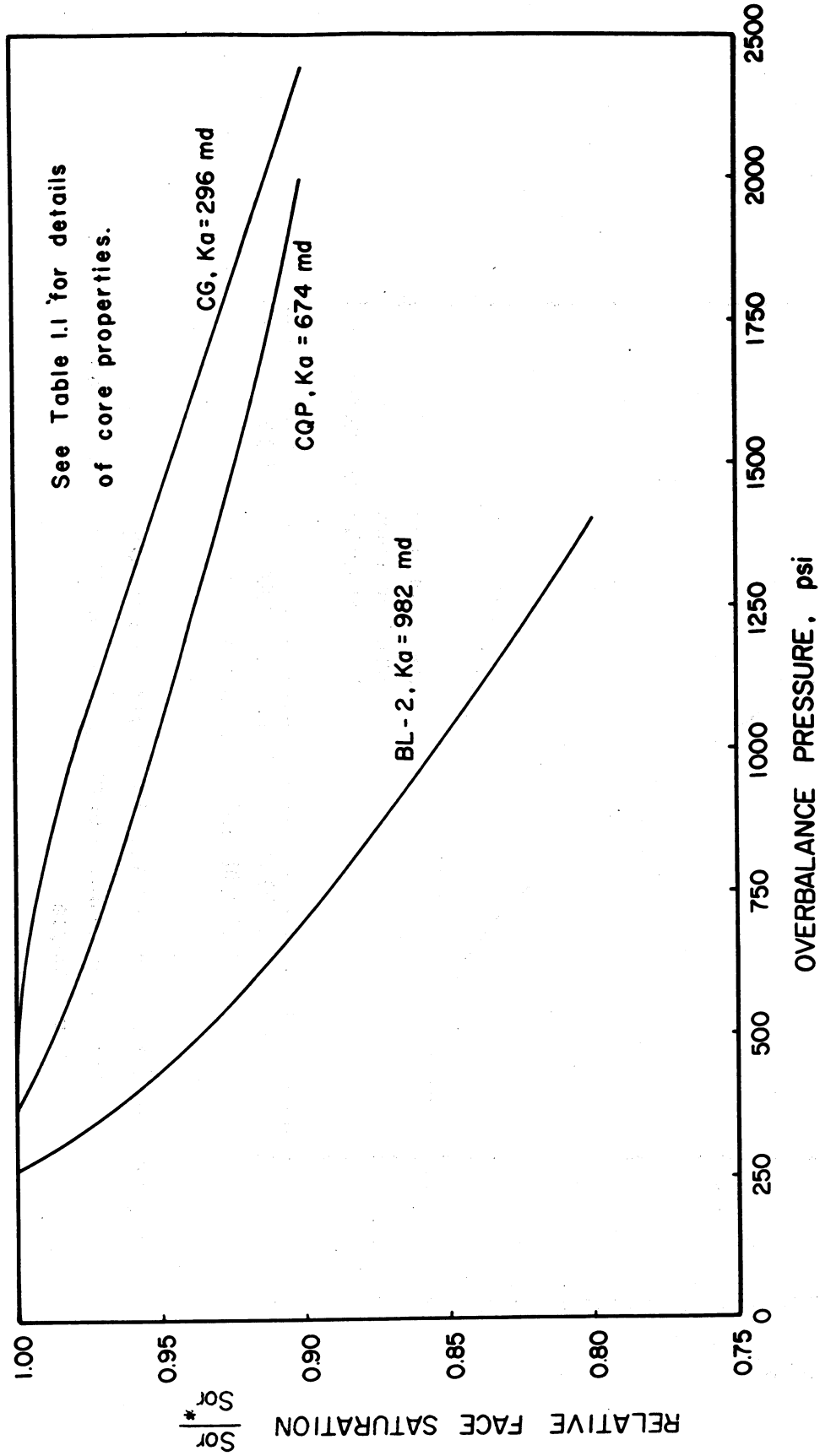


Figure 2.3 Relative saturation at face of wellbore versus overbalance pressure.

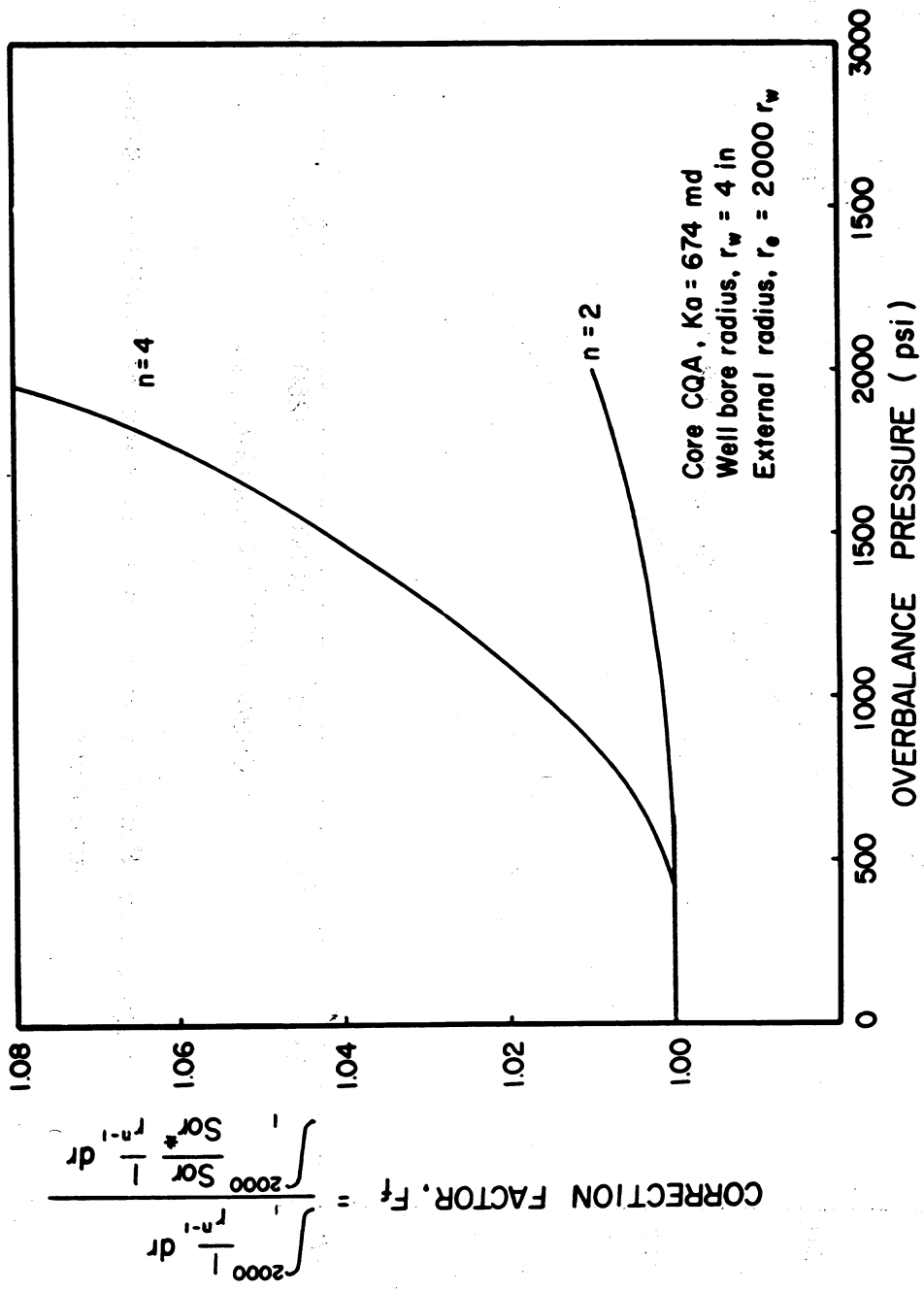


Figure 2.4 Correction factor for flushing for logging tool response proportional to  $\frac{1}{r^2}$  and  $\frac{1}{r^4}$  for 674 md core sample.

$$\text{CORRECTION FACTOR, } F_f = \frac{\int_{2000}^1 \frac{1}{r^{n-1}} dr}{\int_{2000}^1 \frac{1}{Sr^{n-1}} dr}$$

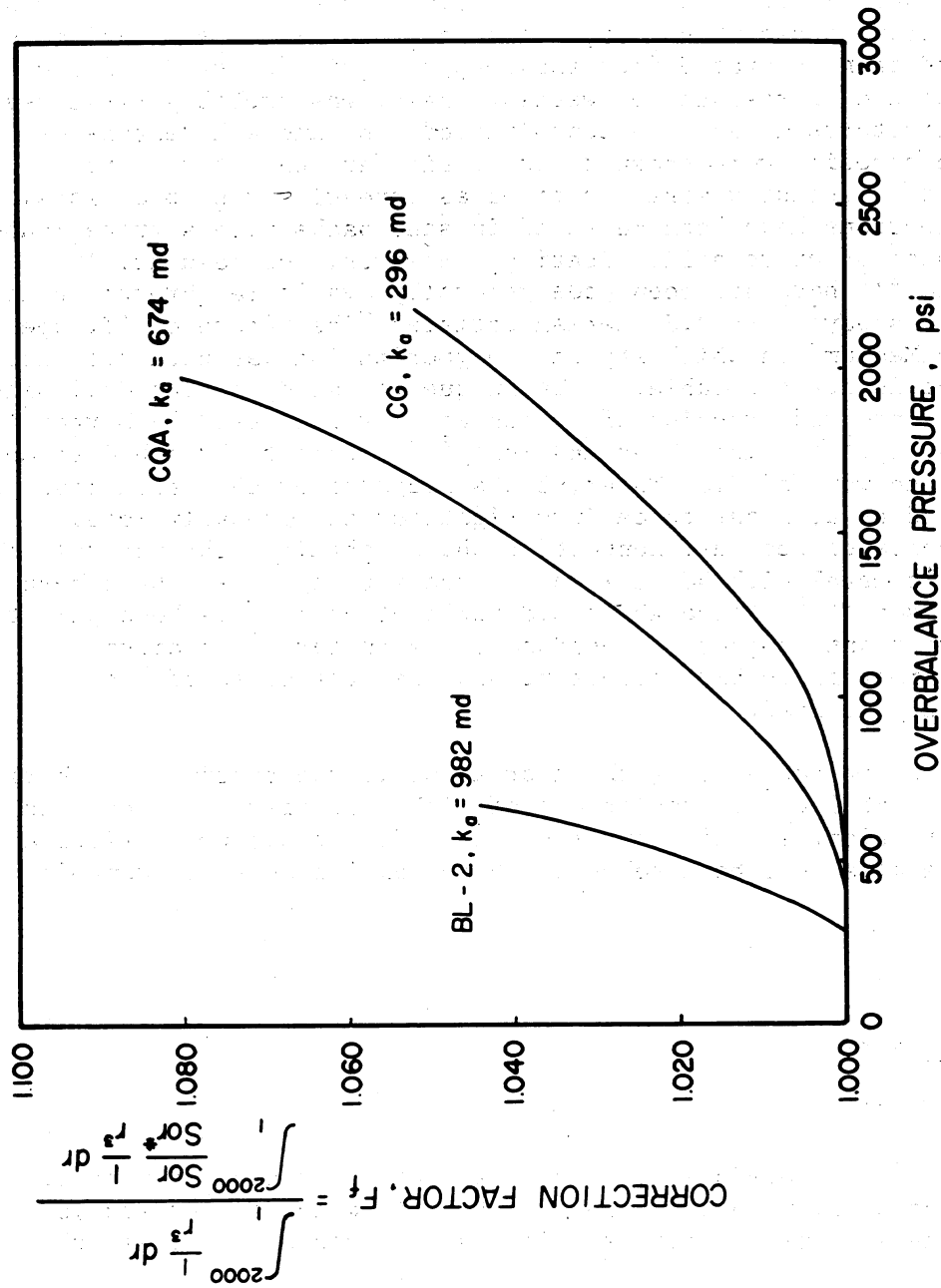


Figure 2.5 Correction factor for flushing for logging tool response proportional to  $\frac{1}{r^4}$  for core samples having air permeabilities of 296 md, 674 md, and 982 md.

### Task 3. Residual Oil Structure

Objective: to develop techniques for the study of the microscopic structure of residual oil and obtain statistics on how residual oil is distributed.

#### Background

In addition to the amount of residual oil, the microscopic distribution of residual oil within the pore spaces of a reservoir rock is also important to the mechanism of tertiary recovery. For example, in modeling the recovery of residual oil, the viscous force required for mobilization is expected to be inversely proportional to ganglia length.<sup>3.1-3.3</sup> The technique of using a nonwetting phase which after flooding to residual saturation, can be solidified and then separated from the porous matrix for study of the microscopic structure of residual nonwetting phase, was probably first used by Craze.<sup>3.4</sup> Structures given by unconsolidated sand and a limestone of intercrystalline porosity were shown to be of similar character. The isolated capillary structures were described as irregularly shaped blobs. Blob size distributions have been measured in sand packs with styrene monomer being the oil phase prior to solidification. However, the results,<sup>3.5</sup> although released,<sup>3.6</sup> have not been made generally available through publication. A previous study<sup>3.7</sup> by J.J. Herman entitled "The Nature of 'Trapped Oil' in a Porous Medium" in which styrene polymerization was used has also been cited<sup>3.5</sup> but is not available. A technique for study of residual oil structures which involved trapping of melted wax has been used by Morrow<sup>3.8</sup> and by R.A. Humphrey.<sup>3.9</sup> Since Reed and Healy<sup>3.9</sup> credit this method to much earlier unpublished work of J.J. Taber, blobs prepared by this technique have been examined by at least three investigations and probably more. Micrographs of casts of residual nonwetting phase, obtained through solidification of Wood's metal with hot toluene as the wetting phase, have been presented by Swanson.<sup>3.10</sup> Although considerable attention has been paid to the obviously important subject of residual oil structure, the amount of quantitative information on blob structure and the statistics of blob populations is very limited.

One of the recent needs for such information is the testing of theories of displacement which lead to predictions of blob size distributions. To obtain such information, satisfactory techniques for preparing statistically representative samples must be developed; these samples must be amenable to analysis.

#### Experimental Procedures

##### (a) Core flooding

The core flooding procedure used for the fluid pair styrene monomer-2% CaCl<sub>2</sub> brine was similar to that used for the oil-water system studied under Task 1. The styrene monomer, serving the purpose of the oleic phase,

contains 1% by weight catalyst so that the trapped styrene could be polymerized after waterflooding. Core samples were coated with epoxy resin before flooding in a modified Hassler type core holder having Teflon end plates. This design ensured that contact of styrene with rubber sleeves was avoided.

(b) Polymerization of trapped styrene monomer

After waterflooding, the core sample with trapped styrene is completely submerged in brine. Polymerization was affected by heating the sample in a temperature controlled oven at 65°C for about 40 hours. This time period had been found to be sufficient for the blobs to become rigid structures of sufficient mechanical strength for size analysis work. Subsequently, the sample with the polystyrene blobs is flooded with IPA and dried with air in order to determine the residual styrene that was actually polymerized.

(c) Leaching procedure for the recovery of polystyrene blobs

The core samples were continuously leached by flowing a 50:50 mixture of concentrated hydrofluoric acid (HF) and water at room temperature. After 8-12 hours of continuous leaching, the cores were reduced to a slurry that consisted of polystyrene blobs, partially dissolved sand, precipitates of HF and rock matter that does not react with HF. The slurry was subsequently filtered and washed with water. The solid matter (residue) was subjected to further leaching in sequence with the following acids: 1) concentrated sulfuric acid; 2) hydrochloric acid; 3) phosphoric acid; and, 4) aqua regia (3:1 mixture of concentrated hydrochloric acid and nitric acid, respectively). At the end of each of the above acid treatments, the contents in the beaker were filtered and washed with water. After these acid treatments, essentially all the rock matter has been leached and only the polystyrene blobs and a very small amount of residual inorganic material remain as solid. Finally, the filtered blobs were given a wash with methanol, dried and weighed. The weight of recovered blobs was used in determining the percent recovery of trapped oil as polymerized blobs.

### Experimental Results

Displacement experiments using the styrene-2% CaCl<sub>2</sub> brine fluid pair system and polymerization of the trapped styrene were performed in, 1) various Berea sandstone samples; 2) in unconsolidated glass beads; and, 3) in micromodels of capillary networks etched in glass. Electron micrographs of typical polystyrene blobs in Berea sandstone are shown in Figure 3.1.

Unpredictable wetting behavior of the styrene monomer in the presence of catalyst was a major difficulty in obtaining capillary structure size distributions of residual oil which were unquestionably characteristic of water-wet rock. For reasons unknown to us at the present, we have experienced the styrene monomer to behave 1) as a nonwetting phase indicative

from the well round-ended surfaces of the blobs (see Figure 3.1a); and 2) mainly intermediate or perhaps even oil-wet rocks as indicated by the shapes of blobs shown in Figure 3.1b.

Similar results have been obtained in glass beads and in glass micro-models with respect to the wetting behavior of the styrene monomer containing the Vazo type catalysts manufactured by DuPont Chemicals.

Recently, benzoyl peroxide (the use of which had been discontinued previously because times required for polymerization were relatively long) has been retested as an alternative for polymerization of styrene in glass beads and in capillary micromodels made of glass with special attention being paid to wetting behavior. The reproducibility of the wetting behavior towards water wetting has been found satisfactory in the micromodels, but the system had finite contact angles of about  $40^\circ$  and would probably be generally regarded as less than strongly water-wet. It now seems almost certain that the major cause of not being able to reproduce strongly water-wet behavior is the presence of catalyst in the styrene monomer. In displacement experiments carried out in micromodels using styrene monomer with no catalyst added to it, strong water wetting was observed. It is anticipated that using fresh styrene monomer without an inhibitor in it (styrene monomer without an inhibitor can be polymerized readily with heat alone), the major obstacle to reproducibility of wetting behavior will likely be overcome.

Measurements of blob size distribution have been made for a number of Berea sandstone samples. The blobs indicative of water wetting shown in Figure 3.1a were characterized using: a) the Coulter Counter technique, dependent mainly on particle volume; and b) the analysis of projected areas which involved use of a Quantimet image analyzer. Number-based and volume-based blob size distributions corresponding to low capillary number, obtained using the Coulter Counter are given in Figure 3.2a and Figure 3.2b respectively. The number based blob size distribution results for the same crop of blobs obtained with the Quantimet are shown in Figure 3.3. In comparing the number based blob size distributions obtained by the Coulter Counter and the Quantimet analysis, respectively, it was found that the minimum and maximum blob size measured are in good agreement; however, the blob size distributions vary considerably. Although this could be due to sampling methods or their artifacts, the difference, which is being further investigated, may well arise because principles of measurement for the two instruments are quite distinct.

The effect of capillary number on blob size distribution under water-wet and intermediate wet conditions is illustrated by the plots of Figures 3.3 and 3.4, respectively. As anticipated, the blob size distribution varies as one moves from low capillary number displacements to displacement conditions well above the critical capillary number. For the case of water-wet conditions and displacement of continuous oil from two Berea samples of similar properties, the blob size distribution was changed drastically when the capillary number was increased from  $2.5 \times 10^{-5}$  to  $1 \times 10^{-4}$ . As can be seen from Figure 3.3, the number fraction of blobs

with size greater than 100  $\mu\text{m}$  decreases from 58% by number at a capillary number of  $2.5 \times 10^{-5}$  to 18% for a capillary number of  $1 \times 10^{-4}$ . Taking into consideration pore structure data of Berea sandstone samples obtained by use of the method of thin sections (e.g., photomicrographic size distribution), the volume average pore diameter is about 50  $\mu\text{m}$  and the largest pore size in Berea sandstone is about 120  $\mu\text{m}$ .<sup>3,11</sup> The blob sizes of residual oil occurring in Berea sandstone under water-wet conditions at capillary number  $1 \times 10^{-4}$  are much greater than the actual size of individual pores, indicating that residual oil blobs occupying two or more adjacent pore bodies are still present under these conditions.

The blob size distribution results under intermediate wetting conditions shown in Figure 3.4 indicate similar qualitative behavior as those in Figure 3.3. However, the blob sizes encountered at intermediate wetting conditions were found to be much larger than the blobs obtained at the same capillary number but under water-wet conditions. This observation is in qualitative agreement with blob size distributions observed in micro-model studies.

### Conclusion

Because of the problems in reproduction of wetting behavior described above, and our limited experience in measurement of blob size distributions, the results presented in Figures 3.3 and 3.4 are considered preliminary. Future work will be aimed at confirming these results, and quantifying the effect of capillary number on blob size distributions under various wetting conditions. Work will also be extended to study trapping in some selected carbonate rocks.

### References

- 3.1 Melrose, J. C. and Brandner, C. F., "Role of Capillary Force in Determining Microscopic Displacement Efficiency for Oil Recovery by Water Flooding," J. Can. Pet. Tech. 13, 42 (1974).
- 3.2 Ng, K. M., Davis, H. T. and Scriven, L. E., "Visualization of Blob Mechanics in Flow Through Porous Media," Chem. Eng. Sci. 33, 1009 (1977).
- 3.3 Morrow, N. R., "Interplay of Capillary, Viscous and Buoyancy Forces in the Mobilization of Residual Oil," J. Can. Pet. Tech. 18, 35 (1979).
- 3.4 Craze, R. C., "Performance of Limestone Reservoirs," Trans. AIME 189, 287 (1950).

- 3.5 Robinson, R. L. and Haring, R. E., "Experimental Study of Residual Oil Configuration in Unconsolidated Sand," Jersey Production Research Company Report, Production Div., Jan. 1962.
- 3.6 Larson, R. G., David, H. T. and Scriven, L. E., "Displacement of Residual Nonwetting Fluid from Porous Media," Chem. Eng. Sci., In Press.
- 3.7 Herman, J. J., "The Nature of 'Trapped Oil' in a Porous Medium," B.S. Thesis, MIT, May 26, 1958.
- 3.8 Morrow, N. R., "Residual Oil," Petroleum Recovery Institute Progress Report, 40, May 1976.
- 3.9 Reed, R. L. and Healy, R. N., "Some Physicochemical Aspects of Micro-emulsion Flooding-A Review," in Improved Oil Recovery by Surfactant Flooding, Ed. Shah and Schechter, Academic Press, 386, New York (1977).
- 3.10 Swanson, B. F., "Visualizing Pores and Nonwetting Phase in Porous Rock," SPE 6857, presented at SPE 52nd Annual Meeting of SPE of AIME, Denver, October 9-12, 1977.
- 3.11 Dullien, F. A. L. and Dhawan, G. K., "Characterization of Pore Structure by a Combination of Quantitative Photomicrography and Mercury Porosimetry," J. Coll. Int. Sci. 47, 337 (1974).



100  $\mu\text{m}$



100  $\mu\text{m}$

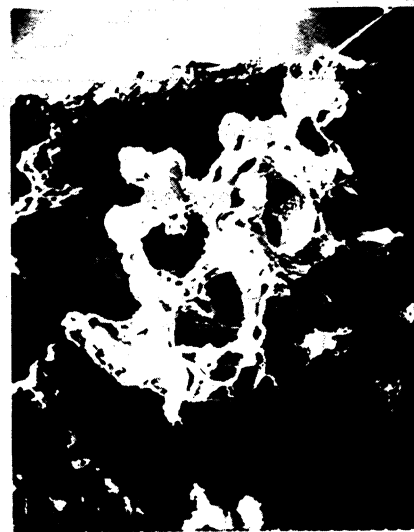


100  $\mu\text{m}$

(a) TRAPPED UNDER WATER - WET CONDITIONS



200  $\mu\text{m}$



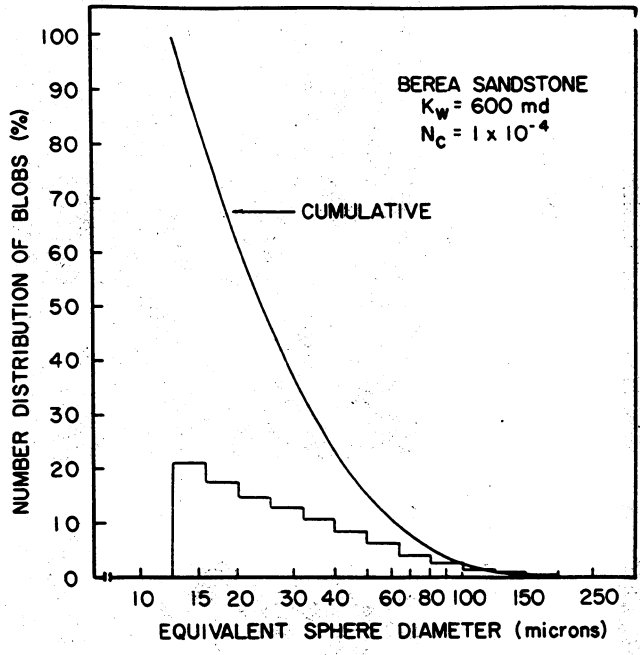
200  $\mu\text{m}$



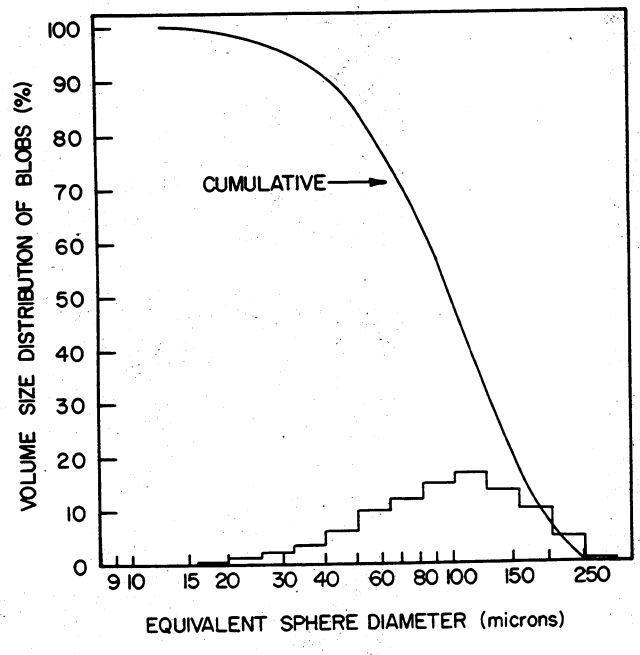
200  $\mu\text{m}$

(b) TRAPPED UNDER INTERMEDIATE WETTING CONDITIONS

Fig 3.1 OIL BLOBS TRAPPED IN BEREA SANDSTONE



(a) number size distribution



(b) volume size distribution

Figure 3.2 Size distributions of oil blobs trapped in Berea sandstone ( $K_w = 600 \text{ md}$ ) under water-wet conditions at  $N_c = 1 \times 10^{-4}$ .

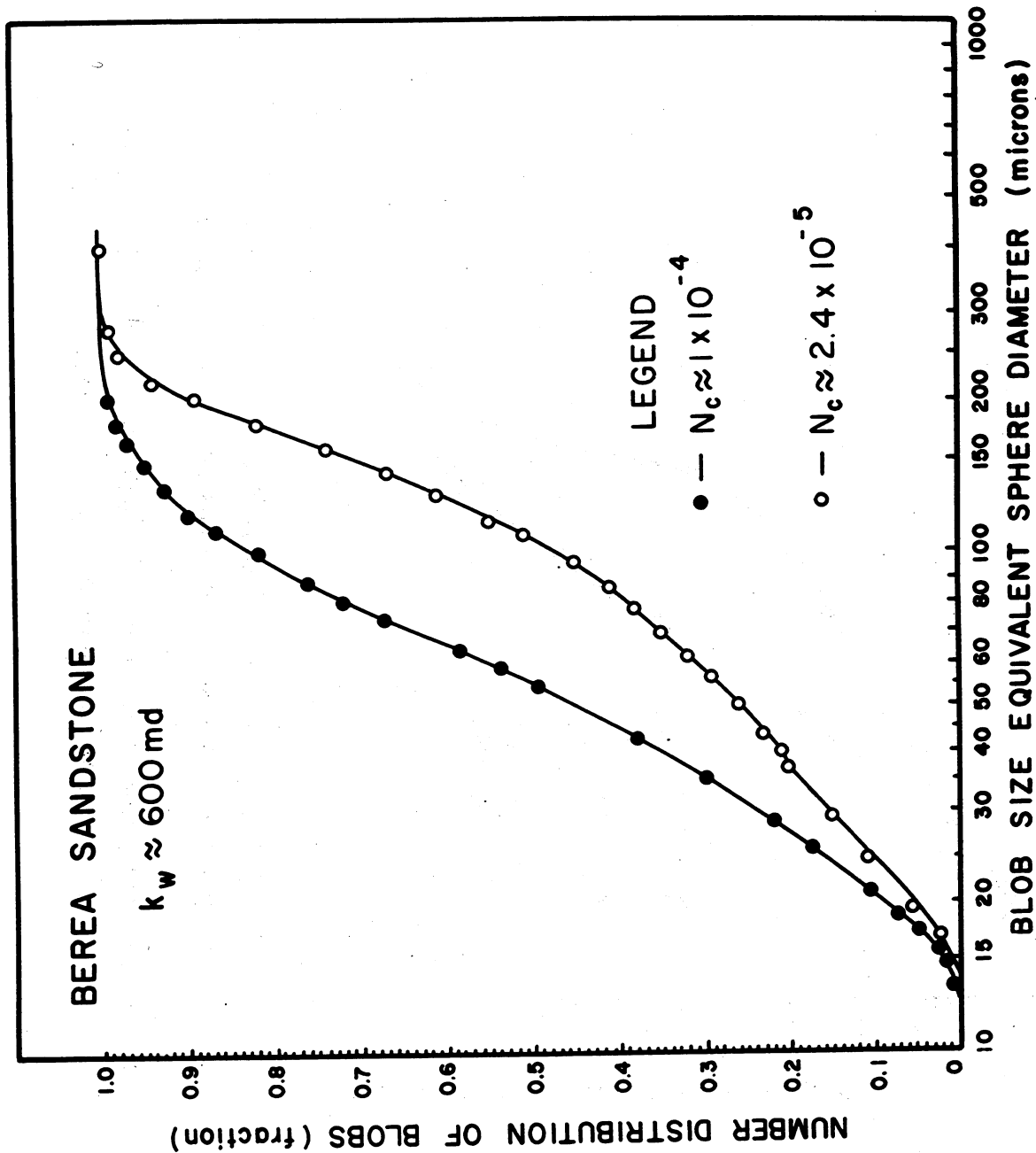


Figure 3.3 Effect of capillary number on blob size distribution.

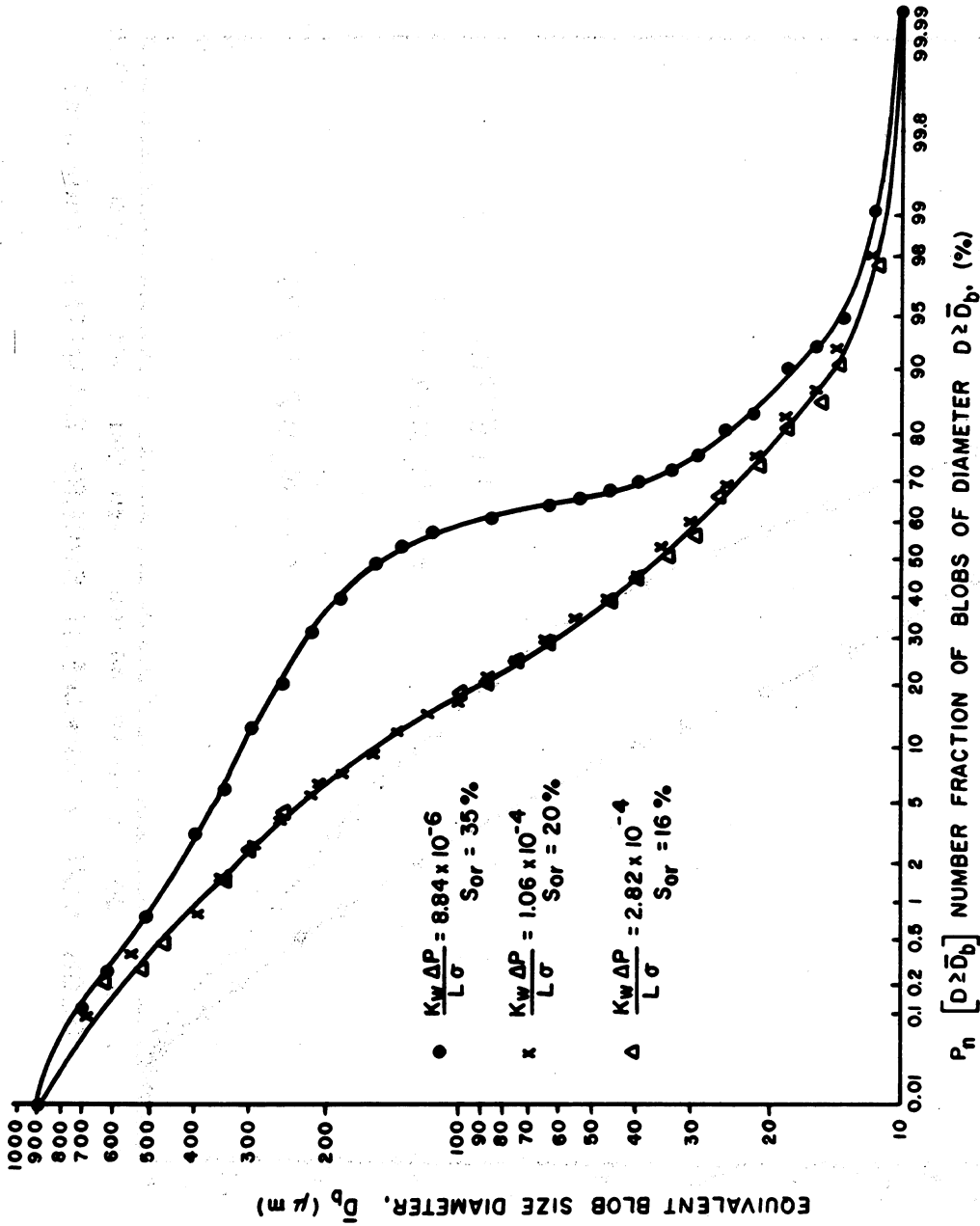


Figure 3.4 Blob size distribution of residual for initially continuous oil in Berea sandstone ( $K_w = 360$  md).

#### Task 4. Effect of Gravity on Residual Saturation

Objective: to develop correlations which relate microscopic displacement efficiency to the ratio of capillary to gravity forces.

At normal oil-water interfacial tensions, capillary forces which retain residual oil far exceed buoyancy forces. However, comparatively little attention has been given to the distinct possibility that when interfacial tensions are lowered as in surfactant flooding, buoyancy forces may have significant effect on both trapping mechanisms and on mobilization.

The ratio of gravity to capillary forces, often termed the Bond number, can be expressed as  $\frac{\Delta\rho g R^2}{\sigma}$ , or in the form  $\frac{\Delta\rho g k}{\sigma}$ , where

$\Delta\rho$  is the density difference

$g$  is the acceleration due to gravity

$\sigma$  is the interfacial tension

$R$  is a characteristic microscopic length (in the present work it is convenient to take  $R$  as the sphere radius)

$k$  is the permeability (for random packings of spheres,  $k \approx 0.00317 R^2$ )

#### Combined Effect of Viscous and Gravity Forces

During the first year of work on this task, an experimental study was made using a mineral oil of 1.42 cp viscosity as the wetting phase and air as the nonwetting phase, and random packings of beads as porous media. This ensured complete wetting (contact angle of zero) by the wetting phase. Bond number was varied by changing sphere radius,  $R$ , and hence permeability, with fluid density difference and surface tension held constant. Capillary number, expressed as  $\frac{v\mu}{\sigma}$ , was varied by changing injection rate in order to determine the combined effect of viscous and gravity forces on trapping.

Details of the experimental procedure have been published.<sup>4.1</sup> In brief, a packed column was first drained to irreducible wetting saturation, and then flooded with oil. Values of residual nonwetting phase saturation obtained for various combinations of capillary and Bond number are presented in Figure 4.1a. When results were replotted as capillary number versus Bond number with residual saturation as parameter, straight line relationships were obtained.<sup>4.1</sup> This showed that the effects of gravity and viscous pressure gradient on the trapping mechanism were equivalent and residual saturation could be correlated with a linear combination of capillary and Bond numbers (Figure 4.1b). The results point to the equivalence of the effect of gravity and viscous forces on the mechanism by which residuals become trapped. A detailed discussion of this mechanism has been presented.<sup>4.1</sup>

## Mobilization of Residuals

An investigation was also made of mobilization of trapped residuals. The increased difficulty of mobilizing trapped fluid relative to prevention of entrapment was immediately apparent. However, at the pressure gradients required for mobilization, it was clearly observable that part of the trapped gas passed into solution at the upstream end of the column and reappeared as gas further down the column. This effect, which was of negligible importance during trapping, made the effect of viscous pressure gradient on mobilization somewhat obscure. However, the results taken at 1 pore volume throughput, are believed to provide a reasonable lower estimate of the reduction in residual saturation due to viscous forces. Results are presented in Figure 4.2 as a plot of microscopic displacement efficiency,  $E_m$ , versus capillary number, where  $E_m$  is defined as

$$E_m = \frac{1 - S_{rr} - S_{wi}}{1 - S_{wi}}$$

$S_{wi}$  is the initial wetting phase saturation (after oilflood)

$S_{rr}$  is the residual or reduced residual nonwetting phase saturation.

The increased difficulty of achieving mobilization, as compared with prevention of trapping, is apparent. Previously reported typical capillary number relationships for mobilization of trapped oil in rocks of narrow and wide pore size distribution are included in Figure 4.2.

## Models of Mobilization and Entrapment

Model calculations have been made for the comparison of mobilization of a blob, which involves drainage and imbibition of the wetting phase, with entrapment which involves only differences in imbibition pressure. The two mechanisms are illustrated in Figure 4.3 for the case of viscous versus capillary forces. Mobilization of discontinuous blobs is estimated to be about 5 times more difficult than prevention of entrapment.<sup>4.1</sup> During the course of this investigation, relative permeabilities at reduced residual saturation were measured; they are included in Figure 4.4 as values of  $k_{rw}$  behind the flood front. The equivalence of gravity and viscous forces was used to determine the pressure gradient in the region of the flood front.<sup>4.1</sup> By equating the Bond number (at low capillary number) required for a given value of residual saturation with the capillary number (at high Bond number) giving the same residual saturation, the relative permeability to the displacing phase at the flood front was calculated as a function of the fraction of residual nonwetting phase displaced. Results are presented on Figure 4.4. The ratio of pressure gradient at the flood front to that behind the front is also shown.

## Effect of Dip Angle

The effect of dip angle on trapping was also investigated. It was found that the effect of buoyancy forces with change in dip angle is greater than that predicted from results for vertical displacement by resolving Bond number according to the angle of dip.<sup>4.1</sup> This is believed to be due to the effect of the three dimensional structure of a finger (potential blob) of fluid which might develop during displacement. On a microscopic scale, even when the column is horizontal, gravity can supplement imbibition pressures because of local vertical height of the potential blob, and this can be sufficient to cause reduction in trapping.

## Buoyancy Effects at Low Interfacial Tension

Results for the effect of buoyancy forces on trapping can be used to determine the possible importance of buoyancy effects in low interfacial tension recovery processes. At ordinary waterflood conditions, the capillary number is about  $10^{-7}$ . This corresponds to a flow rate of about 1 ft/day for water of one centipoise viscosity and an oil-water interfacial tension of 30 dyne/cm. The capillary number for 50% reduction of residual saturations in sphere packings is close to  $10^{-4}$  (Figure 4.1), and would require that interfacial tension be reduced to 0.3 dyne/cm for the above flow rate and viscosity. For vertical displacement at very low capillary numbers, the Bond number at which saturation is reduced 50% by buoyancy forces is about 0.08. If the fluid density difference is  $0.2 \text{ g/cm}^3$ , the sphere radius of the packings required to achieve this Bond number would be 35 microns with corresponding pore radii of about 10 microns. Although the permeability (about 4 Darcys) and porosity (about 38%) are high relative to most reservoir rocks, the pore radius of 10 microns is of the same order as that for good producing zones. With respect to the present discussion, pore size is the more relevant parameter. Results for the effect of dip angle indicate that even for horizontal displacement, buoyancy forces can have a favorable effect on recovery. It follows that in any low tension displacement process, the influence of buoyancy forces on the displacement mechanism may well be significant.

## Trapping of Oleic Phases

In recent work on Task 4, effort was concentrated on obtaining results for trapping and mobilization using an oleic liquid as the nonwetting phase. The two main objectives of this work are:

- (a) Test correlations for the effects of capillary and buoyancy forces on trapping (see Figure 4.1b) which were obtained for entrapment of gas with oil as the wetting phase.

- (b) Obtain results for mobilization of trapped non-wetting phase. (Recall that results obtained for the mobilization of trapped gas<sup>4.1</sup> are of limited reliability because they were seriously affected by solution and dissolution of the gas phase.)

Results are presented in Table 4.1 and are plotted in Figure 4.5 as residual saturation versus Bond number, for a comparatively low capillary number of  $1.01 \times 10^{-5}$ . Thus, most of the reduction in residual saturation can be ascribed to variation in the ratio of gravity to capillary forces. It is seen that apart from the trapped oleic phase saturation being consistently about 1% higher than for trapping of the gaseous phase, the results for the distinctly different fluid systems are very similar. Observed differences may be due to wettability. Advancing and receding contact angles were mostly in the range of  $20^\circ$ - $30^\circ$  for the oil/alcohol/water systems as compared with  $0^\circ$  for the oil/air systems.

In experiments carried out most recently, both the capillary number and Bond number were varied as shown in Table 4.2. These results showed a fairly consistent trend, but did not fit the correlation developed for trapping of gas. One possible explanation of this result is that the trapping mechanism is sensitive to inertial forces associated with relatively high capillary numbers. However, the experimental work proved to be difficult to perform; it is perhaps more likely that deviation from the correlation is due, at least in part, to consistent error in the experimental results. Other approaches to carrying out these experiments are now being tested in an extension of this work.

### Conclusions

- 1) Reduction in residual saturations can be achieved by the effect of buoyancy forces, viscous forces or some combination of both.
- 2) For systems in which the nonwetting phase was a gas, the amount of trapping can be correlated with a linear combination of capillary and Bond number, which accounts for the combined effect of gravity and viscous forces.
- 3) Correlations developed for gas trapping could be used to predict trapping of oleic phases for systems of relatively low capillary number with trapping controlled mainly by buoyancy forces.
- 4) The effect of buoyancy forces on prevention of trapping with change in dip angle is greater than predicted from results for vertical displacement by resolving Bond number according to angle of dip.
- 5) Relative permeability to the wetting phase at the flood front is significantly lower than the relative permeability behind the front.

### Acknowledgement

Measurements on trapping of oleic phases were carried out by Vijaya Dandge and Sandra Nordman.

### References

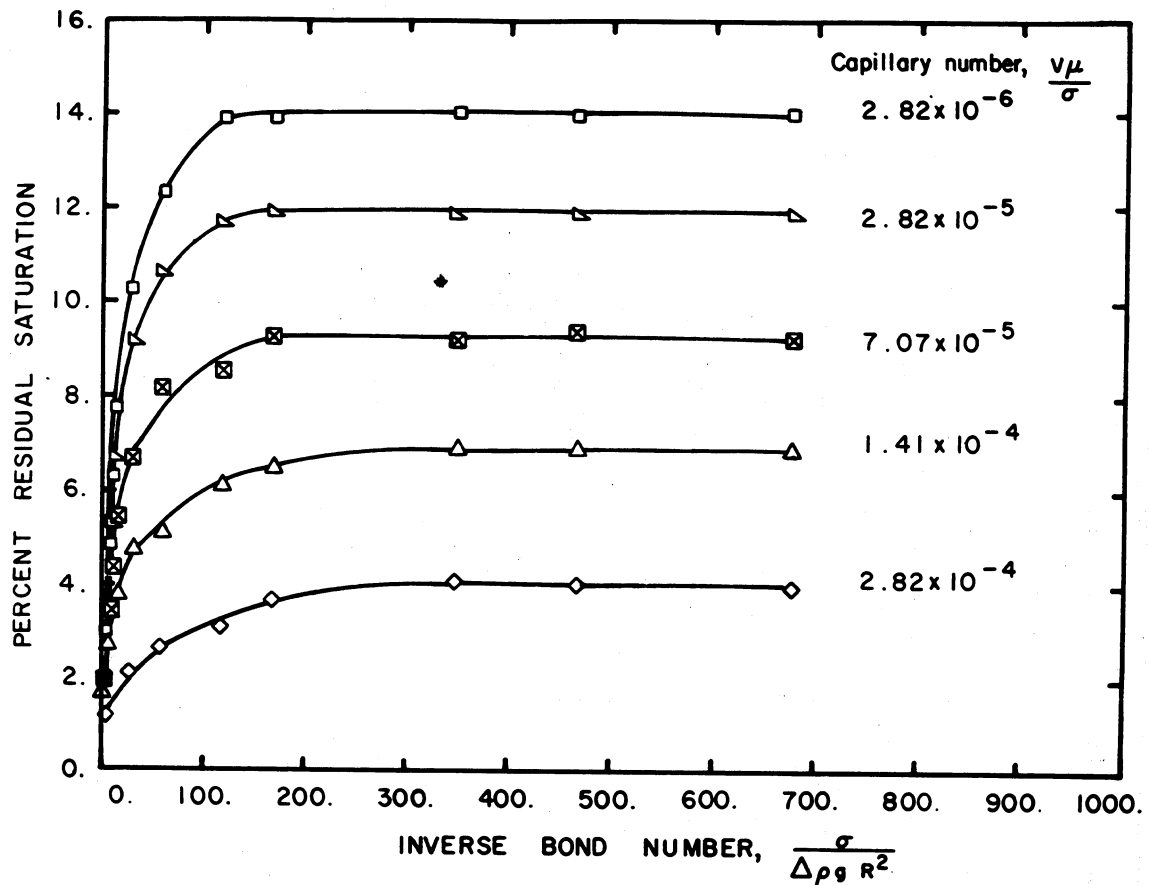
- 4.1 Morrow, N. R. and Songkran, B., "Effect of Viscous and Buoyancy Forces on Nonwetting Phase Trapping in Porous Media," in Surface Phenomena in Enhanced Oil Recovery, Plenum Press. In Press.

Table 4.1 Trapping of Oleic Phase at Various Bond Numbers  
for Capillary Number of  $1.01 \times 10^{-5}$

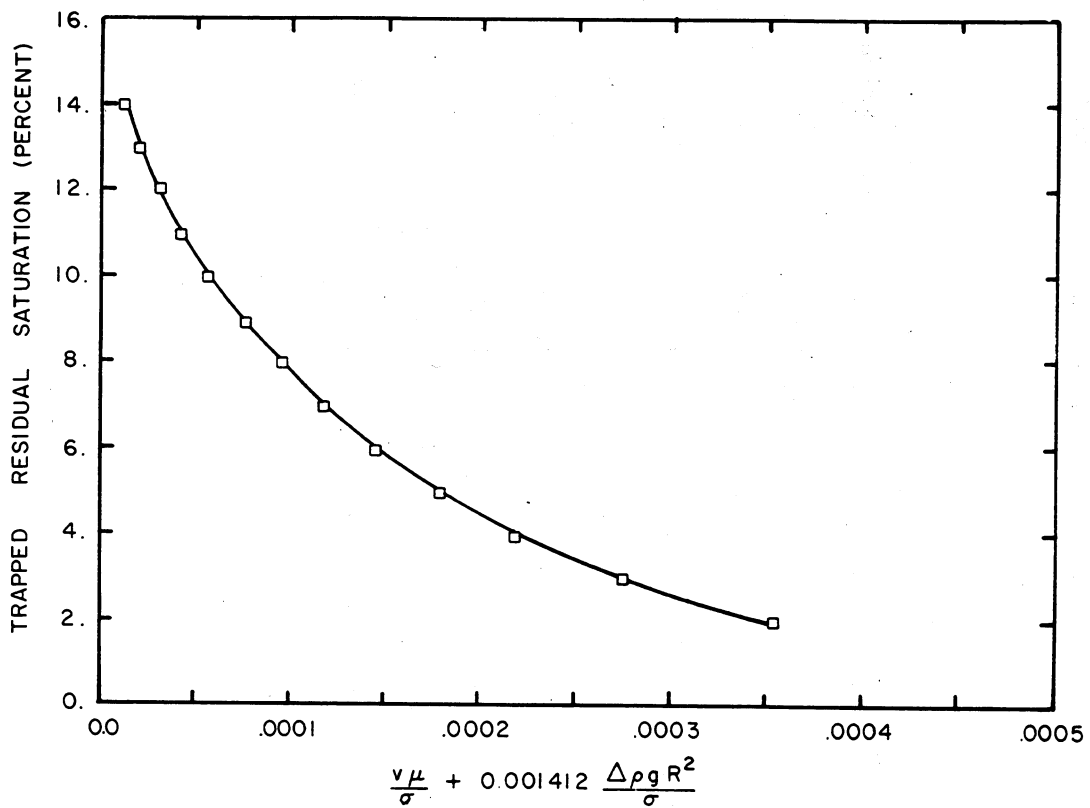
Mesh No.	Mean Radius R (cm)	$\sigma$ (dyne/cm)	$\Delta e$ g/cm <sup>3</sup>	Bond No.	$1/M_B$	Residual Sat. %	Standard Deviation	No. of Runs	$\frac{v\mu}{\sigma} + 0.001412 \frac{\Delta e g R^2}{\sigma}$
70-80	0.00972	22.37	0.3178	0.00132	759.47	15.15	0.61	6	$1.2 \times 10^{-5}$
80-100	0.00819	11.53	0.2995	0.00171	585.05	15.19	0.51	6	$1.25 \times 10^{-5}$
45-50	0.0163	21.05	0.3152	0.0039	256.23	15.16	1.11	8	$1.56 \times 10^{-5}$
35-40	0.0230	21.05	0.3152	0.0078	128.69	14.06	0.55	6	$2.11 \times 10^{-5}$
30-35	0.0274	21.53	0.3174	0.0109	91.74	13.53	1.6	10	$2.55 \times 10^{-5}$
30-35	0.0274	6.65	0.2881	0.0319	31.35	10.94	1.12	7	$5.51 \times 10^{-5}$
18-20	0.0463	10.1	0.2995	0.0624	16.03	7.84	0.81	5	$9.82 \times 10^{-5}$
18-20	0.0463	6.5	0.2887	0.093	10.75	6.42	0.71	6	$1.41 \times 10^{-4}$
16-18	0.0545	6.65	0.2881	0.126	7.82	4.3	1.09	8	$1.88 \times 10^{-4}$
18-20	0.0463	2.5	0.2738	0.23	4.35	3.12	0.88	9	$3.35 \times 10^{-4}$

Table 4.2 Trapping of Oleic Phase in Packings of 80-100 Mesh Beads at  
Various Capillary Numbers for Bond Number of  $1.79 \times 10^{-3}$

Capillary Number	$\sigma$ (dyne/cm)	$\Delta e$ g/cm <sup>3</sup>	Residual Saturation %	Standard Deviation	Number of Runs	$\frac{v\mu}{\sigma} + 0.001412 \frac{\Delta e g R^2}{\sigma}$
$2.5 \times 10^{-6}$	11.53	0.2995	16.1	0.55	7	$4.9 \times 10^{-6}$
$5 \times 10^{-6}$	10.9	0.3000	16.13	0.64	6	$7.6 \times 10^{-6}$
$1.01 \times 10^{-5}$	11.53	0.2995	15.19	0.51	6	$1.25 \times 10^{-5}$
$2.5 \times 10^{-5}$	11.53	0.2995	13.69	0.62	8	$2.74 \times 10^{-5}$
$7.5 \times 10^{-5}$	10.98	0.2991	11.22	0.14	6	$7.75 \times 10^{-5}$
$1.5 \times 10^{-4}$	10.98	0.2991	10.23	1.09	9	$1.525 \times 10^{-4}$
$2.5 \times 10^{-4}$	10.98	0.2991	9.39	0.59	7	$2.525 \times 10^{-4}$
$4 \times 10^{-4}$	10.47	0.2991	7.75	0.55	5	$4.03 \times 10^{-4}$



(a) Trapped residual saturation versus inverse Bond number.



(b) General correlation of above results given by combined linear function of capillary number and Bond number.

Figure 4.1 Combined effect of viscous and gravity forces on residual saturation.

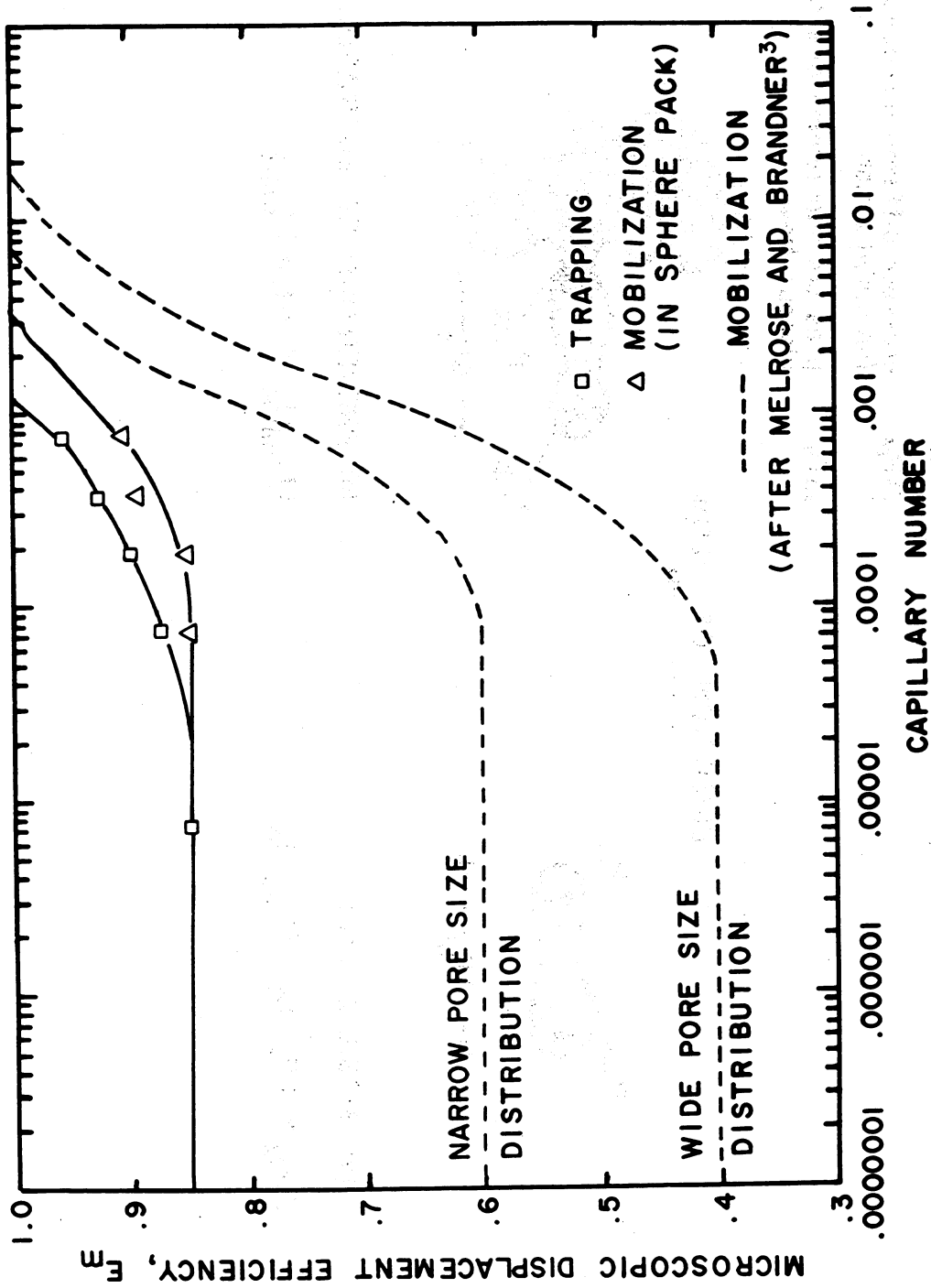
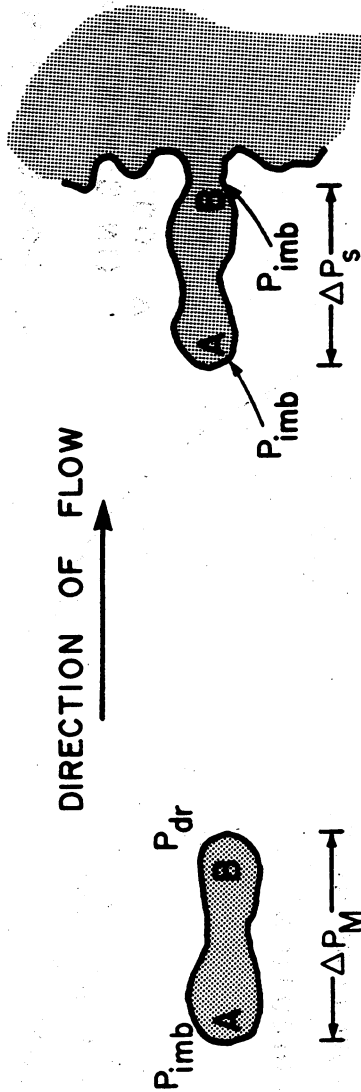


Figure 4.2 Plots of microscopic displacement efficiency versus capillary number ( $v\mu/\phi\sigma$ ).

- $P_{dr}$  drainage capillary pressure
- $P_{imb}$  imbibition capillary pressure
- $\Delta P_M$  pressure difference required for mobilization
- $\Delta P_s$  pressure supplement due to viscous flow



(a) MOBILIZATION

$$\Delta P_M > (P_{dr})_B - (P_{imb})_A$$

(b) PREVENTION OF ENTRAPMENT

$$(P_{imb})_A + \Delta P_s > (P_{imb})_B$$

Figure 4.3 Conditions required for (a) mobilization of a trapped blob, (b) prevention of entrapment of a potential blob.

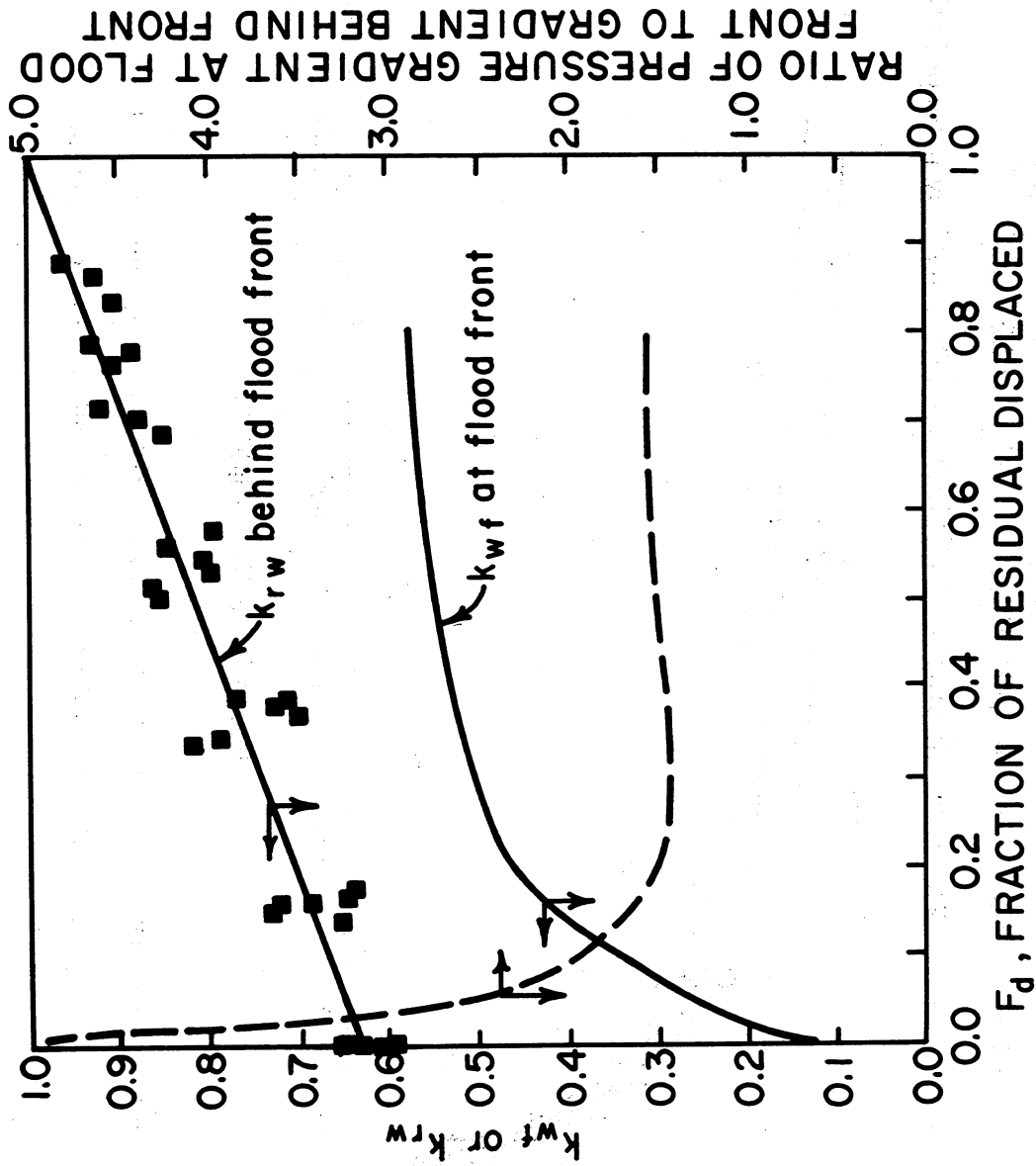


Figure 4.4 Relative permeabilities of wetting phase and ratio of pressure gradient at and behind the flood front vs. fraction of residual nonwetting phase displaced.

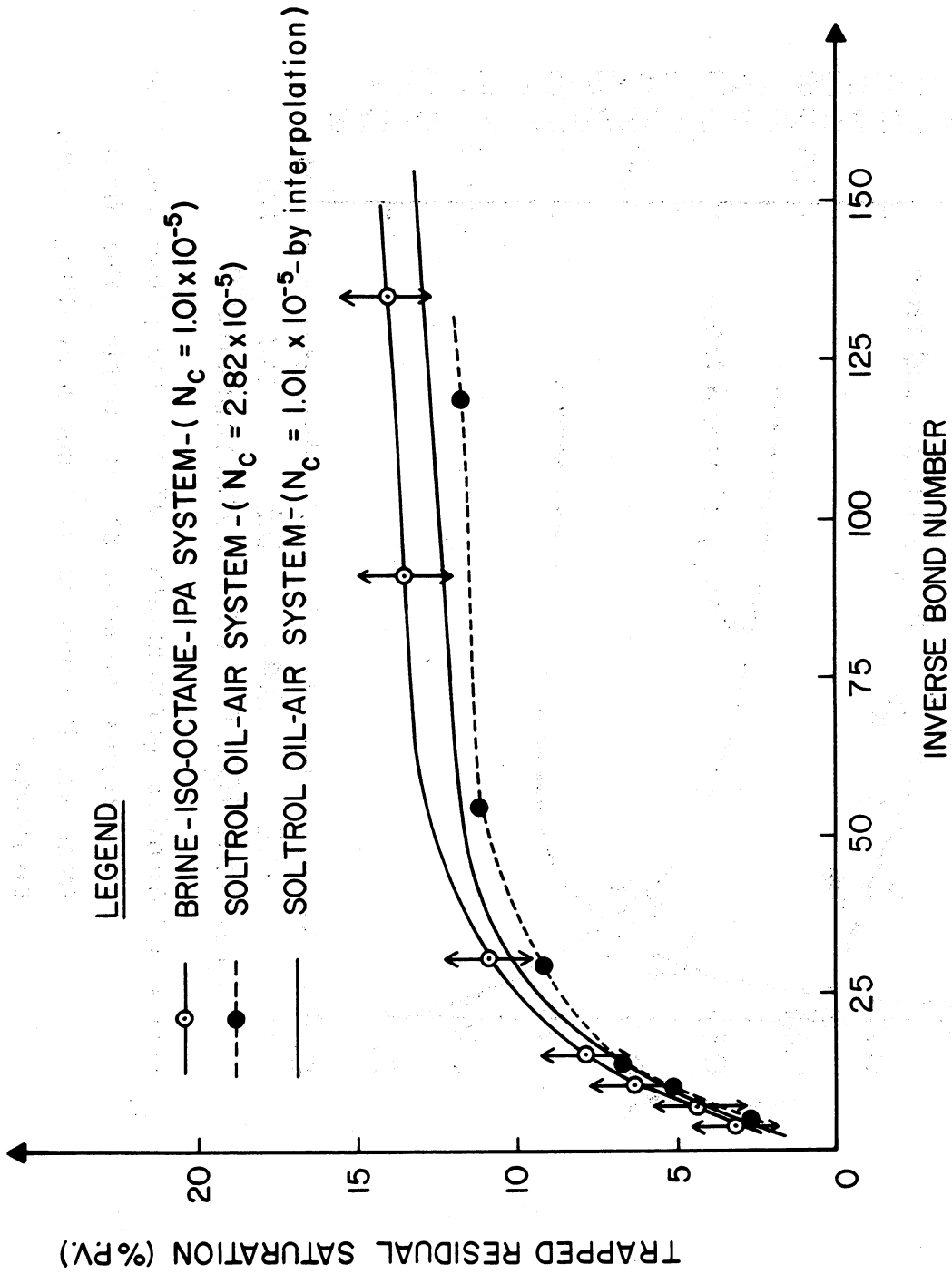


Figure 4.5 Comparison of relationships between trapped residual and inverse Bond number for air-oil and oil-water systems.

## Task 5. Magnitude of Residual Oil Saturation

Objective: to determine the effect on residual oil of particle shape, size distribution and other factors which represent variation in rock and fluid properties.

### Background

A critical factor in the success of a tertiary project is the amount of residual oil available for recovery. Residual oil saturations remaining after waterflooding can range from less than 10% to more than 50% in rocks which may be similar in porosity and permeability. In situ measurements of residual oil give values which, in general, appear to be lower than those indicated by material balance methods and laboratory waterflood tests on reservoir core samples.<sup>5.1</sup> While a major effort has gone into methods of determining residual oil saturation, until recently there has been very little information available on the factors which determine the magnitude of residuals. The complexity of the problem is illustrated by the results of Wardlaw and Cassan<sup>5.2</sup> which showed a general lack of correlation between residual saturations and the more commonly measured rock properties such as porosity and permeability. It can be expected that rock pore geometry and the superimposed effects of wettability determine recovery behavior under normal waterflood conditions. The work carried out under Task 5 was aimed at delineating the effects of pore geometry on trapping of oil in water-wet systems.

The need for such investigation is exemplified by recent controversy concerning the effect of pore size on trapping. A novel and relatively inexpensive approach to estimating residual oil saturation in water-wet carbonate rocks was published recently by Wardlaw and Cassan.<sup>5.3</sup> The method is based on visual examination of thin sections and pore casts. Critical factors in estimating recovery are the proportions of high and low porosity intercrystalline regions, regions of interparticle porosity, regular pores, and the manner in which these regions are distributed relative to each other. Wardlaw and Cassan noted that "for a given pore-to-throat diameter ratio, it is also possible that recovery efficiency decreases as the absolute size of pores and throats decreases, but this has not been investigated experimentally." They showed that recovery efficiencies determined by mercury ejection could be predicted to within  $\pm 10\%$  for 34 out of 36 samples that were studied. Observed recoveries ranged from less than 5% up to 60% of the original in-place nonwetting phase.

In a critique of Wardlaw and Cassan's paper, Magara<sup>5.4</sup> argued the importance of absolute pore size to recovery, stating that "although the effect of absolute pore size may not have been demonstrated experimentally by laboratory methods, it is already well-known among production engineers and geologists." Magara suggests that Wardlaw and Cassan's method would be more reliable if actual pore sizes were taken into account rather than the ratio of throat size to pore size. However, both theoretical considerations and experimental results run counter to a view which Magara regards as common knowledge.

For the most commonly used model of porous media, a bundle of uniform bore capillaries having either equal or a distribution of diameters, there will be no trapping of the nonwetting phase. Complete displacement of the nonwetting phase can also occur in porous media having capillaries of non-uniform cross section, although behavior will now depend on pore shape. For example, trapping would not be expected in cubic packings of uniform spheres. However in contrast to the bundle of uniform capillaries, upon drainage, cubic packings would exhibit an irreducible wetting saturation in the form of pendular rings of liquid retained at contact points between spheres. Provided the ratio of gravity to capillary forces is small, this irreducible saturation is also independent of particle size because similarity principles govern the formation of the irreducible saturation.<sup>5.5</sup>

When displacements are carried out in random sphere packings, both retention of an irreducible wetting phase on drainage, and trapping of non-wetting phase after imbibition are observed. The most convenient direct test of the effect of pore size on trapping is to compare results for trapping in random packings of close-size fractions of spheres or some kind of granular material such as sand. These packings will be geometrically similar in a statistical sense.

## Experimental Procedures, Results and Discussion

### Packing of Equal Spheres

Extensive results which pertain to the effect of pore size on trapping were presented under Task 4. In the initial work on the effect of gravity and capillary number on trapping, Bond number was varied by changing particle size with fluid properties and displacement conditions held constant. Provided the Bond number is less than  $5 \times 10^{-3}$ , the residual saturation is independent of sphere size, and is constant for a given capillary number (see Figure 4.1). Results in Figure 4.1a demonstrate the constancy of residual nonwetting phase saturations in random packings of close-sized spheres having hydraulic radii as tested.

Magara's conclusion as to the effects of pore size are likely related to the observation that residual saturations tend to increase with decrease in permeability. Similar observations have been made for the wetting phase, with the amount of retained wetting phase, commonly identified with reservoir connate water, increasing as the permeability decreases. However, residual wetting phase and residual nonwetting phase saturations for random packings of equal spheres are independent of sphere size. Thus, there is no basis for ascribing variations in residual saturations for naturally occurring porous media to variation in absolute pore size. In the present work, consideration of the effect of absolute pore size has been extended to trapping in composite packings, the manner in which pores of different sizes are distributed relative to each other, and the effect of ratio of pore body size to pore throat size.

## Two Component and Multicomponent Sphere Packings

The apparatus for determination of the effects of gravity and viscous forces, as described in work on Task 4, was used to study the effect of composition of two-component glass-bead aggregates. The aggregates were mixed and added to Soltrol oil, the wetting phase in these experiments, taking care to limit separation of the sphere sizes and to avoid entrapment of air during formation of the packing. After measuring absolute permeability, the pack was drained and the irreducible wetting phase saturation was determined from change in weight. The pack was then flooded at low capillary number and the column was reweighed so that the volume of air trapped in the packing could be determined. Permeabilities at residual saturation were also measured. Results are summarized in Figure 5.1. Absolute permeabilities measured for the two-component packs were in good agreement with values predicted from hydraulic radius theory with the Kozeny factor assumed equal to 5. While porosity goes through the familiar minimum for two-component packs, and permeability increases with the percentage of larger component, the residual saturations of the two-component mixtures were essentially independent of aggregate composition. When similar experiments were carried out on wider size distributions of beads (see Table 5.1), the residual saturations were very close to the value of 14% obtained for the one and two-component bead packs.

### Heterogeneous Packs

In order to demonstrate how high residual saturations can develop because of heterogeneities, a number of configurations, as shown in Figure 5.2, involving high and low permeability regions were tested. The beads were separated into regions of small beads (regions denoted in Figure 5.2 as S) and large beads (regions denoted as L). In some cases the included regions were very lightly sintered to prevent mixing during preparation of the packings.

#### (a) clusters of small beads surrounded by large beads

When the configuration shown in Figure 5.2a is drained, the small-bead regions can be expected to remain 100% saturated with the wetting phase because continuity through the coarse beads is lost before the capillary pressure is sufficient to drain the smaller pores associated with the small beads. Thus, for the packing studied, trapping cannot occur in 18.7% of the pore space. If the saturation of the trapped nonwetting phase in the large bead region is 14% as observed for packings of close-sized spheres, the predicted residual saturation for the packing as a whole would be 11.4% which compares well with a measured value of 11.6%.

#### (b) clusters of large beads surrounded by small beads

As an illustration of how heterogeneities in packing structure can give high residual saturations, clusters of large beads surrounded by small beads giving larger pores surrounded by smaller pores as illustrated in Figure 5.2b,

were investigated. When this structure is drained, both the small pore and large pore regions can be expected to drain to low irreducible wetting phase saturations of about 8%, the measured value being 7.5%. Upon flooding, the wetting phase will invade the smaller pores and the large beads become surrounded before invasion can occur. This should leave the matrix of smaller pores with a residual nonwetting phase saturation of 14% and the pockets of larger pores with saturations of about 92.5%. For the system studied, the predicted contributions to total residual saturation are 10% for small beads and 26.4% for the large beads, giving an overall saturation of 36.4%. This falls close to the 35.7% which was measured.

(c) aspect ratio

The ratio of pore body to pore throat diameter, often referred to as the aspect ratio, was found by Wardlaw to have significant effects on trapping. It can be shown directly for displacements in two-dimensional micromodels that if the aspect ratio is above a critical value, not yet established, but probably in the range of 3 to 4, oil becomes trapped as singlets within the pore body. Photographs of trapping in micromodels having high and low aspect ratios shown in Figures 5.3a and 5.3b respectively demonstrate the differences in blob size that can arise because of aspect ratio.

(d) vugular pores

Vugular pores are important in nature and are a special case of high aspect ratio whereby both the neighboring pore throat and the neighboring pore body diameters are very much smaller than the diameter of the vug. In water-wet rocks residual oil can be expected to remain trapped in the vugs, leading to low recoveries and high residual oil saturations.

### Mobilization of Trapped Oil

The mechanism by which trapping occurs in a single pore because of high aspect ratio is somewhat analogous to trapping in clusters of relatively large pores. However, it seems likely that there will be very distinct differences in ease of mobilization. Oil trapped in pore clusters will be more easily moved for two reasons:

- 1) blob length will be much larger than for blobs held in single pores
- 2) the high aspect ratio that leads to large-scale trapping of oil in single pores will also be a hindrance to mobilization

In actual rocks, the amount of oil which becomes trapped will likely result from a combination of the effects of the examples of heterogeneity

outlined above. In addition to the amount of oil trapped in a given rock sample, microscopic distribution and structure of the trapped oil, which depend on the relative contributions of the various trapping mechanisms, are also likely to be important with respect to the efficacy of a tertiary recovery process.

### Conclusions

For strongly water-wet rocks,

- 1) Residual saturations are independent of pore size per se in systems of similar pore geometry.
- 2) Well mixed aggregates of spheres gave virtually the same residual saturations as random packings of equal spheres.
- 3) High connate water saturations, due to clusters of fine particles which remain saturated, reduce the space available for trapping.
- 4) Clusters of large pores cause high residual saturations. This oil will tend to be amenable to tertiary recovery.
- 5) High aspect ratios tend to cause entrapment of oil as a large number of relatively small blobs held in single pores. Oil distributed in this form will be difficult to mobilize.
- 6) Vugs are a special case of high aspect ratio pores and will tend to retain oil during waterflood.

For wetting properties other than strongly water-wet, rock wettability and heterogeneity of rock wettability will modify the trapping mechanisms described above according to the effects which wettability will have on the sequence by which pores are able to fill or empty. For example, oil is likely to be recovered from vugs in rocks which are oil-wet or of intermediate wettability<sup>5.5</sup> because water will preferentially invade the larger pores.

### Acknowledgement

Most of the reported measurements were made by H. T. Lim.

## References

- 5.1 Interstate Oil Compact Commission, Determination of Residual Oil Saturation, June 1978.
- 5.2 Wardlaw, N. C. and Cassan, J. P., "Oil Recovery Efficiency and the Rock-Pore Properties of Some Sandstone Reservoirs," Bull. of Can. Pet. Geol., Vol. 27, No. 2 (June 1979) 117-138.
- 5.3 Wardlaw, N. C. and Cassan, J. P., "Estimation of Recovery Efficiency by Visual Observation of Pore Systems in Reservoir Rocks," Bull. of Can. Pet. Geol., Vol. 26, No. 4 (December 1978) 572-585.
- 5.4 Magara, K., "Estimation of Recovery Efficiency by Visual Observation of Pore Systems in Reservoir Rocks: Discussion," Bull. of Can. Pet. Geol., Vol. 27, No. 3 (September 1979) 400-401.
- 5.5 Morrow, N. R. and Songkran, B., "Effect of Viscous and Buoyancy Forces on Nonwetting Phase Trapping in Porous Media," in Surface Phenomena in Enhanced Oil Recovery, Plenum Press. In Press.

Table 5.1 Residual Saturations in Packings Formed  
from a Range of Bead Sizes

Sieve Analysis		Expt. No.	Residual Saturation	
Mesh Size (Tyler)	Cumulative Wt. % Undersize		Wetting	Nonwetting
24	98.54	1	6.97	15.93
32	88.66	2	7.15	15.57
48	20.81	3	7.51	15.75
60	2.21	4	6.97	15.93
65	0.28			
80	0.093	Mean	7.15	15.80
115	0	Standard Deviation	0.255	0.172

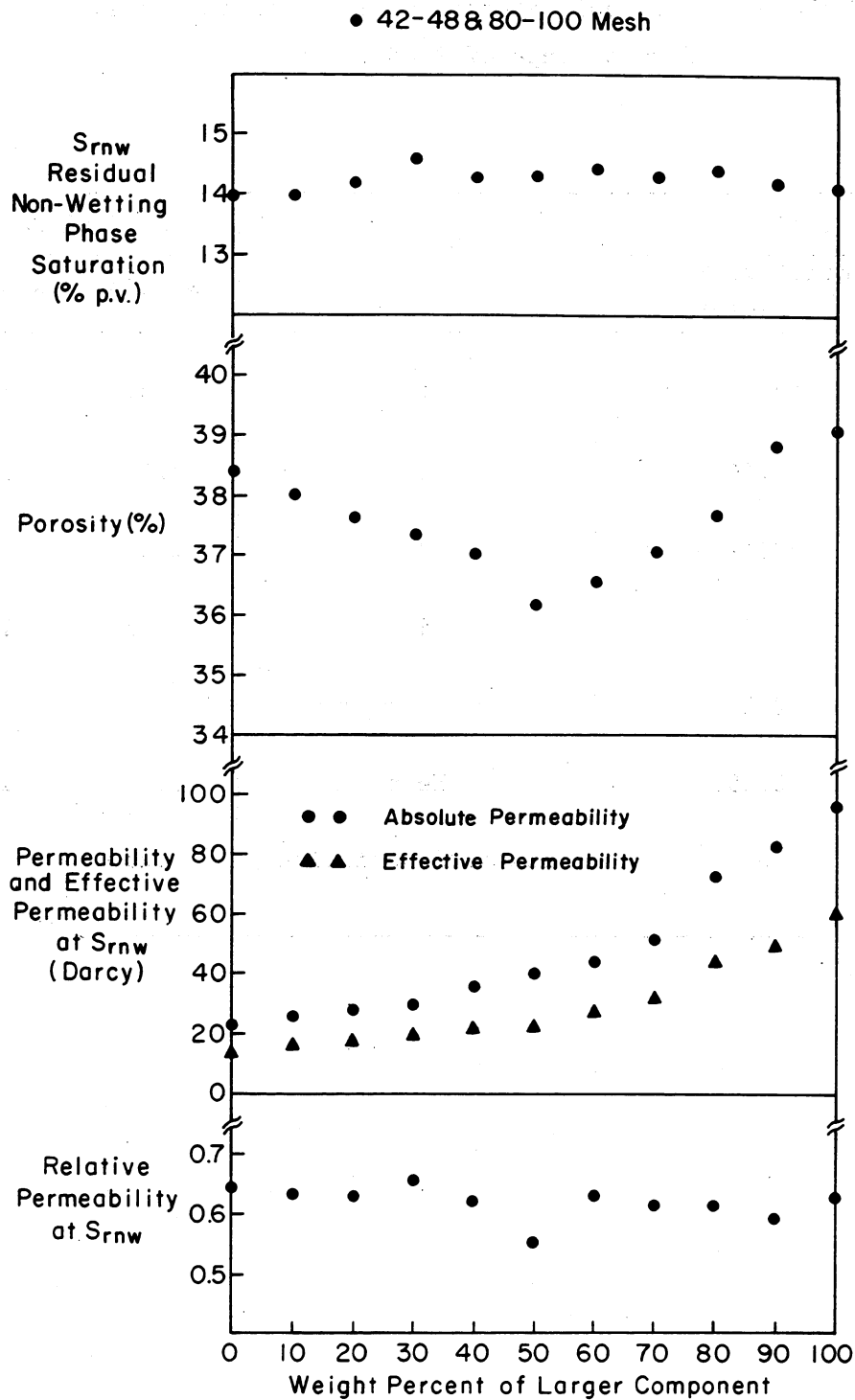
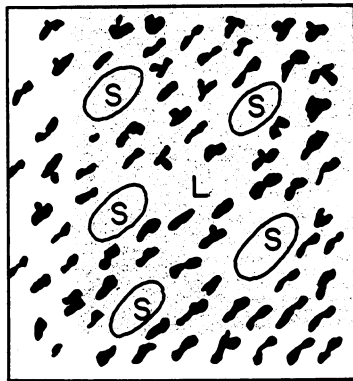


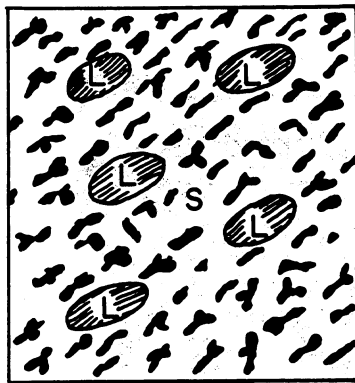
Figure 5.1 Residual nonwetting phase, porosity, absolute, effective, and relative permeabilities at residual nonwetting phase saturation for two component bead mixtures, (42-48 mesh and 80-100 mesh), air and oil.



 Dispersed Residual Oil Blobs  
 Regions which remain 100% water saturated

Results for smaller pores 19% of  
 of total volume:  
 Predicted residual 11.4%  
 Measured 11.6%

(a) Illustration of cluster of small pores (S) in a matrix of large pores (L).

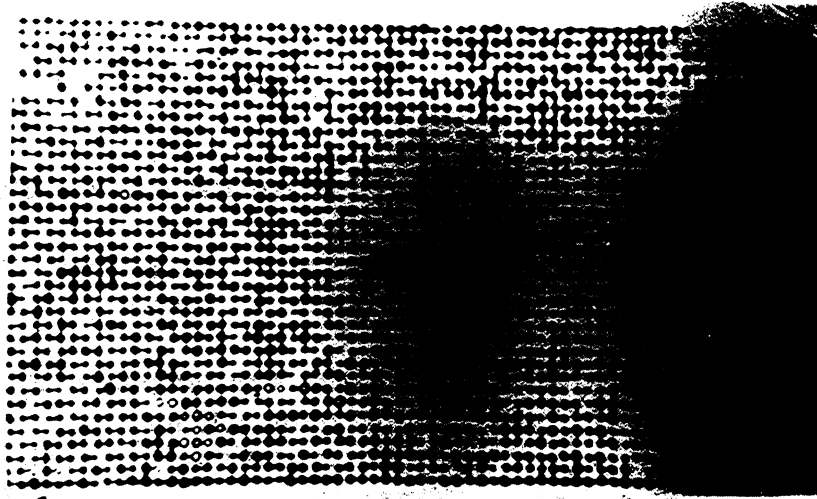


 Dispersed Residual Oil Blobs  
 Regions which retain high oil saturation

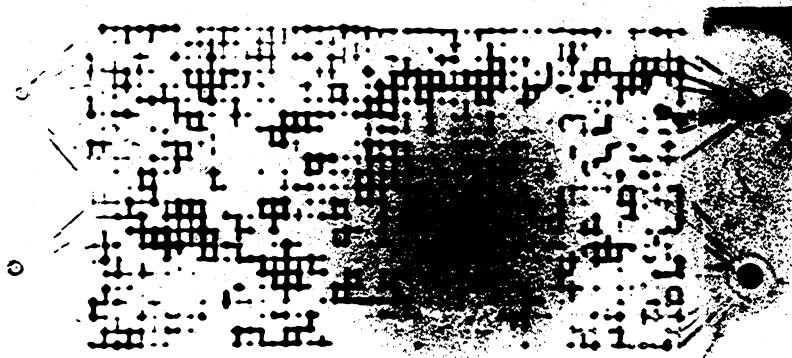
Results for larger pores 28.5% of  
 total volume:  
 Predicted residual 36.4%  
 Measured residual 35.7%

(b) Illustration of clusters of large pores (L) in a matrix of small pores (S).

Figure 5.2 Effect of heterogeneities on magnitude and distribution of residual oil.



(a) High aspect ratio causes high oil saturations trapped as small blobs.



(b) Trapping with blobs having a wide size distribution.

Figure 5.3 Effect of pore structure on trapping.

## Task 6. Effects of Wettability on Capillary Number Relationships

- Objectives: (a) to advance the theory of the effect of wettability on capillary number relationships.
- (b) to investigate the effect of interface velocity on contact angle at rough surfaces for advancing and receding conditions.

### Background

Two examples of the significance of wettability in enhanced recovery are the effect of wetting on residual oil<sup>6.1</sup> and the relationship between contact angle and salinity of microemulsion systems.<sup>6.2</sup> It has been suggested that a particular value of contact angle is associated with optimal salinity. However, there is no general agreement, even on a qualitative basis, of the effect of wetting, per se, on enhanced recovery.

The broad approach being taken to treatment of the effect of wetting on microscopic displacement mechanism is to consider effects of wettability on capillary number for three broad classes of wetting behavior for both mobilization of residual oil and prevention of entrapment. The classes of wetting conditions are: wetted, in which the reference phase is capable of spontaneous displacement of the non-reference phase; intermediate, in which neither phase is capable of spontaneously displacing the other; non-wetted, in which the non-reference phase can spontaneously displace the reference phase. It has been shown, from the results presented under Task 4, that reduction in trapping of continuous non-reference fluid in a wetted system can be achieved by small local changes in imbibition mechanism. In contrast, the forces required for mobilization of trapped blobs involve differences between drainage and imbibition capillary pressures. Interesting predictions of the effect of contact angle on recovery result when these mechanisms are considered for systems of finite contact angle. For wetted systems, mobilization of discontinuous blobs becomes more difficult as the contact angle increases because contact angle hysteresis tends to increase these differences; however, prevention of entrapment should be easier because increase in advancing contact angle should cause relative differences in imbibition pressures to decrease. The two mechanisms are illustrated in Figure 6.1.

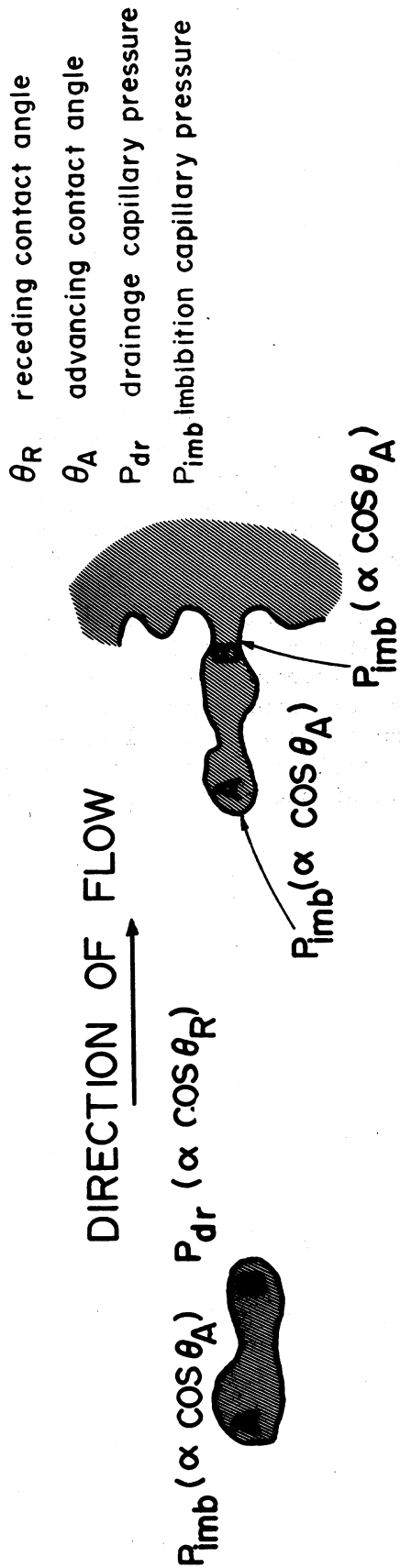
At intermediate wetting (no spontaneous imbibition of either phase), change in pore filling sequence is expected, whereby the invading fluid, be it one phase or the other, tends to advance through the larger pore spaces, rather than the smaller pores as in spontaneous imbibition of a wetting fluid. Immiscible displacement of irreducible wetting fluid in a wetted system or residual non-reference fluid in a non-wetted system is equivalent to attempting to displace connate water from a water-wet core and is extremely difficult to achieve.

In work so far completed in objective (a), blob mobilization has been studied in pores of well defined geometry formed by the space between two

rods and a flat plate.<sup>6.3</sup> An account of this work is presented in Appendix I. In previous studies<sup>6.4</sup> of the effect of wettability on imbibition capillary pressures and imbibition rates, results suggested that dynamic effects might be important in systems which are not strongly wetted, and that objective (b), investigation of dynamic contact angles at rough surfaces, would provide resolution of this issue. Results of the investigation<sup>6.3</sup> are presented in Appendix II. In brief, the dynamic contact angles showed remarkably little sensitivity to interface velocity for velocities from zero to two orders of magnitude greater than normal field rates of frontal advance.

### References

- 6.1 Salathiel, R. A., "Oil Recovery by Surface Film Drainage in Mixed-Wettability Rocks," Trans. AIME (1973) 1216-1224.
- 6.2 Reed, R. L. and Healy, R. N., "Contact Angles for Equilibrated Micro-emulsion Systems," SPE 8262, presented at 59th Annual Fall Meeting of SPE of AIME, Las Vegas, September 23-26, 1979.
- 6.3 Nguyen, M. D., "Aspects of Wettability Related to Oil Recovery," M.S. Thesis, New Mexico Institute of Mining and Technology, February 1980.
- 6.4 Morrow, N. R. and McCaffery, F. G., "Displacement Studies in Uniformly Wetted Porous Media," Wetting, Spreading and Adhesion, J.F. Padday, ed. Academic Press, 1978, 289-319.



DIFFICULTY INCREASES  
 WITH  $\theta$   
 (a) mobilization

DIFFICULTY DECREASES  
 WITH  $\theta$  ( $\theta < 62^\circ$ )  
 (b) prevention of entrapment

FIGURE 6.1: Effect of wettability (for systems which spontaneously imbibe) on (a) difficulty of mobilization of a trapped blob, (b) prevention of entrapment of a potential blob.

## Appendix I

(Work carried out under Task 6a)

### The Effects of Contact Angle Hysteresis and Pore Geometry on Blob Mobilization

#### SUMMARY

Interface curvatures for a range of wetting conditions have been determined from height of rise in capillaries formed by two parallel rods and a flat plate in mutual contact. Pore shape correction factors for height of rise in rod-plate pores were determined using a liquid giving a contact angle of zero. Curvature correction factors which account for the interaction of pore shape and contact angle were determined from height of rise in systems of known wetting properties. Results were used to predict conditions for mobilization of blobs for pairs of rod-plate pores of different size ratio and wetting properties. Experimental measurements of mobilization conditions agreed to within better than 10% with predicted values. Results support previous observations for porous media of random pore structure, that displacement pressures are strongly dependent on contact angle and that the interaction of pore geometry and contact angle on displacement pressures has relatively minor effect.

## Introduction

Many investigations, especially within the petroleum production industry, have been made of trapping and mobilization of fluids in porous media. The factors which control entrapment of oil may be summarized as follows:

- 1) Pore geometry of the rock matrix: pore shape, size and distribution of pores with respect to each other;
- 2) Fluid-rock interactions: wettability and behavior of clays and fine particles;
- 3) Fluid-properties: viscosities, densities, interfacial tensions, phase behavior; and
- 4) Displacement conditions: viscous and hydrostatic pressure gradients.

Laboratory studies have shown that residual oil can be recovered if the ratio of viscous to capillary forces, expressed as the capillary number,  $N_c (= \frac{v\mu}{\sigma})$ , where  $v$  is the fluid velocity,  $\mu$  the viscosity of the displacing phase, and  $\sigma$  the interfacial tension), is sufficient to overcome the capillary forces which hold the oil. Analyses of field test results of micellar-polymer tertiary recovery processes indicate a relationship between oil recovery and capillary numbers achieved in the formation.<sup>1</sup> Although the importance of capillary numbers in oil recovery is well recognized, there is little reliable information on how capillary number relationships will be affected by wetting behavior. The following is an account of the effect of wetting on mobilization of single blobs in systems of well defined geometry and wetting behavior.

In a previous study, mobilization of single blobs within the pore geometry given by a cubic array of spheres against a plate was shown to be highly sensitive to small changes in blob length.<sup>2</sup> Although the sphere/plate system was of simple geometry compared with natural porous media, this sensitivity, caused by the continuous variation in pore cross section, which underly the periodic variation from one sphere to the next, hindered interpretation of the effects of wettability on displacement. In the present work, this disadvantage was avoided by forming pores by mutual contact between two rods and a plate. Requirements for blob mobilization could then be determined for pairs of pores having similar cross section with individual pores having constant cross sections. Interaction of pore geometry and contact angle could then be accounted for by relatively simple relations obtained by measurement. A major consideration in choosing the rod-plate system was to have a system where, in subsequent studies, surfaces forming the pores are readily accessible for treatments such as roughening by sand blasting.

## Theory of Blob Mobilization

Recently, Melrose and Brandner<sup>3</sup> developed a theory for mobilization of oil blobs. When at rest, the external and internal pressures are uniform. All liquid-fluid interfaces of the blob will have the same curvature. A viscous or hydrostatic pressure gradient causes the blob to change shape. If the blob moves through pore spaces, there must be drainage at the leading part of the blob and imbibition at the trailing part. The pressure drop,  $\Delta P_c$ , through the blob can be expressed as

$$\Delta P_c = P_{dr} - P_{imb} \quad (1)$$

A detailed discussion of blob movement with illustrations has been prepared by Ng, et al.<sup>4</sup>

In considering the effect of displacement on ease of mobilization, the effect of wettability on drainage and imbibition pressures must be taken into account. If  $C_{dr}$  is the drainage curvature in the region where the blob is receding and  $C_{imb}$  the imbibition curvature in the region where the blob is advancing, the pressure drop for mobilization is

$$\Delta P_m = \sigma(C_{dr} - C_{imb}) \quad (2)$$

when  $\sigma$  is the interfacial tension. Equations (1) and (2) are general and should hold for all wetting conditions. When the contact angle is zero, the capillary pressure for drainage can be used to define a pore radius for drainage,  $r_{dr}$ , from

$$P_{dr} = \frac{2\sigma}{r_{dr}} \quad (3a)$$

Similarly for imbibition at  $\theta = 0^\circ$

$$P_{imb} = \frac{2\sigma}{r_{imb}} \quad (3b)$$

For blob mobilization at zero contact angle

$$\Delta P_m = 2\sigma \left( \frac{1}{r_{dr}} - \frac{1}{r_{imb}} \right) \quad (4)$$

In the present work displacement of blobs was carried out in pores formed by an assembly of rods and a flat plate, as shown in Figure A1.1. If the draining (higher curvature) interface is associated with the smaller rods, radius  $R_1$ , and the imbibing, lower curvature interface, with rods of radius  $R_2$ , then by similarity, assuming gravity effects to be negligible

$$r_{dr} = F R_1 \quad (5a)$$

and  $r_{imb} = F R_2 \quad (5b)$

where  $F$  is the interface shape factor for zero contact angle. Thus, for a completely wetted system

$$\Delta P_m = \frac{2\sigma}{F} \left( \frac{1}{R_1} - \frac{1}{R_2} \right) \quad (6a)$$

Inscribed radii  $r_1$  and  $r_2$  provide better approximations of the actual pore sizes giving an equation of the form

$$\Delta P_m = \frac{2\sigma}{f_o} \left( \frac{1}{r_1} - \frac{1}{r_2} \right) \quad (6b)$$

where  $f_o$  is the scaled ( $f_o = 4F$ ) curvature correction factor.

When the contact angle is finite, the drainage curvature will be determined by the interaction of pore geometry and the receding contact angle,  $\theta_R$ , and the imbibition curvature by the interaction of pore geometry with the advancing contact angle,  $\theta_A$ .

Forms of equations (6a) and (6b) which take contact angle variation into account can be expressed in various ways, but they are all basically of the form

$$\Delta P_m = \frac{2\sigma}{f_o} \left( \frac{\cos\theta_R}{f_\theta(\theta_R)} - \frac{\cos\theta_A}{f_\theta(\theta_A)} \right) \quad (7)$$

where  $f_\theta$  is a factor which accounts for change in surface curvature from that given by a circular capillary. The need for this factor is ascribed to the interaction of pore geometry and wetting properties.

Interfaces formed between the rods and a plate have been complicated, non-symmetrical shapes which are far from being convenient to compute. Interaction factors for the given pore geometry and a range of contact angles were therefore determined from experimental measurements of capillary rise. Once the interaction factors are known, conditions for blob mobilization can be predicted. Measurement and application of these factors is considered further under presentation and discussion of results.

#### Experimental Materials and Procedures

Rod materials were selected according to desired wetting conditions.

Steel rods and an aliphatic hydrocarbon with air as the second phase were used to obtain complete wetting of the steel and lucite surfaces. A low surface energy material, polytetrafluoroethylene (PTFE), was chosen for study of wettability effects. Rod diameters are listed in Table Al.1. For the PTFE, choice of liquids gave systems with intrinsic contact angles,  $\theta_E$ , (angles measured at smooth surfaces) as listed in Table Al.2. When Teflon rods were used, a thin transparent film of Teflon was placed between the lucite cover plate and the Teflon rods. From previous experience with PTFE surfaces, it was assumed that the advancing and receding contact angles at the rod and film surfaces gave Class II hysteresis behavior. Values of advancing and receding angles are included in Table Al.2.

Steel and lucite pore models were cleaned with acetone. PTFE surfaces were cleaned with chromic acid, followed by washing with distilled water and drying in air at 80°C.

Capillary constants for the rod-plate pores were calculated from measurement of capillary rise in individual pores. The model was set vertically and connected via a PTFE tube to a reservoir which contained the test liquid. A cathetometer was used to measure the difference in height between the interface in the reservoir and that in the model pore. For the steel rods (contact angle 0°), the height of rise was independent of the direction of motion of the interface. When Teflon rods were used, the height of rise between the large rods and the plate was usually measured under advancing conditions because in displacement of blobs imbibition occurs in the larger pores. Capillary rise for the smaller rods was usually measured under receding conditions because blob displacement involves drainage in the smaller pores. Measurements were corrected for capillary rise in the reservoir.

Rods of selected diameters were butted together as shown in Figure Al.1 to give a large pore connected to a small pore. The rods were set up in a lucite trough with appropriate spacers to ensure that the rods were properly placed. The pairs of rods used to form the butted pore model are listed in Table Al.1.

The experimental model is mounted so that it can be slowly adjusted to any angle of inclination (Figure Al.1). The model is tilted from the horizontal to angle  $\alpha$  until  $\alpha_{cr}$  is reached at which, for a given blob length, the blob just penetrates the smaller pore throat and starts moving upward under buoyancy force. The blob length and  $\alpha_{cr}$  are recorded.

## Results and Discussion

### Height of Rise in a Completely Wetted System

Capillary rise in rod-plate pores was measured using isooctane and N-dodecane. An equation showing the height of rise of a completely wetting liquid ( $\theta = 0^\circ$ ) in the pore model can be written

$$\Delta h = \frac{2\sigma}{\Delta\rho g f_0 r_i} \quad (8)$$

where

$r_i$  is the radius of inscribed circle of model pore  
 $\Delta\rho$  is the density difference between liquid and air  
 $g$  = Acceleration due to gravity  
 $f_0$  = Pore shape correction factor, related to  $F$  of equation 5 by  $f_0 r_i = FR$

For the zero contact angle systems, height of rise was independent of direction of interface movement. Values of height of rise and calculated values of  $f_0$  are given in Table A1.3.

Interface shape and height of capillary rise can be affected by the ratio of gravity to capillary forces acting within the region of the interface. This ratio is usually expressed as some form of Bond number  $\frac{\Delta\rho g R^2}{\sigma}$  where  $R$  is some microscopic length which scales with pore size. (In this work we used the rod diameter,  $R$ .) As a check that observed values of  $f_0$  were not unduly dependent on variation in interface shape because of gravity, values of  $f_0$  were plotted against Bond number (see Figure A1.2).

Results for the region over which  $f_0$  was essentially independent of Bond number were used to obtain an average value of  $f_0$  for a range of rod sizes. These results also provide a conservative estimate of deviation from constant curvature of the interface for systems of finite contact angle for which the interface will always tend to be less curved. Hence, curvature variation of the interface due to gravity will always tend to be less than that observed for zero contact angle, other properties being the same.

#### Height of Rise for Zero Contact Angle

Results for capillary rise of two liquids in rod-plate pores formed from five sizes of steel rod are presented in Table A1.3. No hysteresis in capillary rise was observed when the contact angle was zero. From the result,  $f_0 = 1.26$ , for the rod-plate systems the height of capillary rise is given by

$$h = \frac{2\sigma}{1.26\Delta\rho g r_i} \quad (9)$$

#### Height of Rise in Finite Contact Angle Systems

Results of height of rise of eight different liquids measured in a Teflon system are presented in Table A1.4 with pairs of rod sizes as listed. The results show height of rise to depend on whether the interface was advanced or receded in the pore. Results can be used to calculate a

factor  $f_\theta$  which will depend on pore shape and the interaction of contact angle and pore geometry.

$$\Delta h = \frac{2\sigma}{\Delta\rho g f_o f_\theta r_i} \quad (10)$$

The results in Table A1.4 show the factor  $f_\theta$  to depend on advancing or receding conditions, but at a given intrinsic contact angle the results were consistent for different sizes of rods. Values of  $f_\theta$  pertaining to advancing and receding conditions are designated  $f_A$  and  $f_R$  respectively. The average values of the  $f$  factors (calculated for each angle and rod size) were obtained from a series of experiments on rod-plate pores which gave the results listed in Table A1.4.

Curvature corrections are presented in two forms. In Figure A1.3, curvature correction factors for drainage and imbibition are presented for Class II contact angle hysteresis behavior whereby

$$P_c = \frac{2\sigma \cos\theta_E}{f_o f_\theta r_i} \quad (11)$$

where  $\theta_E$  is the intrinsic contact angle.

In Figure A1.4, plots of a curvature correction angle,  $\alpha$ , are presented where  $\alpha$  is defined by

$$P_c = \frac{2\sigma \cos(\theta_E - \alpha)}{f_o r_i} \quad (12)$$

A physically significant feature of the results, apparent from the plot of  $\alpha$  against  $\theta_E$ , is that the correction to contact angle barely ever exceeds  $20^\circ$  showing that the correction to capillary rise because of pore geometry and contact angle interaction is relatively minor. This result is consistent with previously reported<sup>5</sup> capillary pressure measurements on porous media of complex pore geometry. However, it may be noted that much larger correction factors for interaction have been computed for pores having the shapes of doughnuts,<sup>6</sup> sphere packs<sup>7</sup> and cones<sup>8</sup> which have local variation in cross section.

### Conclusions

Calculations of conditions for blob mobilization in a system where operative advancing and receding contact angles, pore shape factors for displacement curvatures and pore geometry/contact angle interaction factors were known were in good agreement with experimental results. The pore geometry/contact angle interaction for pores of uniform cross section is relatively small, as was found for much more complex synthetic porous media.

Results obtained for the rod-plate pore system provide a basis for studying more complex phenomena of oil recovery such as effects of surface roughness and wetting behavior of high energy surfaces.

#### References

1. Lake, L. W. and Pope, G. A., "Status of Micellar-Polymer Field Tests," Pet. Eng. Intl. (November 1979) 38-58.
2. Morrow, N. R., "Interplay of Capillary, Viscous and Buoyancy Forces in the Mobilization of Residual Oil," J. Can. Pet. Tech., 13, 42 (1974).
3. Melrose, J. C. and Brandner, C. F., "Displacement Efficiency for Oil Recovery by Waterflooding," J. Can. Pet. Tech., 13, 42 (1974).
4. Ng, K. M., Davis, H. T. and Scriven, L. E., "Visualization of Blob Mechanics in Flow Through Porous Media," Chem. Eng. Sci., 33, 1009 (1978).
5. Morrow, N. R., "Capillary Pressure Correlations for Uniformly Wetted Porous Media," J. Can. Pet. Tech., 15, 49 (1976).
6. Purcell, W. R., "Interpretation of Capillary Pressure Data," Trans., AIME, 189, 369 (1950).
7. Melrose, J. C., "Wettability as Related to Capillary Action in Porous Media," Soc. Pet. Eng. J. 259 (September 1965).
8. Philip, J. R., "Limitations on Scaling by Contact Angle," Soil Sci. Soc. Amer. Proc., 35, 507 (1971).

Table A1.1 Rod Sizes Used in the Butted Rod-Plate Pore Models

Designation	Diameter of Small Rod (in.)	Diameter of Large Rod (in.)	Inscribed Circle Radius (cm.)	
			$r_{in}$ Narrow Pore	$r_{iw}$ Wide Pore
$R_1-R_2$	1/8 ( $R_1$ )	1/4 ( $R_2$ )	.039688	.079375
$R_1-R_3$		1/5 ( $R_3$ )		.063500
$R_1-R_4$		1/6 ( $R_4$ )		.052917
$R_1-R_5$		1/7 ( $R_5$ )		.045357

Table AI.2 Properties of Tested Liquids

Liquid	Density (g/cm <sup>3</sup> )	Surface Tension (dyne/cm)	Viscosity (cp)	Contact Angle		
				$\theta_E$ (Int.)	$\theta_A$ (Adv.)	$\theta_R$ (Rec.)
Isooctane	.6940	18.77	.49	26°	30°	5°
N - Dodecane	.7430	24.90	1.48	42°	48°	23°
N - Tetradecane	.7599	26.20	2.25	44°	50°	25°
Dioctyl Ether	.8007	24.83	3.52	49°	56°	31°
Hexachlorobutadiene	1.681	36.00	3.174	60°	68°	42°
$\alpha$ -Bromonaphthalene	1.4739	43.00	4.75	73°	83°	58°
Ethylene Glycol	1.1081	47.60	18.20	90°	103°	78°
Distilled Water	1.001	70.55	1.000	108°	123°	98°

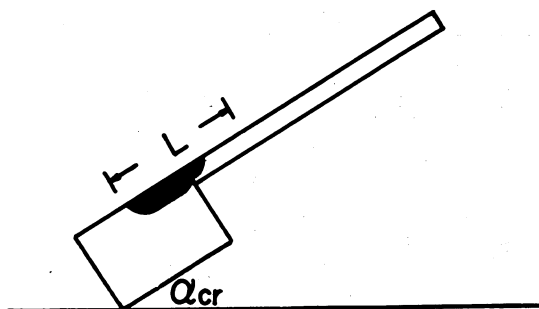
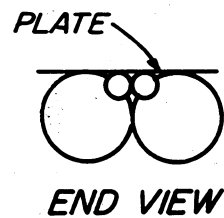
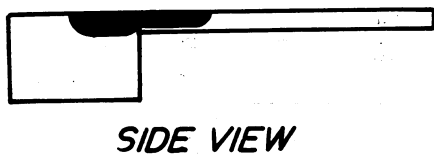
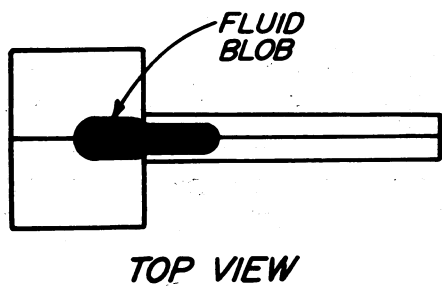
Table A1.3 Results and Calculated Shape Factors for Wetted Systems

Fluids		Steel Rods				
		R <sub>1</sub>	R <sub>2</sub>	R <sub>3</sub>	R <sub>4</sub>	R <sub>5</sub>
Isooctane	radius of inscribed circle, r <sub>i</sub>	.079375	.063500	.052917	.045357	.039688
	height of rise, h(cm)	.5660	.6850	.8220	.9625	1.0950
	capillary constant					
	$F_o = \frac{2\sigma}{\Delta\rho g h r_i}$	1.232	1.272	1.272	1.268	1.273
	$F_o$ (mean)	1.26				
N-Dodecane	height of rise, h(cm)	.6950	.8410	1.0020	1.1950	1.4030
	$F_o = \frac{2\sigma}{\Delta\rho g h r_i}$	1.243	1.284	1.293	1.265	1.231
	$F_o$ (mean)	1.26				

Table A1.4 Comparison of the Predicted and Observed Forces Required for Mobilization of a Single Blob for Systems of Finite Contact Angle

Fluids	$\theta_E$	Class II Contact Angle Hysteresis		Correction Factors				$\frac{g\Delta\rho L \sin\alpha}{\sigma} \text{ cr (cm}^{-1}\text{)}$				
		$\theta_R$	$\theta_A$	$f_o f_{\theta_R}$	$f_o f_{\theta_A}$	$f_{\theta_R}$	$f_{\theta_A}$	*	$\frac{1}{8/4}$	$\frac{1}{8/5}$	$\frac{1}{8/6}$	$\frac{1}{8/7}$
Isooctane	26°	4.56°	29.64°	1.244	1.137	.985	.900	(1)	20.86	16.63	10.53	6.99
								(2)	20.50	16.69	11.01	6.57
								(3)	2%	.4%	5%	6%
N-Dodecane	42°	22.80°	47.88°	1.227	.990	.971	.784	(1)	20.70	16.27	11.85	7.43
								(2)	21.90	16.59	10.84	7.43
								(3)	6%	2%	9%	0%
N-Tetradecane	44°	25.08°	50.16°	1.207	.950	.956	.752	(1)	20.82	16.59	12.37	8.14
								(2)	21.48	16.26	11.73	8.41
								(3)	3%	2%	5%	3%
Dioctyl Ether	49°	30.78°	55.86°	1.208	.907	.956	.718	(1)	20.25	16.35	12.45	8.56
								(2)	20.10	16.75	11.95	8.75
								(3)	1%	2%	4%	2%
Hexachlorobutadiene	60°	42.32°	68.40°	1.14	.725	.910	.574	(1)	20.49	17.91	13.49	10.30
								(2)	22.22	16.37	13.63	11.57
								(3)	8%	9%	1%	10%
$\alpha$ -Bromonaphthalene	73°	58.14°	83.22°	.945	.374	.748	.296	(1)	20.19	18.21	16.22	14.23
								(2)	20.83	18.69	16.22	14.40
								(3)	3%	2.5%	0%	1%
Ethylene Glycol	90°	77.52°	102.60°	.748	.732	.592	.580	(1)	22.06	23.94	25.82	27.70
								(2)	21.91	21.98	25.03	26.11
								(3)	.7%	8%	3%	6%

\* (1) Predicted value  
(2) Observed value  
(3) % Difference



POSITION OF BLOB AT  $Q_{cr}$   
(ONSET OF INSTABILITY)



ENLARGED VIEW  
OF PORE CROSS-SECTION

Figure A1.1 Essential features of apparatus for measurement of blob instability in rod-plate model.

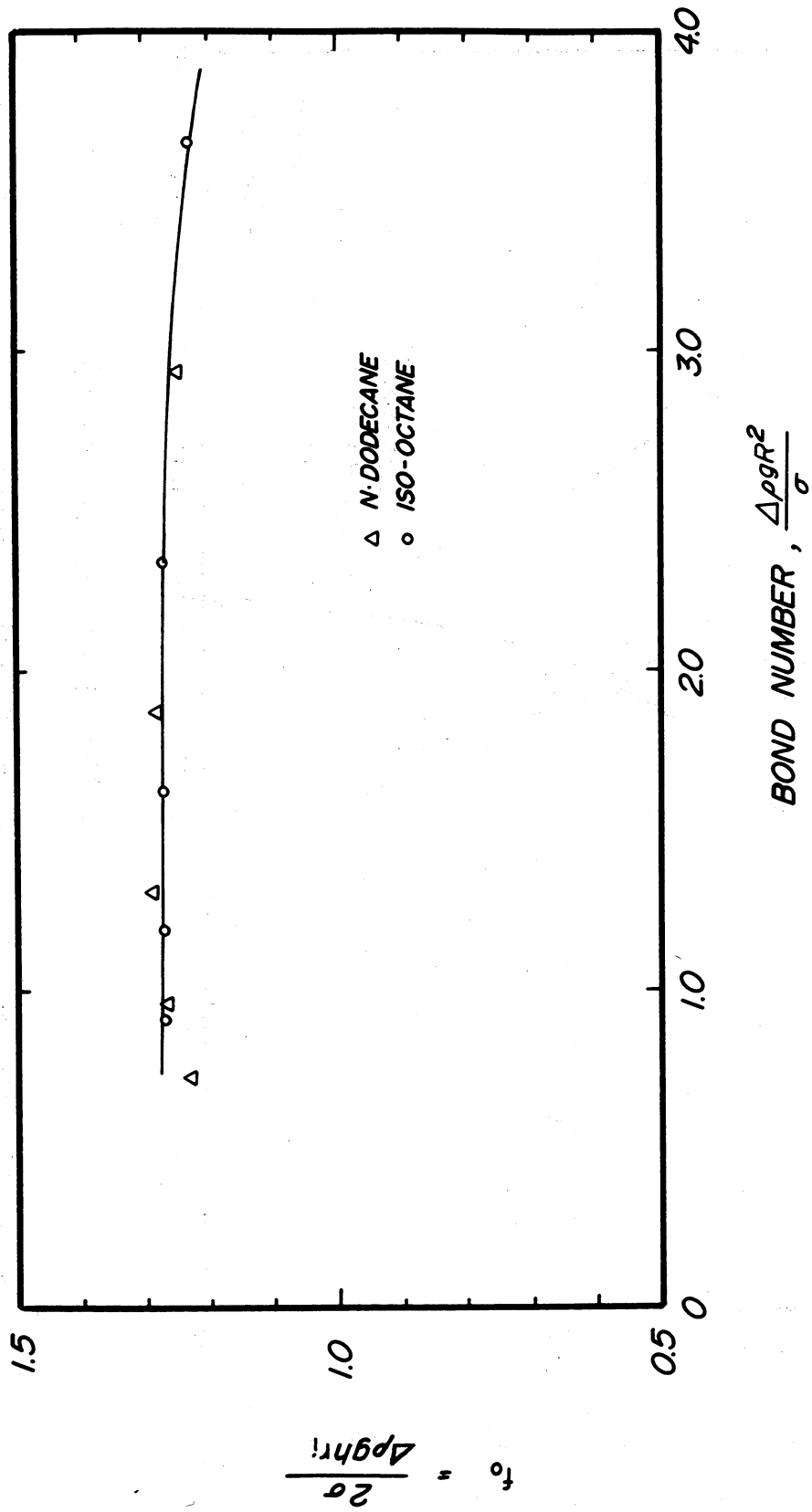


Figure A1.2 Pore shape correction factor,  $f_0$  vs Bond number for wetted systems.

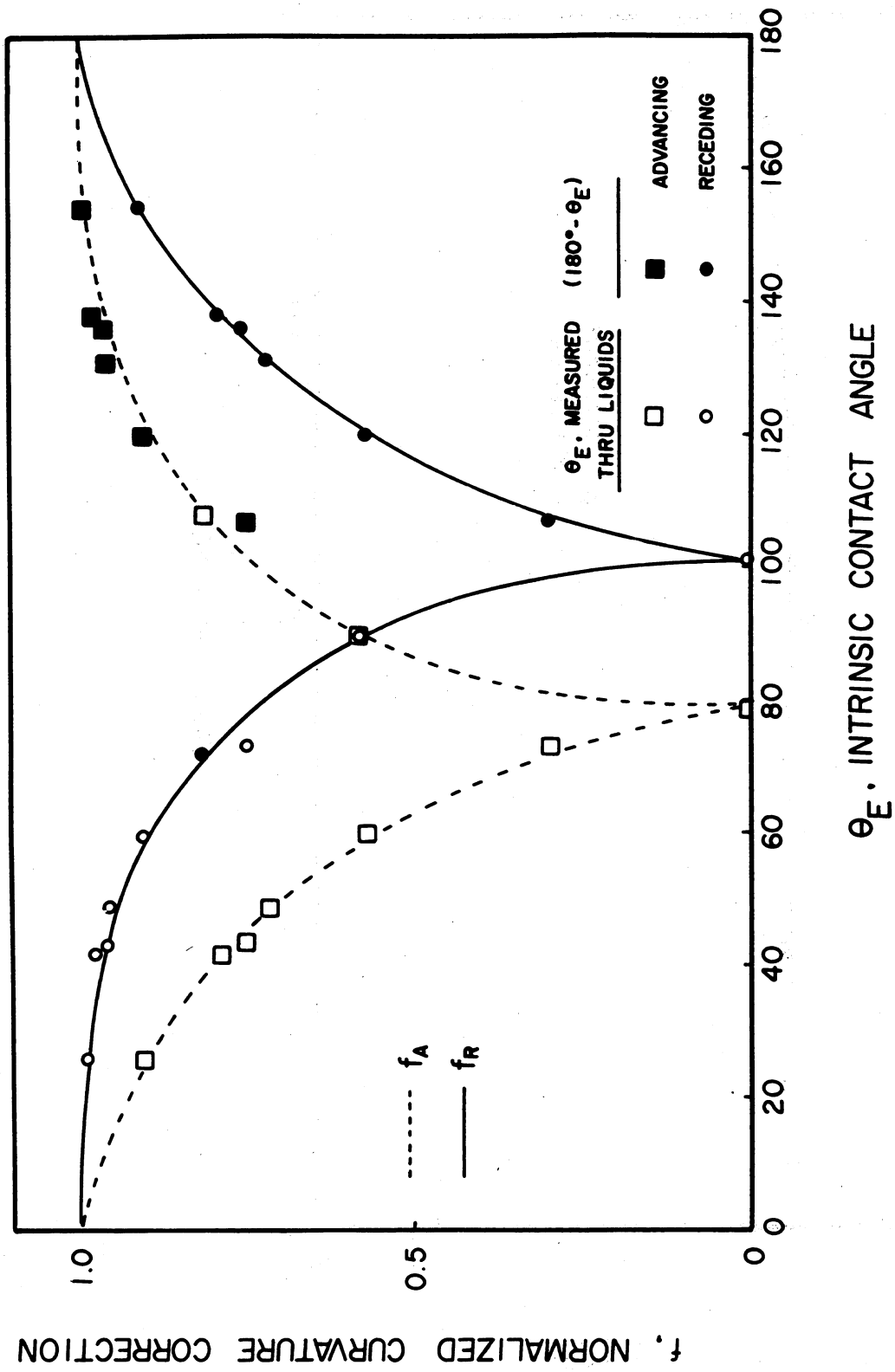
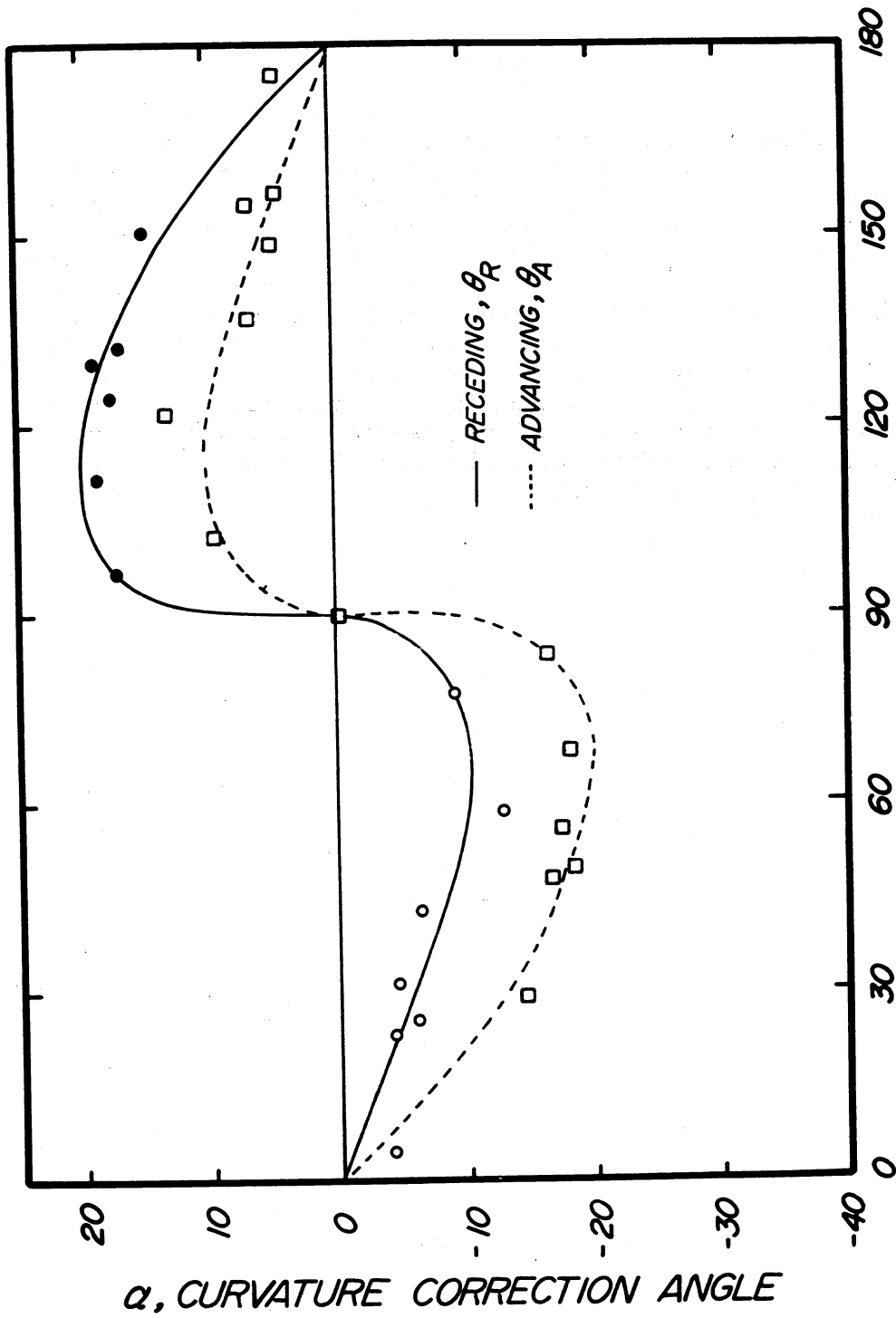


Figure A1.3 Normalized curvature correction factor,  $f_A$  (or  $f_R$ ) vs intrinsic contact angle,  $\theta_E$ .



CONTACT ANGLE,  $\theta_{RII}$  or  $\theta_{AII}$

Figure A1.4 Curvature correction angle,  $\alpha$  vs intrinsic contact angle,  $\theta_E$ .

## Appendix II

(Work carried out under Task 6b)

### Effect of Interfacial Velocity on Dynamic Contact Angles at Rough Surfaces

#### SUMMARY

Dynamic advancing and receding contact angles determined from capillary rise at roughened polytetrafluoroethylene (PTFE) surfaces are reported for eight liquids having intrinsic angles ranging from  $22^\circ$  to  $108^\circ$ . Comparative results for an unroughened tube are also presented. Interface velocities ranged from zero to  $2.0 \times 10^{-2}$  cm/sec. Advancing contact angles tended to increase slightly with interface velocity and receding angles decreased slightly. However, the change was always less than 3 degrees and could be due to experimental artifact. It is concluded that contact angles are very nearly independent of interface velocity for systems in which non-equilibrium compositional changes in surface regions due to processes such as adsorption are absent, and interface velocities are sufficiently slow that interface shape is altered only slightly by viscous forces.

## Introduction

The wetting behavior of solid surfaces is of importance to a wide range of problems of practical interest. In multiphase flow of fluids in porous media, wettability has a dominant influence on fluid distribution and flow behavior. In a previous study it was shown that displacement behavior could be systematically related to wettability as defined by contact angle.<sup>1</sup> Hysteresis in contact angle caused by surface roughness could be closely related to hysteresis in displacement capillary pressures where receding contact angles are operative during drainage and advancing contact angles are operative during imbibition.<sup>2</sup> Relative permeability behavior of flowing phases was also consistent with the effect of wettability on displacement mechanisms.<sup>3</sup> However, in investigation of the effects of wettability on rates of spontaneous imbibition, it was found that imbibition rates were significantly lower than expected.<sup>4,5</sup>

One possible explanation is that the operative contact angle, which for imbibition is the advancing angle, changes with interface velocity. Numerous studies of the effect of interface velocity on contact angle have been reported. Huh and Scriven<sup>6</sup> have provided an informative review of work on interface movement and enumerate the problems involved in modelling interface movement. Displacements of interfaces formed by two liquids present particularly complex behavior.<sup>7-10</sup> Many of the reported experimental studies were made at velocities for which the effect of viscous forces on interface shape is important. Schwartz and Tejada<sup>10</sup> describe three modes of dynamic contact angle behavior. Hoffman<sup>11</sup> correlated observed dynamic contact angles with capillary number (ratio of viscous to capillary forces) plus a shift factor which was a function of the static contact angle. Jiang, et al.<sup>12</sup> present correlations of dynamic contact angles for liquid-air interfaces measured by a variety of techniques. A comprehensive review of dynamic contact angles and interface motion was recently prepared by Dussan.<sup>13</sup> However, data on contact angle behavior pertaining to the conditions under which the aforementioned anomalous imbibition behavior was observed are sparse and conflicting.<sup>14-16</sup> Most reported measurements were obtained for smooth surfaces. The surfaces of the type of PTFE porous media in which the imbibition experiments were carried out are known from electron micrographs to be very rough. There is abundant evidence from published electron micrographs that many other types of porous media, which are of more direct practical interest, such as hydrocarbon reservoir rocks, also have surfaces which can be broadly described as being microscopically rough. A detailed understanding of displacement mechanisms in such systems requires knowledge of interface behavior under dynamic conditions. A study of dynamic contact angles at rough surfaces was therefore undertaken for systems giving a wide range of controlled wetting conditions.

## Experimental

Polytetrafluoroethylene (PTFE) was chosen as substrate with pure

liquids and air as fluids. This choice ensured that observed hysteresis behavior was not due to phenomena such as adsorption behavior.

### Liquid Properties

Surface tensions were checked by du Nuoy ring tensiometer and viscosities were measured with Cannon-Fenske and Brookfield viscometers. Densities were measured by density bottle calibrated with distilled water. Properties of test liquids including intrinsic contact angles<sup>17</sup> at smooth PTFE surfaces are presented in Table A2.1.

Most of the measurements of contact angle were determined indirectly from capillary rise in PTFE cylindrical tubes of radii and designation given in Table A2.2. Static and dynamic contact angles were measured for one tube as supplied and for two roughened tubes of distinctly different diameters. Roughening of internal surfaces was achieved by packing a tube with 80-100 mesh dolomite powder and then rolling the tube between two flat metal plates.

The narrower tube (Tube 1) was rolled by displacing the upper plate about 10 cm, 100 times, with a force of about 15 kg. on the upper plate. The wider tube (Tube 2) was rolled 50 times with a force of about 10 kg. on the upper plate. Most of the powdered dolomite was removed by shaking and the remainder by soaking the tube in warm (50°-60°C) concentrated chromic acid for 30 minutes, followed by rinsing in warm (50°-60°C) distilled water for 30 minutes. The tubes were then dried in an oven at about 80°C.

Accurate measurements of tube radii,  $R$ , were determined (after roughening for Tubes 1 and 2) from the weight and length of a mercury thread contained in a given tube. Radii were checked by measurements of capillary rise using normal heptane which was known to give contact angles extremely close to zero at roughened surfaces.<sup>1</sup> Measurements of radii were in good agreement (see Table A2.2).

In initial experiments the interface was caused to move along a horizontal or slightly tilted tube by hydrostatic pressure difference. In theory, the tilt of the tube could be made to exactly compensate for the change in pressure drop due to viscous forces as the interface moved in the tube. In practice the interface tended to stick, especially at the low interface velocities of interest in the present work.

The reported measurements of dynamic advancing and receding contact angles,  $\theta_{AD}$  and  $\theta_{RD}$  respectively, were obtained using a modified capillary rise method in which the tube was vertical and could be moved at constant velocity,  $V$ . Static contact angles were determined from measurements of capillary rise obtained after lowering or raising a tube to some set position. Main features of the apparatus are shown in Figure A2.1. With this method, sticking during dynamic measurements was always overcome by the changing hydrostatic pressure. Hydrodynamically, movement of the tube relative to the liquid is equivalent to movement of liquid in a stationary

tube. Capillary rise,  $h$ , in the moving tube was observed to be essentially constant over the time periods of a few minutes needed for each measurement of capillary rise. This technique also permitted the tube properties to be held more nearly constant by keeping the observed interface in the same region of the tube for all of the measurements. Reproducibility of calculated angles was generally better than  $\pm 1^\circ$ .

#### Calculation of Dynamic Contact Angles from Capillary Rise

Advancing and receding contact angles for an interface moving at a velocity,  $V$ , (positive when tube is moving upwards) were calculated as follows. Boundary effects at the end of the tube<sup>1,8</sup> and in the region of the interface were neglected as was pressure drop due to gas flow. Pressure drop due to viscous flow in the tube,  $\Delta P_1$ , was determined from the Hagen-Poiseuille equation:

$$\Delta P_1 = \frac{8\mu\Delta LV}{R^2} \quad (1)$$

where  $\mu$  is the liquid viscosity, and  $\Delta L$  is the length of the tube occupied by liquid. Neglecting change in interface curvature caused by gravity, the pressure drop across the interface in a narrow tube when the contact angle is  $\theta_D$  and the interface maintains a surface of minimum area with respect to the prevailing contact angle boundary conditions, is given by:

$$\Delta P_2 = \frac{2\sigma\cos\theta_D}{R} \quad (2)$$

The total pressure drop for the liquid in the tube is given by:

$$\Delta P = \Delta\rho gh \quad (3)$$

where  $h$  is the volumetric mean height of rise as corrected<sup>1</sup> for interface shape.

The hydrostatic pressure is equal to the sum,  $\Delta P_1 + \Delta P_2$ ; hence, dynamic contact angle,  $\theta_D$ , is given by:

$$\theta_D = \cos^{-1} \left[ \frac{\Delta\rho ghR - \frac{8\mu\Delta LV}{R}}{2\sigma} \right]$$

## Results and Discussion

### Static Angles

Static advancing and receding contact angles measured for Tube Nos. 1 and 2 are presented in Figure A2.2. For systems such as pure liquid and air against PTFE there is essentially no contact angle hysteresis if the solid surface is smooth;<sup>17</sup> the choice of fluid phase through which intrinsic angle,  $\theta_E$ , is defined is somewhat arbitrary. Advancing and receding angles measured with respect to one fluid phase giving an intrinsic contact angle,  $\theta_E$ , can be treated respectively as receding and advancing contact angles for the other phase (intrinsic angle  $180-\theta_E$ ).<sup>1</sup> Each data point can be plotted twice as shown in Figure A2.2 to provide an account of hysteresis behavior over the complete range of uniformly wetted (as defined by intrinsic contact angle) systems.

In discussing results, three classes of static contact angle behavior defined in previous work according to surface condition will be referred to as:

#### Class I - Smooth Surfaces: (ideal behavior)

No contact angle hysteresis  $\theta_E = \theta_R = \theta_A$

#### Class II - Tubes as Supplied or Slightly Roughened:

Advancing and receding angles show limited contact angle hysteresis.

##### Advancing Contact Angles - Class II

$$0^\circ < \theta_E < 158^\circ; \theta_A = 1.14 \theta_E$$
$$158^\circ < \theta_E < 180^\circ; \theta_A = 180^\circ$$

##### Receding Contact Angles - Class II

$$0^\circ < \theta_E < 22^\circ; \theta_R = 0^\circ$$
$$22^\circ < \theta_E < 180^\circ; \theta_R = 1.14 (\theta_E - 22^\circ)$$

#### Class III - Well-Roughened Tubes:

Generally large contact angle hysteresis.

##### Advancing Contact Angles - Class III

$$0^\circ < \theta_E < 21.6^\circ; \theta_A = 0^\circ$$
$$21.6^\circ < \theta_E < 92.4^\circ; \theta_A = 2 (\theta_E - 21.6^\circ)$$

$$92.4^\circ < \theta_E < 158.4^\circ; \theta_A = 181.5 - 4.051e^{-0.05\theta_E}$$

$$158.4^\circ < \theta_E < 180^\circ; \theta_A = 180^\circ$$

#### Receding Contact Angles - Class III

$$0^\circ < \theta_E < 21.6^\circ; \theta_R = 0^\circ$$

$$21.6^\circ < \theta_E < 87.6^\circ; \theta_R = 0.5e^{0.05\theta_E} - 1.5$$

$$87.6^\circ < \theta_E < 158.4^\circ; \theta_R = 2(\theta_E - 68.4^\circ)$$

$$158.4^\circ < \theta_E < 180^\circ; \theta_R = 180^\circ$$

Static results obtained in the present work are generally in good agreement with a correlation<sup>1</sup> developed for systems exhibiting Class III behavior which is included in Figure A2.2. Class II and III are by no means the only types of contact angle hysteresis behavior but from experience they are considered the most likely. Contact angle behavior falling between Class II and Class III behavior has been reported recently by Batycky.<sup>19</sup>

Electron micrographs of Tubes 1 and 2 are shown in Figure A2.3. Tube 1 appears distinctly rougher than Tube 2 as might be expected from the more severe roughening procedure used for Tube 1. However, both tubes gave essentially the same results. This was consistent with previous observations that once a surface was made sufficiently rough, further roughening had no significant effect on contact angle hysteresis.<sup>1</sup>

#### Dynamic Contact Angles

Results for advancing and receding contact angles at velocities ranging from 0 to  $2 \times 10^{-2}$  cm/sec are presented in Figures A2.4 and A2.5 respectively. At higher velocities, vibration caused the receding angles to increase and advancing angles to decrease in an erratic manner which made observation of the interface difficult. This could likely be eliminated by refinement of the mechanism for raising or lowering the tube. However, the velocity of  $2 \times 10^{-2}$  cm/sec was well in excess of the mean rates of liquid advance<sup>4</sup> in porous media which were of primary interest in the present study. Johnson, et al.<sup>16</sup> were successful in making measurements at smooth surfaces for velocities of up to  $4 \times 10^{-1}$  cm/sec. They point out that this is to be expected because random vibrations allow free energy barriers surrounding metastable states to be overcome. On the other hand, impressed motion in one direction or the other will have the opposite effect. These authors also suggest that systems showing large hysteresis in static contact angles will tend to be more susceptible to change in contact angle with velocity because they will have a greater number of metastable states. However, for the range of impressed velocities studied, it is seen from Figures A2.4 and A2.5 that, for a wide range of wetting conditions, receding and advancing contact angles changed by no more than a few degrees with interface velocity. It

is concluded that the difference between the static and maximum or minimum possible angles which gives rise to hysteresis in dynamic contact angles is very small for rough surfaces. Johnson et al. noted that the foregoing rationale only applies where the time for liquids to undergo spontaneous movement is fast compared to the overall rate of movement of the three phase line of contact.

Results for the unroughened tube (Tube 3) are shown in Figure A2.6, together with some of the results obtained for one of the roughened tubes (Tube 1). Changes in contact angle hysteresis due to roughening are apparent. Advancing contact angles for  $\alpha$ -bromonaphthalene ( $\theta_E = 73^\circ$ ) and ethylene glycol ( $\theta_E = 90^\circ$ ) were consistent with Class II behavior. However, receding angles were lower (about  $40^\circ$  instead of  $77^\circ$  for ethylene glycol and  $17^\circ$  instead of  $48^\circ$  for  $\alpha$ -bromonaphthalene). A possible explanation is that Tube 1 was rougher than the tubes used in the series of experiments which established the correlation for Class II behavior; receding angles may be more sensitive to surface condition than the advancing angles, for roughness conditions intermediate to those giving Class II and Class III behavior.

A significant aspect of the results presented in Figure A2.6, is that dynamic contact angles for two distinctly different surface conditions are close to independent of interface velocity. This lack of dependency of contact angle on velocity virtually eliminates the possibility that the apparent anomalies in rates of spontaneous imbibition mentioned in the introduction to this paper were caused by change in advancing contact angle with rate of interface motion.

Elliot and Riddiford<sup>15</sup> reported changes in contact angle with interface velocity; they interpreted their results in terms of molecular reorientation. In general, results of the present study support the conclusions of Johnson, et al. regarding this interpretation, in that no significant changes in contact angle with velocity which might be ascribed to molecular reorientation were observed for either relatively smooth or roughened surfaces.

Caution must be exercised with respect to the effects of surface roughness and interface velocity on systems in which the solid substrate is a high energy solid. Dynamic contact angles, measured on monolayers deposited on glass slides, for interface speeds up to 0.4 cm/sec showed in most cases that contact angle had only minor if not negligible dependence on velocity.<sup>16</sup> In two instances, where changes of up to  $10^\circ$  and  $15^\circ$  were observed, results were ascribed to heterogeneity of the adsorbed monolayer.

In recent studies of wetting properties of microemulsion systems, Reed and Healy showed contact angle, within the limits of particularly difficult experimentation caused by ultralow interfacial tensions, to be constant and free of hysteresis for a variety of high energy substrates.<sup>20</sup> This suggests that wetting behavior of these systems would not be altered if the solid substrate were heterogeneous. Under these circumstances, it seems reasonable to assume that results for the effect of wettability, as

defined by contact angle, on displacement behavior obtained using porous media formed from a low energy solid will be applicable to microemulsion systems in porous media. It is also expected that microemulsion systems can exhibit contact angle hysteresis at rough surfaces. Because of likely adsorption mechanisms<sup>20</sup> related to microemulsion wetting behavior, assumptions as to the effects of interface velocity on wetting behavior would need to be tested.

### Conclusion

Dynamic advancing and receding contact angles, at both rough and smooth low energy surfaces are essentially independent of interface velocity provided viscous forces do not cause significant change in interface shape.

### References

1. Morrow, N. R., "Capillary Pressure Correlations for Uniformly Wetted Porous Media," J. Can. Pet. Tech. 15, 49 (1976).
2. Morrow, N. R., "The Effects of Surface Roughness on Contact Angle with Special Reference to Petroleum Recovery," J. Can. Pet. Tech. 14, 42 (1975).
3. McCaffery, F. G. and Bennion, D. W., "The Effect of Wettability on Two-Phase Relative Permeabilities," J. Can. Pet. Tech. 13, 42 (1974).
4. McCaffery, F. G. and Bennion, D. W., "Experimental Study of the Relationship of Contact Angles to Imbibition in Porous Media," Preprints: 48th National Colloid Symposium at University of Texas, Austin, Texas. American Chemical Society (1974) 124-129.
5. Morrow, N. R. and McCaffery, F. G., "Displacement Studies in Uniformly Wetted Porous Media," Wetting, Spreading and Adhesion, J.F. Padday, ed. Academic Press (1978) 289-319.
6. Huh, C. and Scriven, L. E., "Hydrodynamic Model of Steady Movement of a Solid/Liquid/Fluid Contact Line," J. Coll. Inter. Sci. 35, 85-101 (1971).
7. Chittenden, D. H. and Spinney, D. U., "An Experimental Study of the Surface Composition Effect on Two-Phase Flow in a Glass Capillary Tube," J. Coll. Inter. Sci. 22, 250-256 (1966).
8. Blake, T. D. and Haynes, J. M., "Kinetics of Liquid/Liquid Displacement," J. Coll. Inter. Sci. 30, 421-423 (1969).
9. Hansen, R. J. and Toong, T. Y., "Dynamic Contact Angle and Its Relationship to Forces of Hydrodynamic Origin," J. Coll. Inter. Sci. 37, 196-207 (1971).

10. Schwartz, A. M. and Tejada, S. B., "Studies of Dynamic Contact Angles on Solids," J. Coll. Inter. Sci. 38, 359-375 (Feb. 1972).
11. Hoffman, R. L., "A Study of Advancing Interface-Interface Shape in Liquid Gas System," J. Coll. Inter. Sci. 50, 228-240 (Feb. 1975).
12. Jiang, T., Oh, S. and Slattery, J. C., "Correlation of Dynamic Contact Angle," J. Coll. Inter. Sci. 69, 74-77 (Mar. 1979).
13. Dussan, V., "On the Spreading of Liquids on Solid Surfaces: Static and Dynamic Contact Lines," Ann. Rev. Fluid Mech. 11, 371 (1979).
14. Elliot, G. E. P. and Riddiford, A. C., "Dynamic Contact Angle--The Effect of Impressed Motion," J. Coll. Inter. Sci. 23, 389-398 (1967).
15. Elliot, G. E. P. and Riddiford, A. C., "Dynamic Contact Angles and Rates of Adsorption," Nature 195, 795 (1962).
16. Johnson, R. E., Dettre, R. H. and Brandreth, D. A., "Dynamic Contact Angle and Contact Angle Hysteresis," J. Coll. Inter. Sci. 62, 205 (1977).
17. Fox, H. W. and Zisman, W. A., "The Spreading of Liquids on Low Energy Surfaces. I. Polytetrafluoroethylene," J. Coll. Inter. Sci. 5, 514 (1950).
18. Bird, R. B., Stewart, W. E. and Lightfoot, E. N., Transport Phenomena, John Wiley & Sons, Inc. (1960).
19. Batycky, J. P., "Dependence of Residual Oil Mobilization on Wetting and Roughness," Symposium on Surface Phenomena in Enhanced Oil Recovery, Third International Conference on Surface and Colloid Science, Stockholm, August 20-25, 1979.
20. Reed, R. L. and Healy, R. N., "Contact Angles for Equilibrated Micro-emulsion Systems," SPE paper No. 8262, presented at 59th Annual Fall Meeting of SPE of AIME, Las Vegas, September 23-26, 1979.

Table A2.1 Measurement of Internal Radius of Teflon Tube

<u>Tube</u>	<u>Mercury Thread Method</u>	<u>N. Heptane</u>
1 *	.0331 cm	.0331 cm
2 *	.0711 cm	.0716 cm
3 +	.0740 cm	---

\* Tube as measured gives class #3 behavior

+ Tube as supplied

Table A2.2 Properties of Test Liquids

Liquid	Density (g/cm <sup>3</sup> )	Density Difference (g/cm <sup>3</sup> )	Surface Tension (dyne/cm)	Viscosity (cp)	Intrinsic Contact Angle*
N - Heptane	.6800	.6788	18.89	.404	22°
N - Decane	.7251	.7239	23.66	.933	35°
N - Tetradecane	.7599	.7587	26.20	2.25	44°
Diocetyl Ether	.8007	.7995	24.83	3.52	49°
Hexachlorobutadiene	1.681	1.680	36.00	3.174	60°
α-Bromonaphthalene	1.4739	1.4727	43.00	4.75	73°
Ethylene Glycol	1.1081	1.1063	47.60	18.20	90°
Distilled Water	1.001	1.000	70.55	1.00	108°

\*Reported by Fox & Zisman<sup>17</sup>

Table A2.3 Comparison of Measured Advancing and Receding Static Contact Angles at Rough Surfaces with Correlations Based on Previous Studies.

No.	Liquid	$\theta_E$	$\theta_A$		$\theta_R$	
			From Experiment	From Correlation	From Experiment	From Correlation
1.	N - Heptane	22°	0°	1°	0°	0°
2.	N - Decane	35°	27°01	27°	2°	1°
3.	N - Tetradecane	44°	41°	44°80	4°	3°
4.	Dioctyl Ether	49°	49°	55°	5°	4°
5.	Hexachlorobutadiene	60°	71°	77°	18°	9°
6.	$\alpha$ -Bromonaphthalene	73°	87°	103°	18°	18°
7.	Ethylene Glycol	90°	131°	137°	32°	43°
8.	Distilled Water	108°	167°	163°	83°	79°

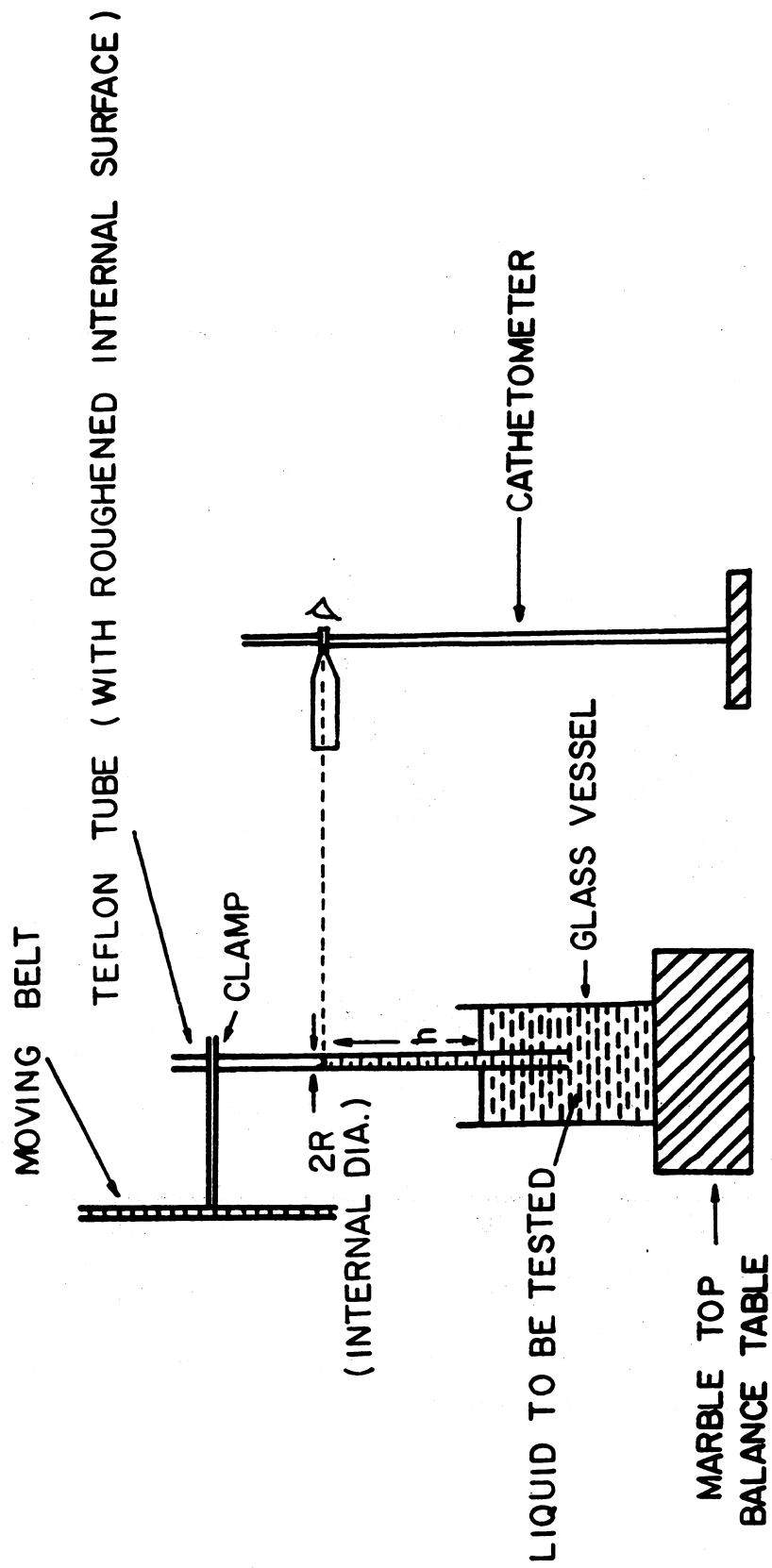


Figure A2.1 Apparatus for measurement of capillary rise under dynamic conditions.

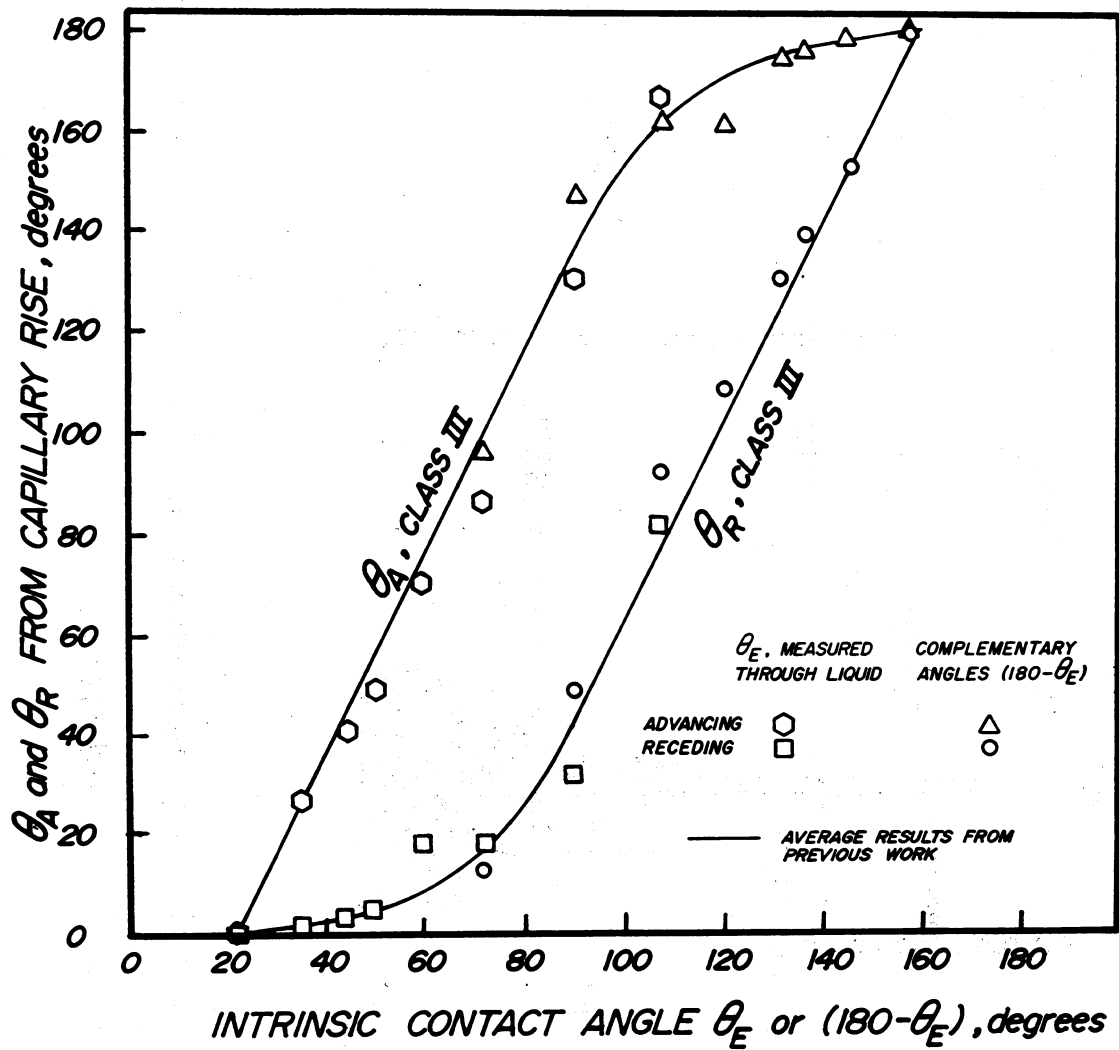


Figure A2.2 Static values of advancing and receding contact angles at rough surfaces versus values at smooth surfaces.



(a) Tube #1 Very Well Roughened (Gave Class III Behavior) - X600



(b) Tube #2 Well Roughened (Gave Class III Behavior) - X600

**Figure A2.3 Electron micrograph of roughened tube surfaces which both gave Class III behavior.**

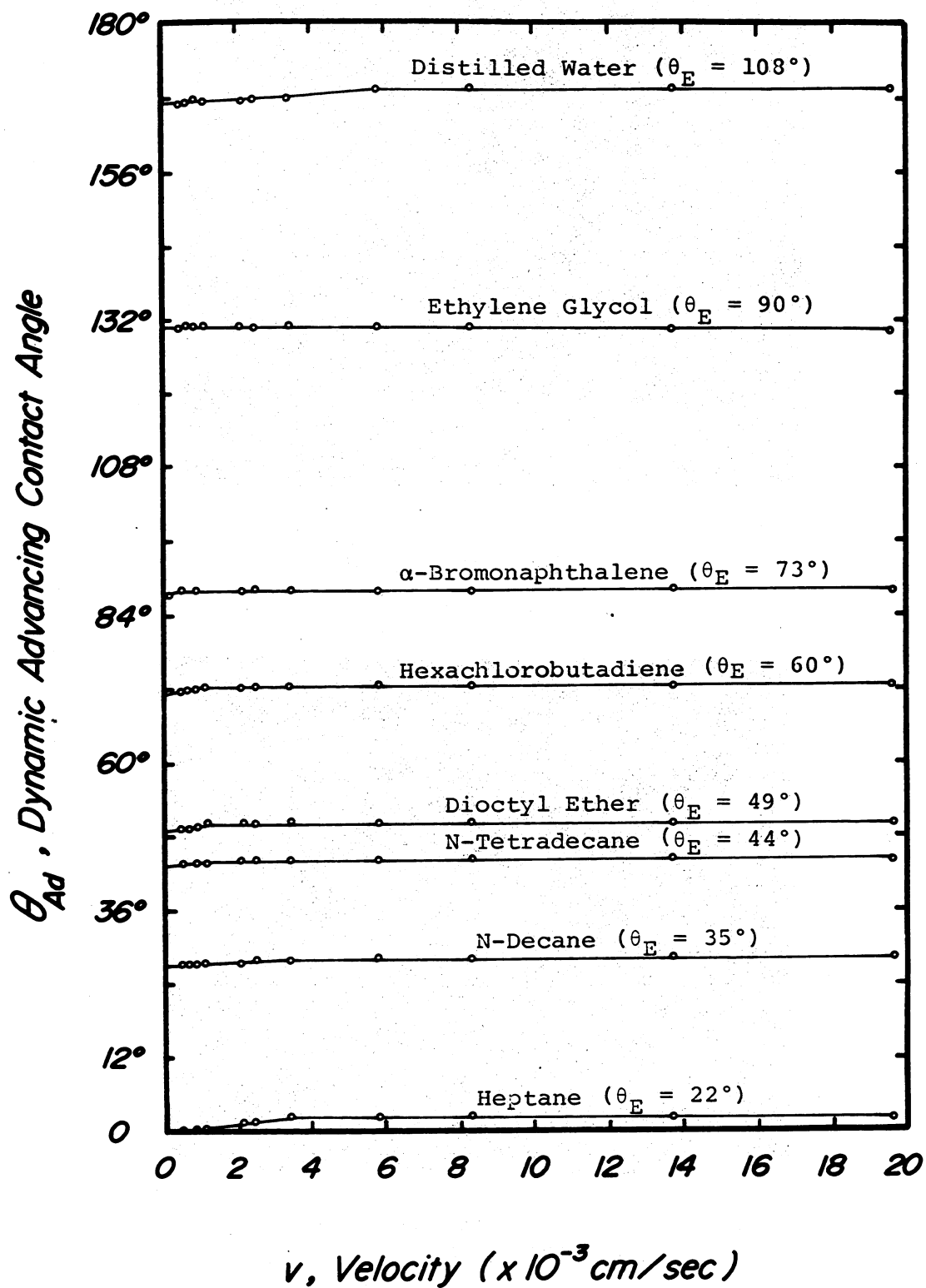


Figure A2.4 Advancing contact angles from capillary rise in a tube being lowered at velocity,  $V$ , for systems of different intrinsic contact angles.

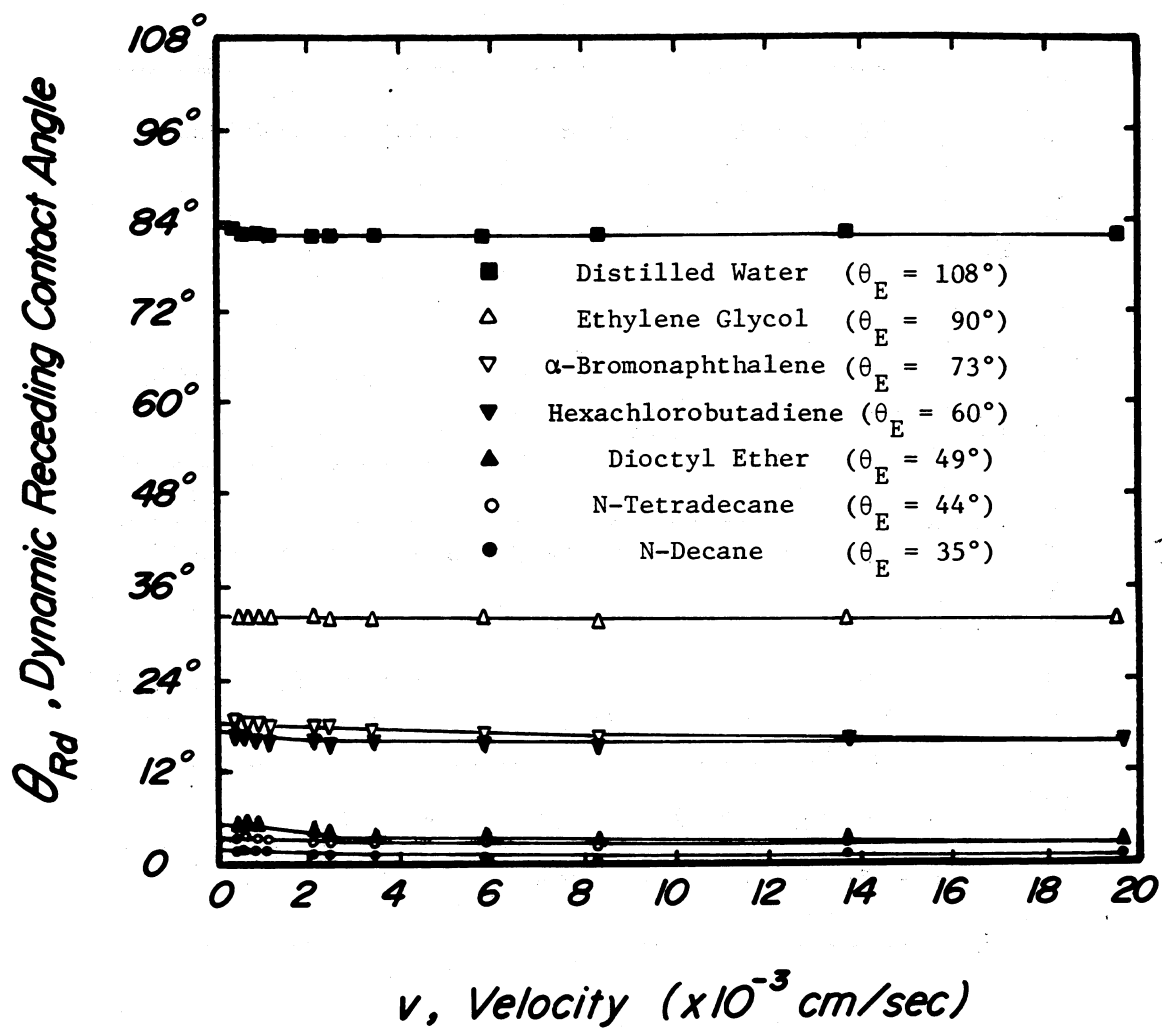


Figure A2.5 Receding contact angles from capillary rise in a tube being raised at velocity,  $V$ , for systems of different intrinsic contact angles.

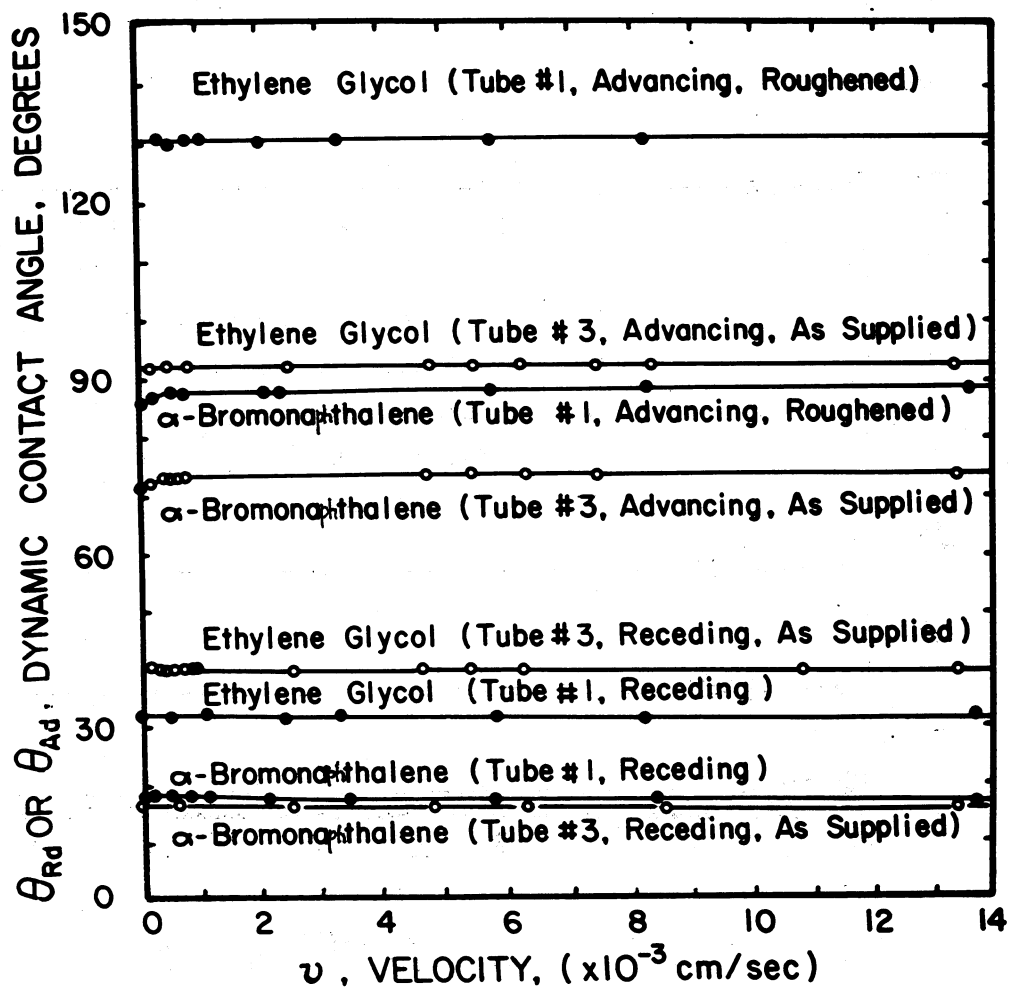


Figure A2.6 Effect of roughening on dynamic contact angle.



